



NKS-408
ISBN 978-87-7893-497-0

Phenomena Threatening Containment Integrity and Evaluating Source Term Characteristics

Veikko Taivassalo¹
Eveliina Takasuo¹
Magnus Strandberg¹
Tero Tyrväinen¹
Ilkka Karanta¹
Anna Nieminen¹

¹VTT Technical Research Centre of Finland Ltd

June 2018

Abstract

To assess phenomena threatening the BWR containment integrity more reliably, long-term debris bed coolability and possibility of hydrogen explosions to occur were analysed deterministically. When comparing VTT's MEWA results on the debris bed post-dryout temperature to KTH's DE-COSIM results, a good agreement was achieved while the temperatures continued to increase, but the stabilized temperatures differed notably. Hydrogen explosions are possible in the containment only if the inertion is lost. This is most probable during the shutdown or start-up.

In addition, factors affecting source term characteristics, i.e. release temperature, altitude and probability were considered for different accident scenarios to further develop the methods and tools for PRA. Source term release height is usually the height of the location where the reactor building leaks or the height of the chimney if release is controlled. The temperature of release from containment is in most cases close to 100 °C but the temperature of radionuclides can potentially change during their migration in the reactor building.

Key words

Debris bed coolability, MEWA, hydrogen explosions, MELCOR, source term, PRA, FinPSA

Phenomena Threatening Containment Integrity and Evaluating Source Term Characteristics

NKS-R SPARC

(Contract: AFT/NKS-R(16)122/12)

Veikko Taivassalo¹, Eveliina Takasuo¹, Magnus Strandberg¹, Tero Tyrväinen¹, Ilkka Karanta¹, Anna Nieminen¹

¹VTT Technical Research Centre of Finland Ltd

Table of contents

	Page
1. Introduction	3
2. Particle debris coolability	3
3. Hydrogen explosions in a Nordic BWR containment	4
3.1 Deterministic analyses	4
3.2. Probabilistic approach	5
4. Source term characteristics	5
4.1 FinPSA containment event tree model	5
5. Conclusions	6
Acknowledgement	7
Disclaimer	7
References	7

1. Introduction

Ensuring the integrity of the containment during a hypothetical severe accident is extremely important since the containment is the last safety barrier preventing radioactive release to the environment. To assess phenomena threatening the Nordic Boiling Water Reactor (BWR) containment integrity more reliably, long-term debris bed coolability and possibility of hydrogen explosions to occur were analysed deterministically.

In addition, factors affecting source term characteristics, i.e. release temperature, altitude and probability were considered for different accident scenarios to further develop the methods and tools for probabilistic risk analysis (PRA).

This report is a summary of the three reports included as annexes.

2. Particle debris coolability

Achieving long-term coolability of molten corium is the main objective in the unlikely event of a severe nuclear reactor accident. The Nordic BWRs rely on cooling the corium in the flooded lower drywell of the containment as a cornerstone of the severe accident management strategy. During the discharge of the corium in the deep water pool, the molten material is fragmented into droplets and subsequently solidified into particles, which settle on the floor of the containment, forming a porous debris bed.

The coolability limit for the debris bed is traditionally based on the minimum dryout heat flux. This approach might be overly conservative, since the temperature may remain on an acceptable level even in the dry zone. Instead of the dryout heat flux, it has been proposed that the coolability limit should be based on the increase of the particle temperature (Atkhen & Berthoud, 2006). To analyse this, the behaviour of conical debris beds was studied by performing MEWA simulations (ANNEX1). Influences of the bed particle size, heating power and porosity were examined. Different heat transfer models available in MEWA and important in predicting the post-dryout temperature field were tested.

Due to the lack of experimental data that could be directly used for code validation, the MEWA results were compared to the DECOSIM results by Yakush & Kudinov (2014) in Figure 1. The simulation results of the MEWA code are not in fully agreement with the DECOSIM results. For small particle cases without temperature stabilization, the codes agree satisfactorily. On the other hand, these cases are not interesting because the maximum particle temperature eventually exceeds the temperatures where zirconium oxidation or even corium remelting begins.

In the other conical bed cases, the beds are coolable but MEWA and DECOSIM predict different transient behaviours and final steady-state conditions. Therefore, before trying to quantify the temperature-based dryout criterion, the origin of the significant differences between the MEWA and DECOSIM results needs to be identified. Some differences in the simulation setups and models are known or probable but most likely they do not cause those large differences in simulation results for post-dryout conditions.

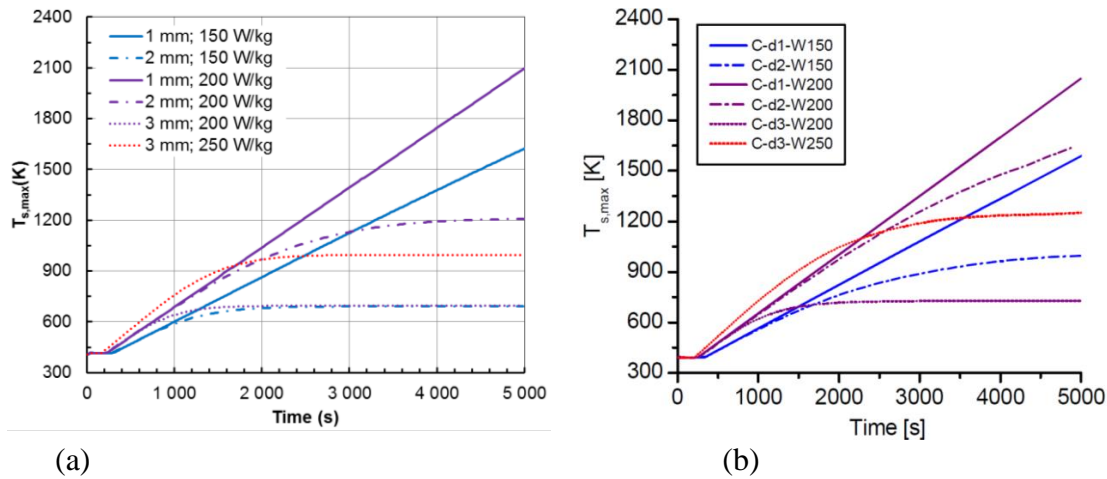


Figure 1. Maximum solid particle temperature as a function of time in the MEWA simulations (a) and in the DECOSIM simulations according to Yakush & Kudinov (2014) (b) for the same conical bed.

3. Hydrogen explosions in a Nordic BWR containment

Accidents that may lead to bypassing the filtered containment venting should be practically eliminated in Nordic BWRs that are inerted with nitrogen to avoid hydrogen explosions. However, if the inertion is lost, hydrogen explosions may be possible in the containment. This is most probable during the shutdown or start-up. In the reactor hall, hydrogen explosion could occur after the loss of containment integrity. This, in turn, has an effect on the timing of the radioactive release and on the quantity also by resuspension of deposited fission products. Hydrogen explosions may also occur in the reactor hall, even if the containment is intact, if containment pressure evolves to a high level increasing the leak.

3.1 Deterministic analyses

The risk of a flammable mixture of hydrogen and air to be formed in the reactor building was studied analysing a station blackout (SBO) scenario for the Nordic BWR plant with MELCOR (ANNEX2). Without assuming an increase in the containment design leak, the results showed such low concentrations that even a hydrogen combustion is considered very unlikely. The total mass of hydrogen also remained low, so that if the local concentrations could be high enough to be theoretically able to result a hydrogen combustion, the assorted energy release would not be very high and this event could not be considered as an explosion.

Also a SBO accident with a non-inerted containment was analysed and this resulted in hydrogen deflagrations in the containment. The total amount of hydrogen burned in the different parts of the containment is illustrated in Figure 2. However, even the non-inerted SBO case did not proceed into detonation i.e. into an explosion. Despite the hydrogen deflagrations caused an increase in the temperature, the pressure remained even on a lower level than in the previous accident analysis, where there was no hydrogen deflagration in the containment. This could be because the burning of hydrogen consumes gas which decreases the pressure.

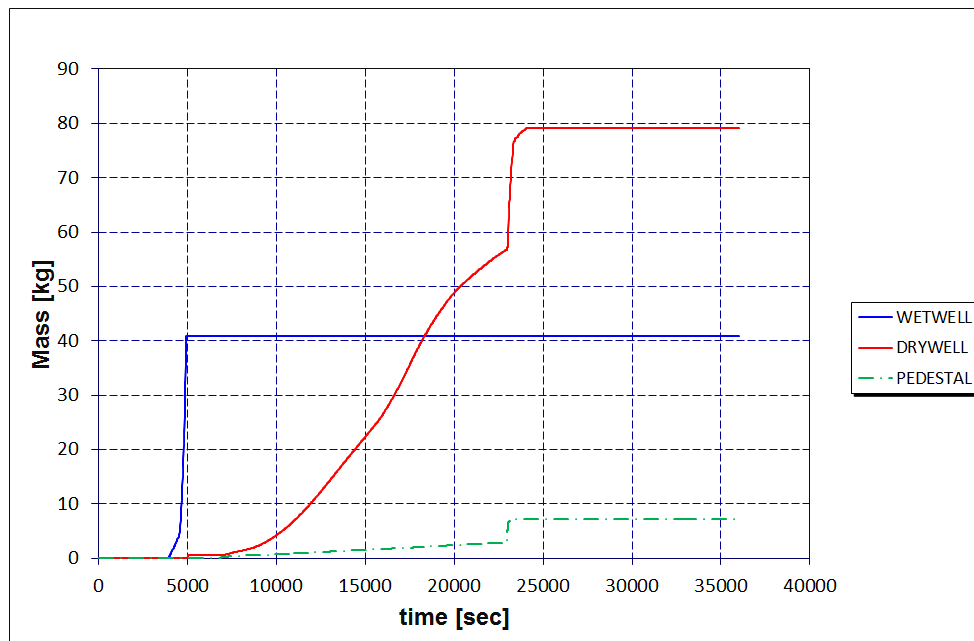


Figure 2. Mass of burned hydrogen in non-inerted containment volumes.

3.2 Probabilistic approach

Hydrogen explosions are typically modelled in level 2 PRAs of BWRs in very simple ways (ANNEX 3). For example, in the FinPSA model probability 0.3 is given for containment not being inert, and if the containment is inert, hydrogen explosion breaks the containment with probability 0.5. These probabilities have been assumed to be conservative. Hydrogen explosions outside the containment, i.e. in the reactor building, are not considered in PRA.

4. Source term characteristics

The height and temperature of radioactive releases have typically not been included in level 2 PRA, even though they are needed as inputs for level 3 PRA (Lee & McCormick, 2011). These source term characteristics are analysed in ANNEX 3. Release height is usually the height of the location where the reactor building leaks (which depends on the containment failure mode), or the height of the chimney if release is controlled. The temperature of release from containment is in most cases close to 100 °C because radioactive substances are usually released among steam, but the temperature of radionuclides can potentially change during their migration in the reactor building. Higher temperatures can be caused by fires and explosions.

4.1 FinPSA containment event tree model

A release height variable and temperature variable were added to the FinPSA containment event tree model for a Nordic BWR. Their values are set always after the containment failure mode is defined. It was assumed that hydrogen explosions and alpha mode steam explosions lead to higher release heights than the other failure modes because they occur high in the containment. Basemat release was assumed to occur at ground level, and the height of the stack was assumed to be 110 meters.

It was assumed that release temperatures are higher than 100 °C if explosions occur. Without explosions, the temperatures were assumed to be 100 °C with exception of basemat melt-through. In that case, it was assumed that the radionuclides are cooled down to a lower

temperature by building structures. These values are not based on any real data at this point but were chosen just for the sake of having an example and they should not be adapted to any real PRA.

In addition, uncertainty analysis was implemented for release probabilities and some results are illustrated in Figure 3 as an example.

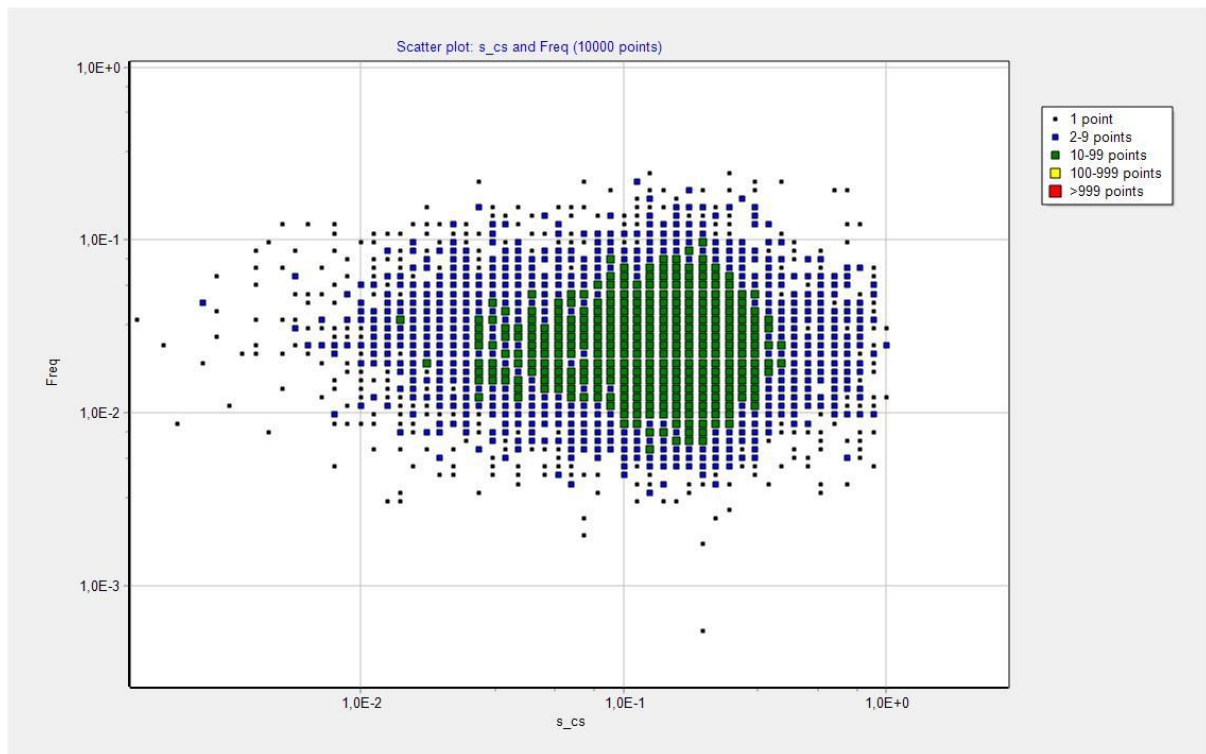


Figure 3. Scatter plot between conditional probability and caesium release fraction in early containment failure based on weighted point values.

5. Conclusions

When comparing VTT's MEWA results on the debris bed post-dryout temperature to KTH's DECOSIM results, a good agreement was achieved while the temperatures continued to increase, but the stabilized temperatures differed notably. Before trying to quantify the temperature-based dryout criterion, the origin of the significant differences between the MEWA and DECOSIM results needs to be identified.

Hydrogen explosions are possible in the containment only if the inertion is lost. This is most probable during the shutdown or start-up. Without assuming an increase in the containment design leak, hydrogen concentration remained so low that even hydrogen combustion is considered very unlikely. When assuming a non-inerted containment, a hydrogen deflagration occurred in the containment.

Source term release height is usually the height of the location where the reactor building leaks (which depends on the containment failure mode), or the height of the chimney if release is controlled. The temperature of release from containment is in most cases close to 100 °C but the temperature of radionuclides can potentially change during their migration in the reactor building, which is not typically considered in PRA.

Acknowledgement

This work has been partly funded by the Finnish Nuclear Power Plant Safety Research Programme SAFIR2018.

NKS conveys its gratitude to all organizations and persons who by means of financial support or contributions in kind have made the work presented in this report possible.

Disclaimer

The views expressed in this document remain the responsibility of the author(s) and do not necessarily reflect those of NKS. In particular, neither NKS nor any other organization or body supporting NKS activities can be held responsible for the material presented in this report.

References

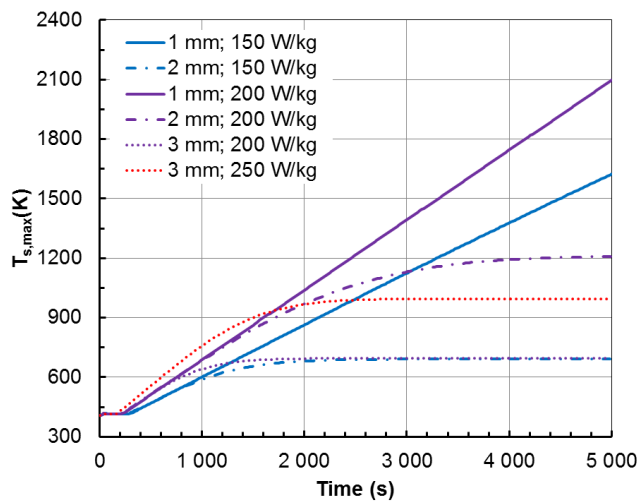
Atkhen, K. & Berthoud, G., 2006. SILFIDE experiment: Coolability in a volumetrically heated debris bed. *Nuclear Engineering and Design*, 236, pp.2126–2134.

Lee, J.C. & McCormick N.J., 2011. *Risk and safety analysis of nuclear systems*. Wiley, Hoboken NJ, USA.

Yakush, S. & Kudinov, P., 2014. A model for prediction of maximum post-dryout temperature in decay-heated debris bed. In *22nd International Conference on Nuclear Engineering*. July 7-11, 2014, Prague, Czech Republic.

ANNEX 1

Predicting debris bed behaviour in post-dryout conditions



Predicting debris bed behaviour in post-dryout conditions

Authors: Veikko Taivassalo, Eveliina Takasuo

Confidentiality: Public

Report's title	
Predicting debris bed behaviour in post-dryout conditions	
Customer, contact person, address	Order reference
SAFIR2018 Research Programme on Nuclear Power Plant Safety 2015 – 2018	SAFIR 6/2016
Project name	Project number/Short name
Comprehensive Analysis of Severe Accidents	108735/CASA
Author(s)	Pages
Veikko Taivassalo, Eveliina Takasuo	28/
Keywords	Report identification code
debris bed, coolability, post-dryout conditions	VTT-R-00762-17
Summary	
<p>Achieving long-term coolability of molten corium is the main objective in the unlikely event of a severe nuclear reactor accident. The Nordic boiling water reactors (BWRs) rely on cooling the corium in the flooded lower drywell. During the discharge of the corium in the flooded drywell, the molten material is fragmented into droplets and subsequently solidified into particles, which settle on the floor of the containment, forming a porous debris bed. In the impressive amount of research on the dryout heat flux and debris bed coolability conducted in recent decades, studies on heat transfer after dryout has occurred are rare. In the post-dryout conditions, the heating power required for dryout and a local loss of water has been reached and, more often than not, exceeded.</p> <p>The coolability limit based on the minimum dryout heat flux might be overly conservative, since the temperature may remain on an acceptable level even in the dry zone. Instead of the dryout heat flux, it has been proposed that the coolability / non-coolability limit should be based on the increase of the particle temperature.</p> <p>In this work, the behaviour of two hypothetical conical debris beds was studied by performing MEWA simulations. Especially the post-dryout conditions were analysed for a reference reactor debris bed and for a conical debris bed studied by Yakush & Kudinov (2014). Influences of the bed particle size, heating power and porosity were examined. Different heat transfer models available in MEWA and important in predicting the post-dryout temperature field were tested. Due to the lack of experimental data that could be directly used for code validation, the MEWA results were compared to the DECOSIM results by Yakush & Kudinov (2014). As the MEWA results clearly differ from the DECOSIM results in cases that could be considered coolable based on temperature stabilization, the origin of the differences needs to be identified before trying to quantify the temperature-based coolability limit.</p>	
Confidentiality	Public
Espoo 10.2.2017	
Written by	Reviewed by
	
Veikko Taivassalo Principal Scientist	Anna Nieminen Research Scientist
Accepted by	
	
Anitta Hämäläinen Research Team Leader	
VTT's contact address	
PO Box 1000, 02044-VTT, Finland	
Distribution (customer and VTT)	
SAFIR2018 Reference Group 2	
<p><i>The use of the name of VTT Technical Research Centre of Finland Ltd in advertising or publishing of a part of this report is only permissible with written authorisation from VTT Technical Research Centre of Finland Ltd.</i></p>	

Contents

Contents.....	2
1. Introduction.....	3
2. Heat transfer models in MEWA.....	4
2.1 Energy balance equation for bed particles.....	4
2.2 Effective thermal conductivity in a dry bed.....	4
2.3 Heat transfer between particles and gas.....	5
3. Conical debris bed of a reference reactor.....	6
3.1 Simulation set-up.....	6
3.2 Simulation results for the base case.....	8
3.3 Results for base-case variants.....	9
3.3.1 Influence of the particle size.....	9
3.3.2 Influence of the porosity.....	9
3.3.3 Effects of heat transfer models.....	9
3.4 Discussion.....	9
4. Conical bed of Yakush & Kudinov.....	15
4.1 Case specifications.....	15
4.2 MEWA results.....	16
4.3 Comparison of the MEWA and DECOSIM results.....	22
4.4 Effects of heat transfer models.....	24
4.5 Discussion.....	24
5. Post-dryout steady-state conditions.....	26
6. Conclusions.....	27
References.....	28

1. Introduction

Achieving long-term coolability of molten corium is the main objective in the unlikely event of a severe nuclear reactor accident. The Nordic boiling water reactors (BWRs) rely on cooling the corium in the flooded lower drywell of the containment as a cornerstone of the severe accident management strategy. During the discharge of the corium in the deep water pool (~10 m), the molten material is fragmented into droplets and subsequently solidified into particles, which settle on the floor of the containment, forming a porous debris bed.

The coolability of heap-shaped (conical) and flat-shaped, top-flooded (cylindrical) debris beds was studied in the COOLOCE experiments, in which the dryout power and heat flux were measured (Takasuo, 2016). In the impressive amount of research on the dryout heat flux and debris bed coolability conducted in recent decades, studies on heat transfer after dryout has occurred are almost impossible to find. In the post-dryout conditions, the heating power required for dryout and a local loss of water has been reached and, more often than not, exceeded.

For debris beds of realistic shapes (heaps and cones), the post-dryout conditions are of interest since the particle temperature may stabilize even though a local dry zone has been formed (Atkhen & Berthoud, 2006). The coolability limit based on the minimum dryout heat flux might be overly conservative, since the temperature may remain on an acceptable level even in the dry zone. Instead of the dryout heat flux, it has been proposed that the coolability / non-coolability limit should be based on the increase of the particle temperature (Takasuo, 2015; Yakush & Kudinov, 2014). It should be noted that in the case of top-flooded bed, local dryout usually leads to temperature increase above corium melting temperature and thus the post-dryout coolability is mainly of interest with the heap-shaped debris beds.

This report presents axisymmetric 2D simulations of the post-dryout behaviour of debris beds. Simulations were performed with the MEWA code (Bürger et al., 2006). Especially heat transfer conditions after dryout has occurred are analysed in two conical debris beds. The various heat transfer models available in MEWA and important in predicting the post-dryout temperature were tested by simulations. The important MEWA heat transfer models are introduced in Section 2. The first modelled geometry is a debris bed for a reference reactor with 200 000 kg of corium. The modelling of the reference reactor debris bed is discussed in Section 3. In addition to the base case, effects of the particle size and porosity were studied. Due to lack of experimental data that could be directly used for code validation, the MEWA results were compared to the DECOSIM results produced in an earlier study by KTH for somewhat different bed characteristics (Yakush & Kudinov, 2014). In addition, a comprehensive verification study was conducted by simulating with MEWA the same conical debris bed studied by Yakush & Kudinov (2014). Section 4 discusses the verification study. Finally, post-dryout conditions after bed temperature stabilization are introduced briefly in Section 5 by comparing MEWA simulation results to an analytical correlation of Yakush & Kudinov (2014).

2. Heat transfer models in MEWA

2.1 Energy balance equation for bed particles

In MEWA simulations, the temperature of the bed particles is computed by solving the energy equation for the solid phase (Rahman, 2013):

$$\frac{\partial}{\partial t} [(1 - \varepsilon)\rho_s h_s] = \nabla \cdot (\lambda_{s,\text{eff}} \nabla T_s) + Q_{\text{decay}} - Q_{s,\text{sat}} - Q_{s,g} - Q_{s,l} \quad (1)$$

In Equation (1), ε is the porosity, ρ the density (kg/m^3), h the specific enthalpy (J/kg), $\lambda_{s,\text{eff}}$ the effective thermal conductivity of the solid phase ($\text{W/m}\cdot\text{K}$) and T the temperature (K). The subscripts s, l and, g refer to the solid, liquid and gas phases. Q_{decay} (W/m^3) represents the internal (decay) heat generation of the debris particles. $Q_{s,\text{sat}}$, $Q_{s,g}$ and $Q_{s,l}$ (W/m^3) are the sources of heat due to the boiling at the particle surfaces (sat) and from the particles to the gas (g) and liquid (l) phases, respectively. Since the focus of this study is on the post-dryout behaviour, in the conditions of interest the solid particles are in contact with the gas phase. Accordingly, boiling and heat transfer from the solid particles directly to the liquid phase are less important. This leaves the models for the effective thermal conductivity $\lambda_{s,\text{eff}}$ and the heat transfer from the particles to the gas phase ($Q_{s,g}$) to play key roles in the post-dryout zones.

2.2 Effective thermal conductivity in a dry bed

The effective thermal conductivity $\lambda_{s,\text{eff}}$ is a bulk property, which describes the ability of multi-component porous medium to conduct heat. It accounts for the combined effects of conduction through the contact points of the solid particles and through the fluid, and possibly radiation across the fluid space and convection in the pores.

In MEWA, there are two alternative basic approaches for calculating the effective thermal conductivity for a dry bed:

- (i) The first approach is the conductivity model of Imura (Imura & Takegoshi, 1974) combined with a radiation model. For the radiation model, there are three options: the Yagi (Yagi & Kunii, 1957), Vortmeyer (1978) and Luikov (Luikov et al., 1968) models.
- (ii) The second approach is the Maxwell model for predicting the properties of a heterogeneous medium (Maxwell 1873, p. 365).

The Maxwell model does not include radiative heat transfer, and it is best suited for particles dispersed in a continuous medium (very large porosity). Therefore, the other conduction-radiation combinations can be considered as the primary models for calculating the effective thermal conductivity in packed low-porosity beds. In MEWA, the default model for the effective dry-bed thermal conductivity $\lambda_{s,\text{eff}}$ is the Imura conductivity model with the radiation model of Yagi.

It should be noted that the MEWA documentation does not quote all the original references of the models for the effective thermal conductivity $\lambda_{s,\text{eff}}$ in a dry particle bed. The model references given here are as found in the public literature by the authors.

2.3 Heat transfer between particles and gas

In MEWA the heat transfer rate from the particles to the gas phase is given by

$$Q_{s,g} = a_{s,g} \kappa_{s,g} (T_s - T_g) \quad (2)$$

where the interfacial area density $a_{s,g}$ is given by

$$a_{s,g} = \frac{6(1 - \varepsilon) (\alpha_v - 0.7)}{D_p \cdot 0.3} \quad (3)$$

if $\alpha_v \geq 0.7$ (continuous gas phase) otherwise $a_{s,g} = 0$. D_p is the particle diameter (m) and α_v the gas (vapor) volume fraction. The heat transfer coefficient $\kappa_{s,g}$ (W/m²K) in Eq. (2) is calculated on the basis of the Nusselt number $Nu_{s,g}$ as follows

$$\kappa_{s,g} = \frac{Nu_{s,g} \lambda_g}{D_p} \quad (4)$$

Here λ_g is the thermal conductivity of the gas phase (W/m·K).

There are three alternatives in MEWA to define the heat transfer coefficient $\kappa_{s,g}$ for heat transfer from the solid particles to the gas phase. In practice, a user selects a method to determine the Nusselt number $Nu_{s,g}$.

- (i) In the default model, the Nusselt number is calculated from a simple formula

$$Nu_{s,g} = 2 + 0.6 \sqrt{Re_g} \quad (5)$$

In Eq. (5), Re_g is the dimensionless Reynolds number

$$Re_g = \frac{|\vec{v}_g \rho_g D_p|}{\eta_g} \quad (6)$$

where \vec{v}_g is the gas velocity (m/s) and η_g is the gas viscosity (Pa·s).

- (ii) The second option is the model of Gnielinski (Stephan et. al., 2010, p. 743), in which both the laminar and turbulent Nusselt numbers are calculated as follows

$$Nu_{s,g}^{lam} = 0.644 \sqrt{Re_g^3 Pr_g} \quad (7)$$

$$Nu_{s,g}^{turb} = 0.037 \frac{Re_g^{0.8} Pr_g}{1 + 2.443 Re_g^{-0.1} (Pr_g^{\frac{2}{3}} - 1)} \quad (8)$$

Here Pr_g is the Prandtl number

$$Pr_g = \frac{\eta_g c_{p,g}}{\lambda_g} \quad (9)$$

where $c_{p,g}$ is the specific heat capacity of the gas phase (J/kgK). The heat transfer coefficient is calculated from Eq. (4) using the Nusselt number obtained from the following formula

$$Nu_{s,g} = \left[2 + \sqrt{(Nu_{s,g}^{lam})^2 + (Nu_{s,g}^{turb})^2} \right] \left[1 + \frac{2}{3}(1 - \varepsilon) \right] \quad (10)$$

- (iii) A user defined constant value is the third alternative to determine the Nusselt number. This option was not used in this study.

3. Conical debris bed of a reference reactor

3.1 Simulation set-up

Because no small-scale or other experimental data exist on the post-dryout conditions, there is no reason to study the post-dryout conditions in a small scale (e.g., by using the COOLOCE test facility models). In addition, it is likely that the results for a laboratory-sized bed would not be scalable to a larger scale. In the reactor scale, the gas velocity is greater for the same particle size and porosity enhancing heat transfer in the large scale.

The bed geometry selected for modelling was the reference reactor presented in Takasuo (2015, pp. 88-91) with the same Cartesian 2D mesh of 5 cm cell size. The height of the bed is 3.265 m and diameter 7.25 m. The water pool measures 4 m in height and 9 m in diameter. The computational domain and mesh with the bed shape are shown in Figure 1. The domain and mesh are axisymmetric respect to the vertical axis. The mesh consists of 90 x 80 cells.

The conical bed represented by axisymmetric mesh is illustrated in Figure 2. The mirror image is included for visualization purposes. Figure 2 also shows the results of a simulation with a heating power just above the dryout power.

In the base simulation case, the presumed melt mass is 200 000 kg corresponding to a large release from the reactor pressure vessel. The porosity was set to 0.5 and the particle diameter to 1 mm. Since the particle shape and size variations, present in realistic debris beds, are not taken into account in the constitutive closure models, the particle diameter is the *effective* diameter. This does not mean that the debris particles are expected to have a uniform diameter of 1 mm, or that their surface area-weighted average diameter is 1 mm. Instead, the effective diameter is best described as a characteristic size that represents thermal and hydrodynamical properties of a realistic bed with an acceptable accuracy. A small particle diameter was selected because an earlier study suggests that the beds of random irregular particles yield a large single-phase pressure loss compared to spherical or regular-sized particles (Chikhi et al., 2014). This usually results in a dryout zone, which is also obtained with small homogenous particles.

In the computations predicting the conditions after dryout, the simulation time is naturally longer than in the standard dryout calculations, because the simulations have to be continued beyond the formation of the first dry zone. The time needed for the bed stabilization is roughly proportional to the amount of excess power above the minimum dryout power. A simulation time of 5000 s was used as default.

The selection of the thermal properties for the debris particles is by no means obvious since they may vary depending on the temperature and (local) composition of the corium. The following constant thermal bed properties were used:

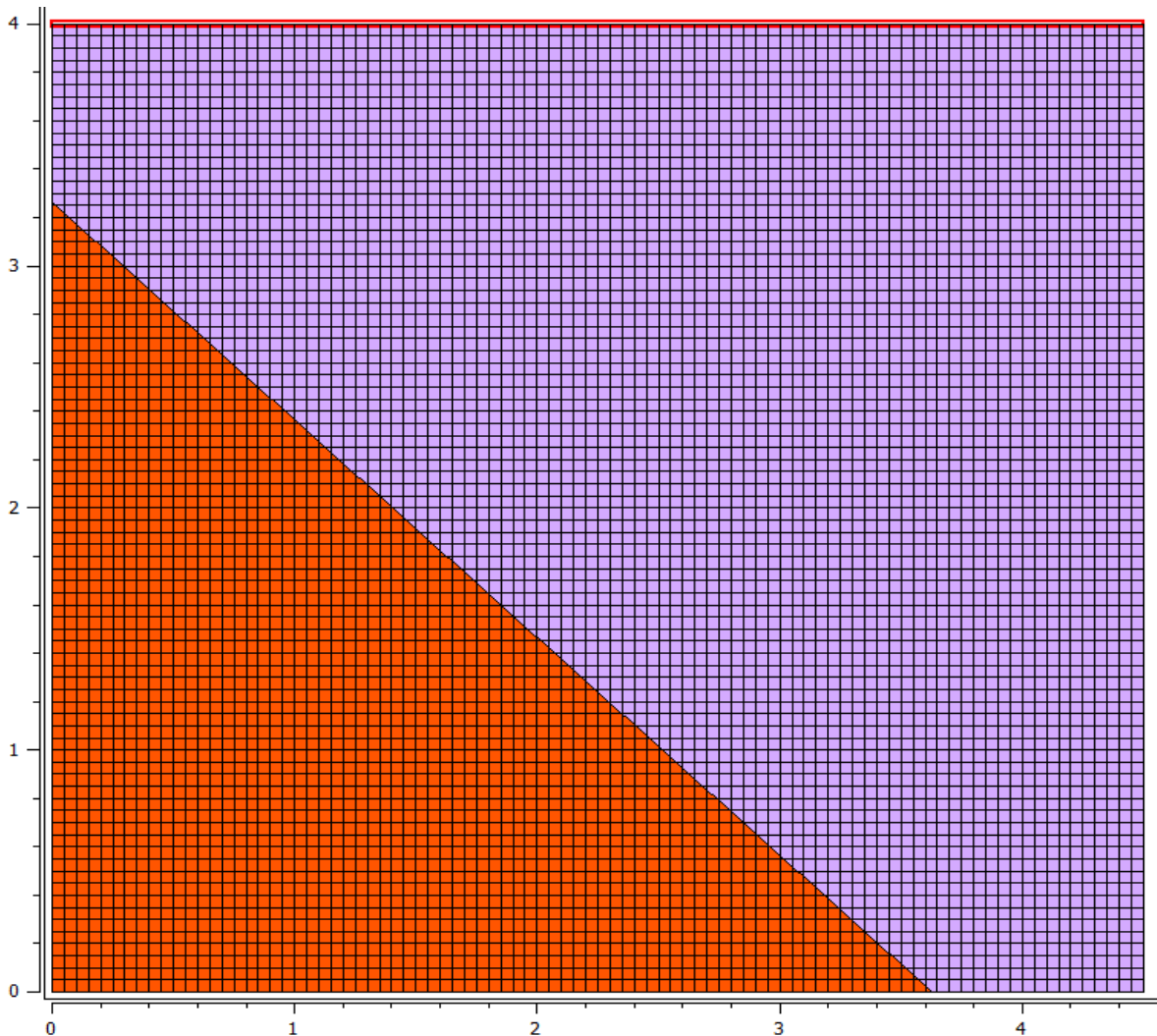


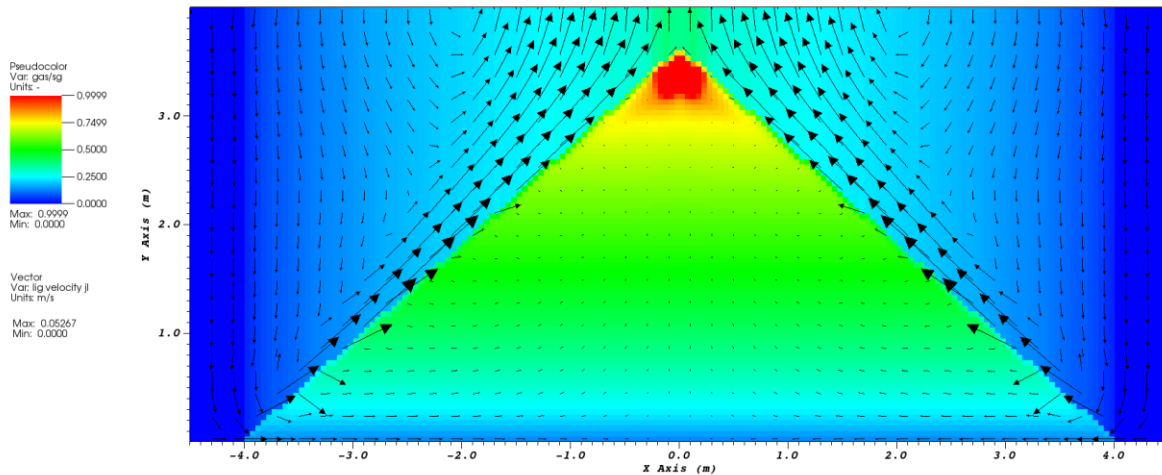
Figure 1. Computational domain, mesh and bed shape in the MEWA simulation for a conical debris bed of a reference reactor.

density: $\rho_s = 8900 \text{ kg/m}^3$,
 specific heat capacity: $c_{p,s} = 566 \text{ J/kgK}$, and
 thermal conductivity: $\lambda_s = 1.9 \text{ W/mK}$.

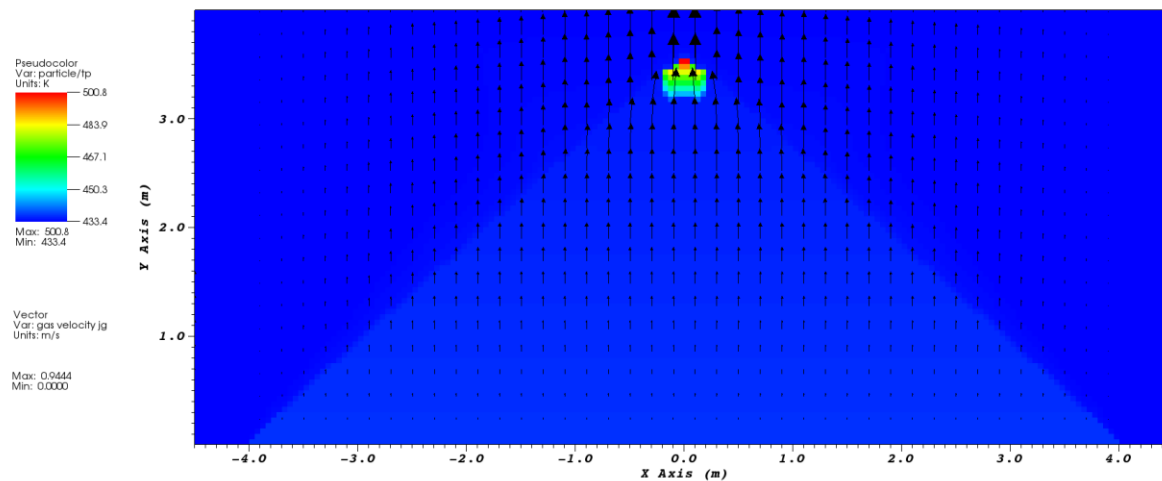
The density of the bed material is based on the study by Song et al. (2006). The values of the specific heat capacity and thermal conductivity were selected to be the same as in the work by Yakush & Kudinov (2014) for comparability. In the simulations, the MEWA model for zirconium oxidation was turned on (Bürger et al., 2006).

The total decay heat power was assumed to be 38 MW (equivalent to 190 W/kg). The pressure at the top boundary is taken to be 3.2 bar.

In the base case simulation, the default models for the effective thermal conductivity of a dry bed $\lambda_{s,\text{eff}}$ (Section 2.2) and for the solid-to-gas heat transfer coefficient $\kappa_{s,g}$ (Section 2.3) are applied. Several variants of the base case were also analysed computationally. In one base-case variant, the particle diameter is increased to be 2 mm. In another variant, the porosity is reduced to the value of 0.4, which was also used in the DECOSIM simulations by Yakush & Kudinov (2014). Furthermore, a set of base-case variants was computed to test the influence of the alternative models for the effective dry-bed thermal conductivity $\lambda_{s,\text{eff}}$ as well as for the solid-to-gas heat transfer coefficient $\kappa_{s,g}$.



(a)



(b)

Figure 2. (a) Void fraction and (b) solid temperature in a MEWA simulation of the conical debris bed of a realistic scale. The dryout power is just exceeded. Vectors of the superficial velocity are shown in (a) for the liquid and (b) for gas phases (Takasuo, 2015).

3.2 Simulation results for the base case

Simulation results for the base case are presented in Figure 3 and Figure 4. shows the void fraction and solid particle temperature as contour plots at the end of the simulation. Dryout has occurred and the dry zone is about 1.5 m high on the axis and the maximum solid temperature is just over 1200 K. The maximum particle temperature is plotted as a function of the simulation time in Figure 4. The bed temperature is close to stabilisation at the time of 5000 s.

Yakush & Kudinov (2014) performed similar simulations with the DECOSIM code for conical and truncated-cone beds. They used particle diameters 1, 2, and 3 mm and specific heating powers 150, 200 and 250 W/kg. By comparing the 1-mm results in Figure 3 and Figure 4 to the DECOSIM results reproduced in Figure 5 and Figure 6, some qualitative differences can be identified. However, comparison is complicated due to several differences in the bed characteristics and simulation set-ups. Accordingly, influences of bed characteristics and heat transfer models were investigated.

3.3 Results for base-case variants

3.3.1 Influence of the particle size

The influence of the particle size was studied by using a particle diameter of 2 mm in a simulation. The void fraction and solid particle temperature at the end of the simulation is depicted in Figure 7. Although dryout is obtained, clearly the larger particle bed cools more effectively due to a reduced flow resistance and the dry zone is small compared to the 1-mm case. The maximum particle temperature is only about 100 K above the saturation temperature. Figure 4 compares the maximum particle temperature as a function of time for the 1 mm and 2 mm particles. In case of the 2 mm particles, the bed stabilizes faster and a steady-state is achieved in about 1000 s, whereas the bed of 1 mm particles requires more than 5000 s.

Comparison of the MEWA results to the 2-mm results of Yakush & Kudinov (2014) (Figure 5 and Figure 6) indicates significant differences in the bed behaviour after dryout. In the DECOSIM simulation, a steady state is not achieved and the maximum particle temperature increases still at the time of 5000 s.

3.3.2 Influence of the porosity

The influence of the porosity was studied by doing the simulation also with a value of 0.4. The porosity is known to influence strongly the particle bed behaviour (Chikhi et al., 2014). The results are shown in Figure 8 and Figure 9. In this case, the results are significantly closer to the DECOSIM results with $D_p = 1$ mm and $P_m = 200$ W/kg presented in Figure 5 and Figure 6. On the other hand, the both codes predict that the bed conditions are not stabilized at the time of 5000 s and the maximum particle temperature is already above the temperature, at which the zirconium oxidization begins.

3.3.3 Effects of heat transfer models

Figure 10 shows the effects of models of the heat transfer coefficient for heat transfer from the solid particles to the gas phase $\kappa_{s,g}$ on the maximum particle temperature. The differences between the curves are at most 1 - 2 K and not readable in the plot.

The influence of the effective dry-bed thermal conductivity $\lambda_{s,eff}$ model selection on the maximum particle temperature is depicted in Figure 11. In this case, too, the differences due to the model selection are insignificant.

3.4 Discussion

In the base simulation case for the reference reactor debris bed (the porosity is 0.5, the particle diameter 1 mm, the total heat power 38 MW) a dry zone is formed and the steady-state post-dryout conditions would be achieved in somewhat more than 5000 s. The maximum steady-state particle temperature would be somewhat above 1200 K. The effects of the models for the effective dry-bed thermal conductivity $\lambda_{s,eff}$ and solid-to-gas heat transfer coefficient $\kappa_{s,g}$ on the maximum particle temperature are within 2 K. The porosity (0.4 vs. 0.5) and particle diameter (1 vs. 2 mm) influence significantly on the simulated transient post-dryout behaviour of the debris bed as well as the achieved steady-state conditions.

The MEWA results differ from the DECOSIM results shown in Figure 5 and Figure 6. The porosity affects strongly the post-dryout bed conditions and the MEWA results with $\varepsilon = 0.4$ are qualitatively close to the DECOSIM results. However, in this case the maximum bed temperature does not stabilize. As relatively small differences in bed characteristics may cause unexpectedly large differences in the simulation results, it was considered worthwhile to repeat the conical bed simulations of Yakush & Kudinov (2014) with the MEWA code.

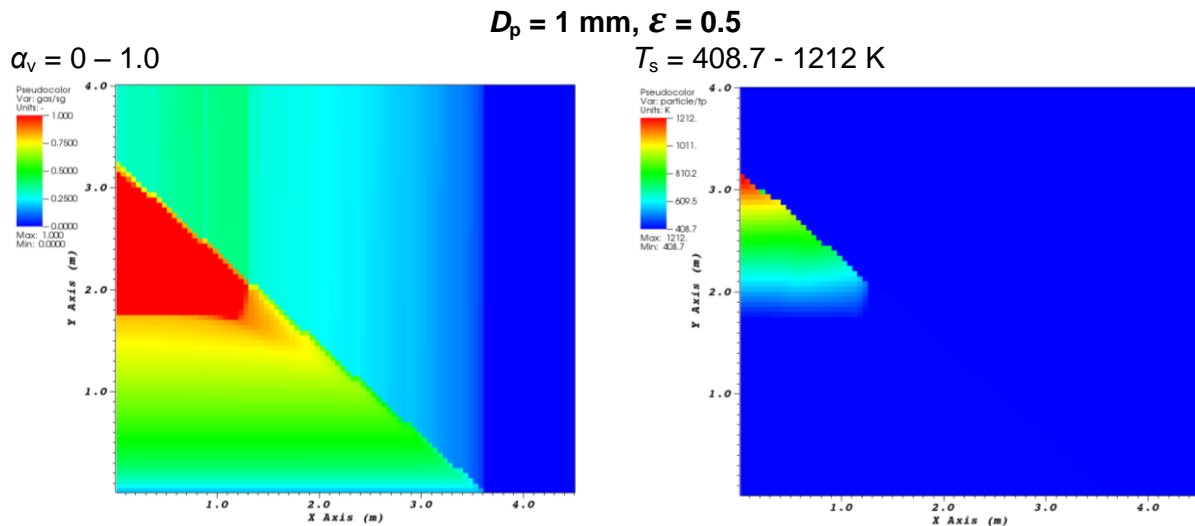


Figure 3. Void fraction (left) and solid particle temperature (right) in the MEWA simulations for the reference reactor debris bed at the time of 5000 s. The default heat transfer models are used.

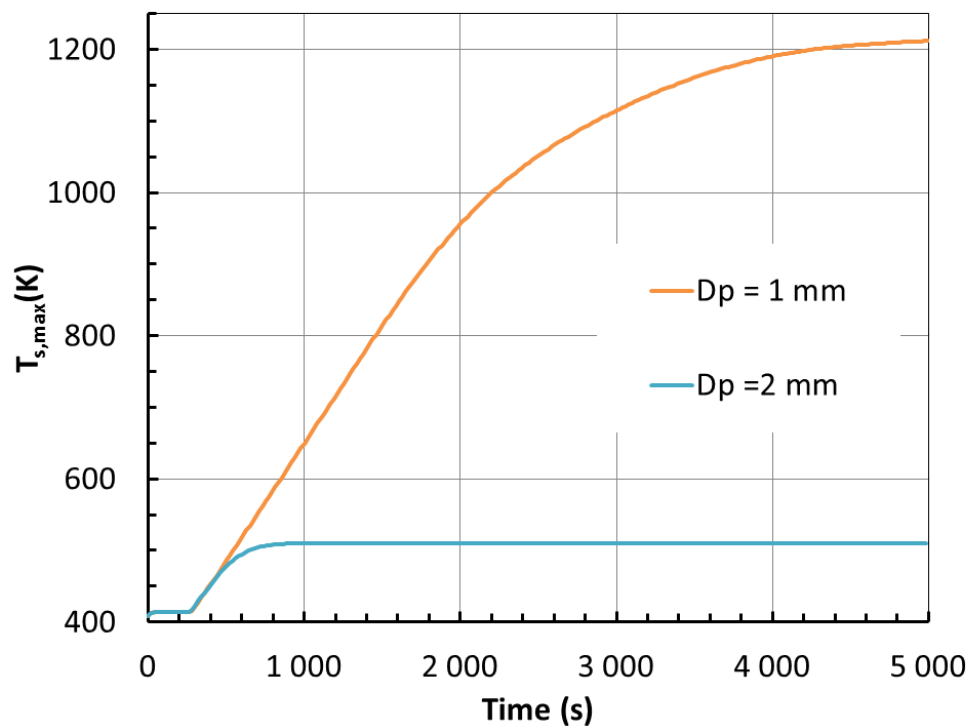
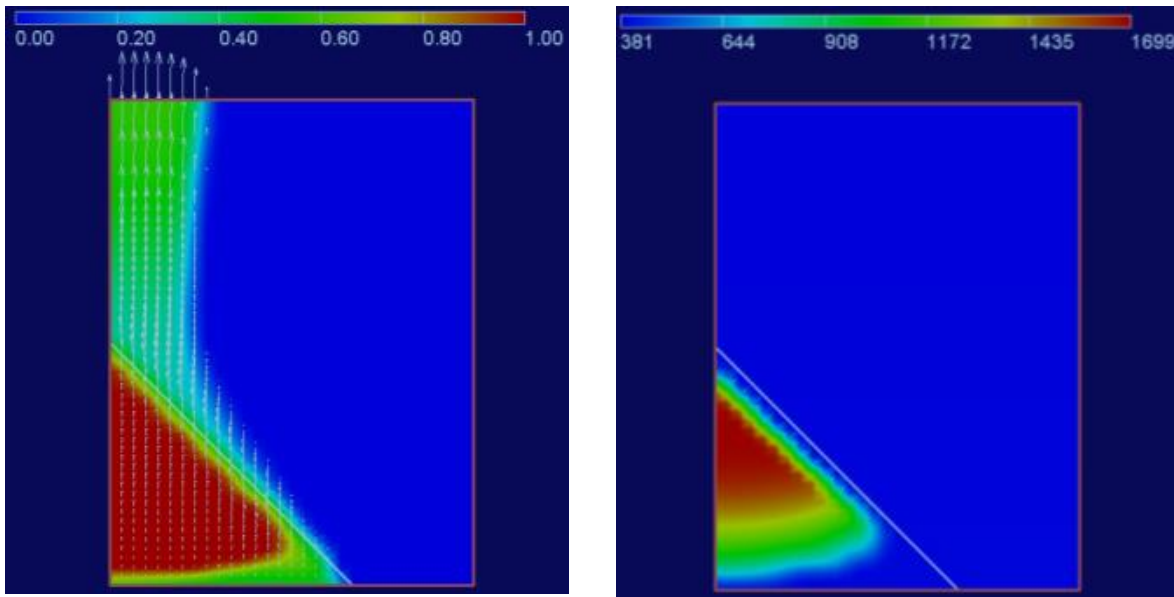


Figure 4. Maximum particle temperature as a function of the simulation time in the MEWA simulations for the reference reactor debris bed in the base case with $D_p = 1 \text{ mm}$ and in a variant case with $D_p = 2 \text{ mm}$. The default heat transfer models are used.

$D = 1 \text{ mm}$, $P_m = 200 \text{ W/kg}$, $t = 4\ 000 \text{ s}$



$D = 2 \text{ mm}$, $P_m = 200 \text{ W/kg}$, $t = 4\ 000 \text{ s}$

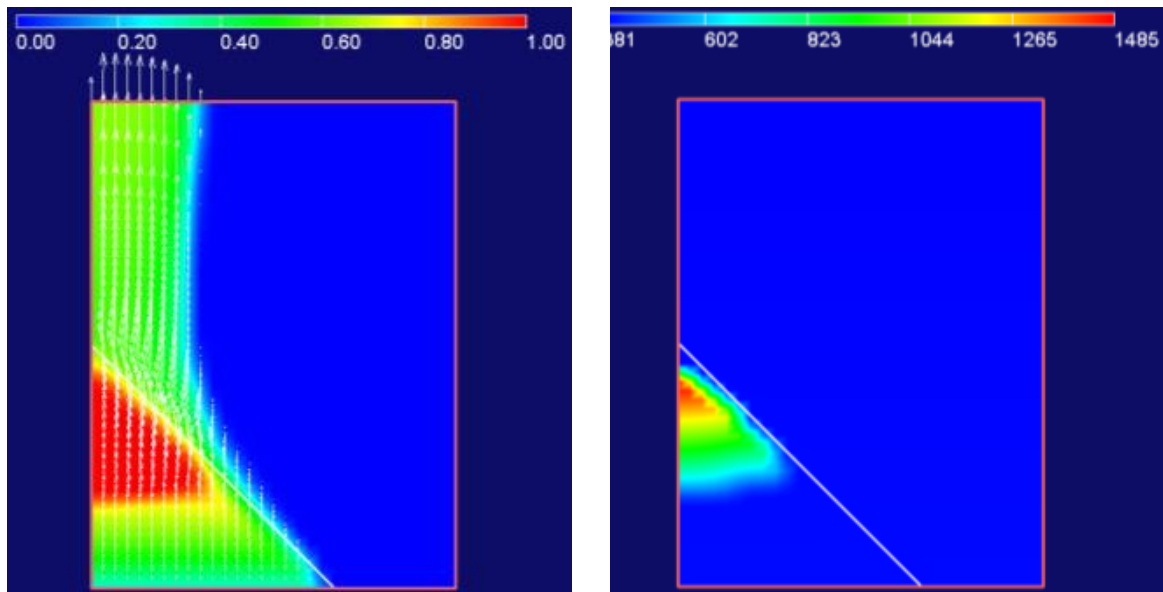


Figure 5. Void fraction (left) and solid particle temperature (right) in the DECOSIM simulations for a conical bed at the time of 4000 s for the cases of 1 and 2 mm bed particles (Yakush & Kudinov, 2014).

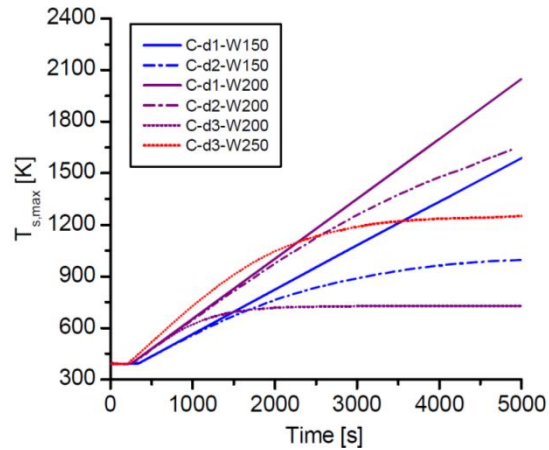


Figure 6. Maximum solid particle temperature as a function of time in the DECOSIM simulations for a conical bed (Yakush & Kudinov, 2014).

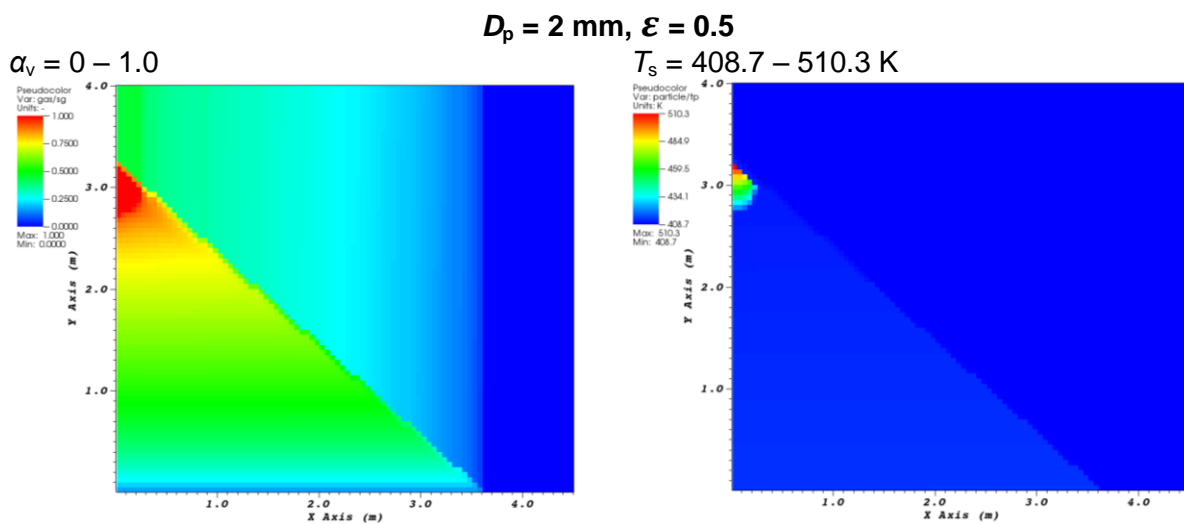


Figure 7. Void fraction (left) and solid particle temperature (right) in the MEWA simulations for the reference reactor debris bed at the time of 5000 s with $D_p = 2 \text{ mm}$. The default heat transfer models are used.

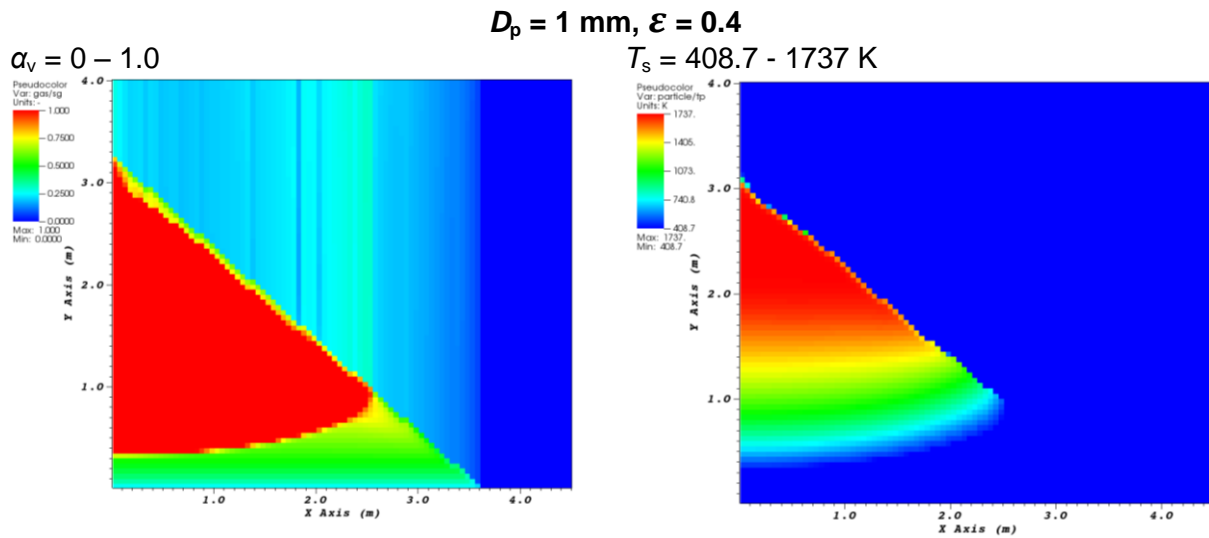


Figure 8. Void fraction (left) and solid particle temperature (right) in the MEWA simulations for the reference reactor debris bed at the time of 5000 s in a case variant of the 0.4 porosity. The default heat transfer models are used.

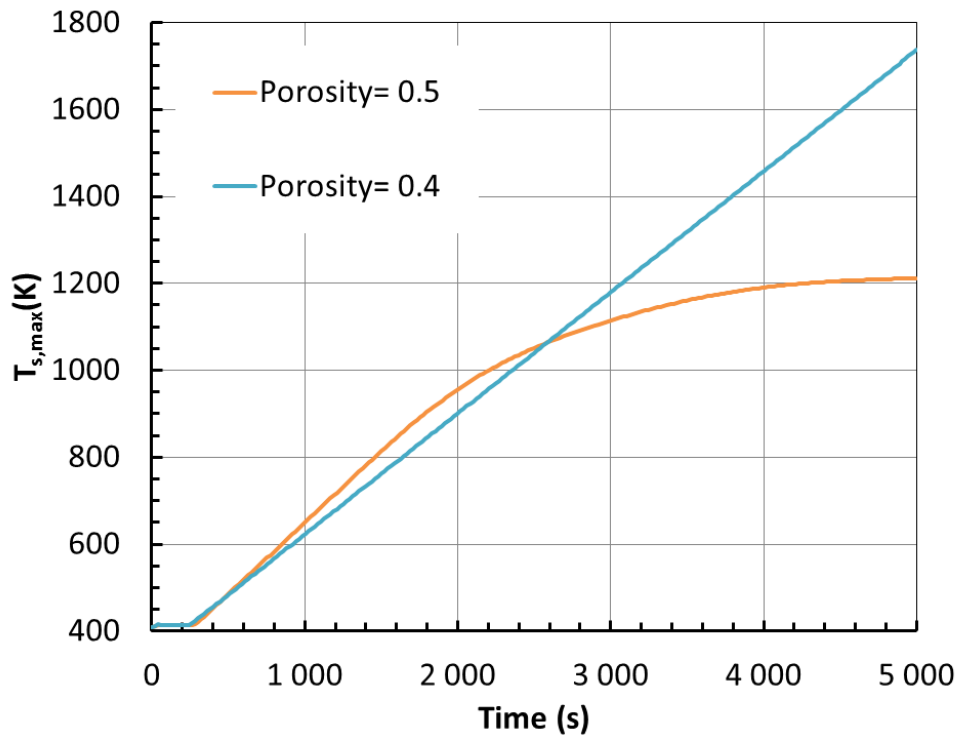


Figure 9. Influence of the bed porosity on the evolution of the maximum particle temperature as a function of the simulation time in the MEWA simulations for the reference reactor debris bed. The default heat transfer models are used.

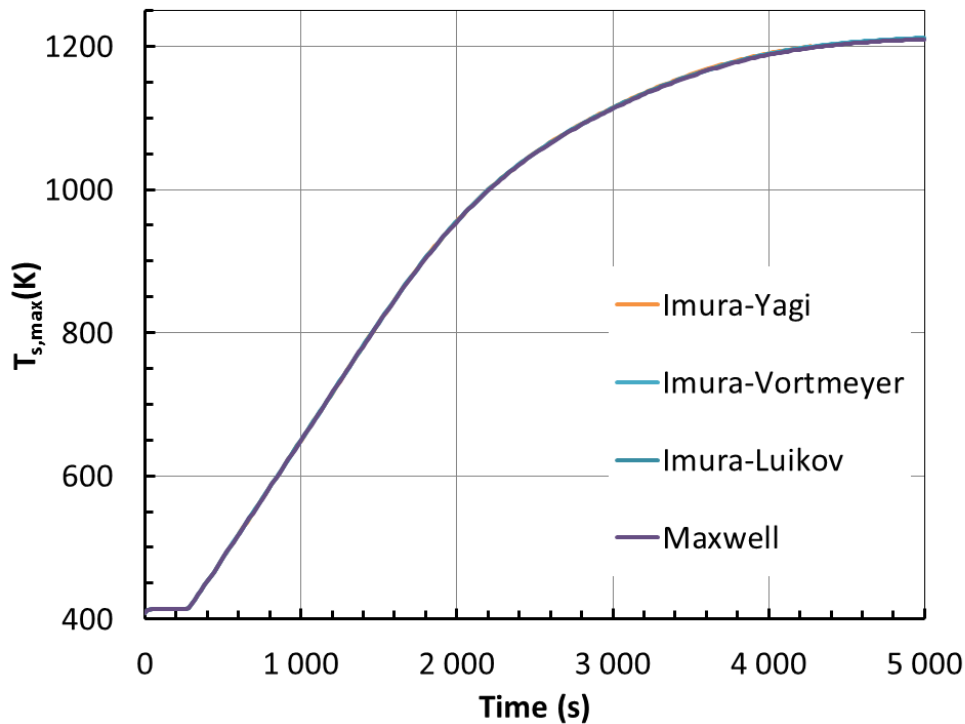


Figure 10. Influence of the model for the effective dry-bed thermal conductivity $\lambda_{s,eff}$ (Section 2.2) on the evolution of the maximum particle temperature in the MEWA simulations for the reference reactor debris bed. The default model is used for the heat transfer coefficient $\kappa_{s,g}$ for heat transfer from the solid particles to the gas phase.

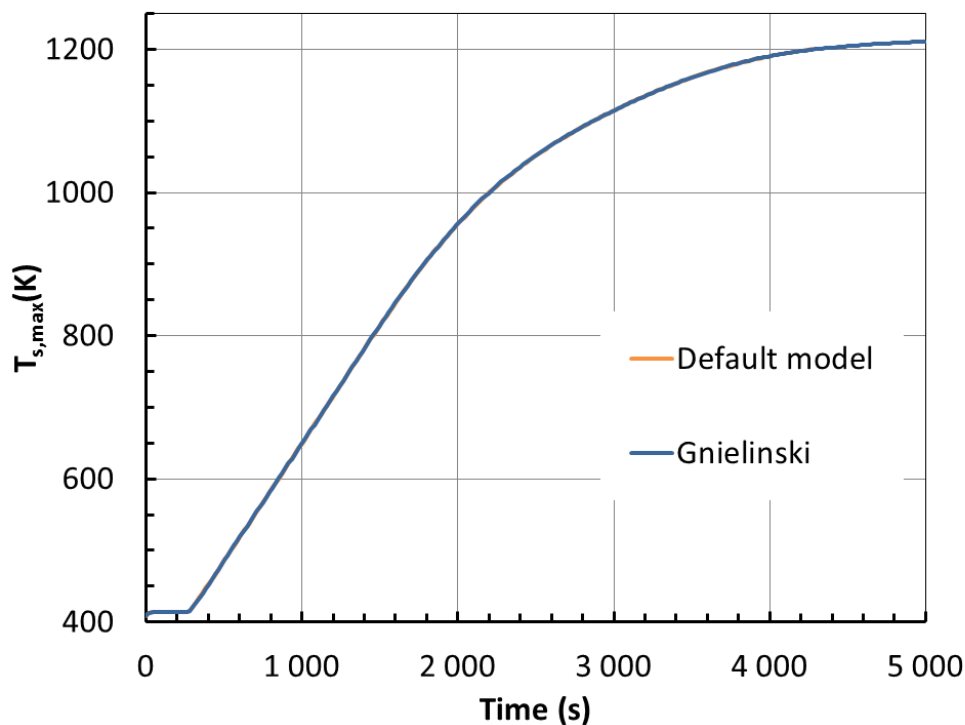


Figure 11. Influence of the model for the solid-to-gas heat transfer coefficient $\kappa_{s,g}$ (Section 2.3) on the evolution of the maximum particle temperature in the MEWA simulations for the reference reactor debris bed. The default model for the effective thermal conductivity of the solid phase is used.

4. Conical bed of Yakush & Kudinov

The MEWA results for the reference reactor debris bed cannot be quantitatively compared to the DECOSIM results of Yakush & Kudinov (2014) for a different kind of conical bed. Therefore, a code-to-code verification exercise was carried out by simulating with MEWA the same conical bed studied by Yakush & Kudinov (2014).

4.1 Case specifications

Yakush & Kudinov (2014) studied conical and truncated-cone beds. In this work, MEWA simulations are performed for their conical bed.

Table 1 summarizes the characteristics of the simulation cases. The heating power varies and different powers were used for different particle sizes. All the computed cases are given in Table 2. Yakush & Kudinov (2014) applied only specific heating powers of 150, 200 and 250 W/kg but in the MEWA simulations lower and higher heating powers were used to demonstrate the influence of the heating power also in cases in which dryout or steady-state post-dryout conditions is not reached.

The computational domain and mesh with the bed shape are shown in Figure 1. The MEWA mesh is very similar to the mesh in the DECOSIM simulations. In the radial direction, the mesh has 30 15-cm cell columns. Vertically there are 51 cell layers with a varying thickness.

Table 1. Characteristics of the conical debris beds studied at KTH (Yakush & Kudinov,2014).

Height of the debris bed (m)	3
Diameter of the debris bed (m)	6
Diameter of the water pool (m)	9
Height of the water pool (m)	6*
Pressure at the top boundary (bar)	3
Porosity of the debris bed (-)	0.4
Diameter of the bed particles (mm)	1, 2, or 3
Density of corium (kg/m ³)	8285
Specific heat capacity of corium (J/kgK)	566
Thermal conductivity of corium(W/Km)	1.9

*Measured from a figure in Yakush & Kudinov (2014).

Table 2. Cases computed with MEWA for the conical debris bed studied at KTH (Yakush & Kudinov,2014) and the maximum solid temperature computed with MEWA.

Specific power (W/kg)	Maximum particle temperature (K)		
	Particle diameter (mm)		
	1	2	3
50	415*		
100	1462	416*	
150	2700**	691	416*
200	2700**	1211	695
250		2285	996
300		2700**	1365
350			1953
400			2552

*No dryout.

**Melting temperature in the MEWA simulations.

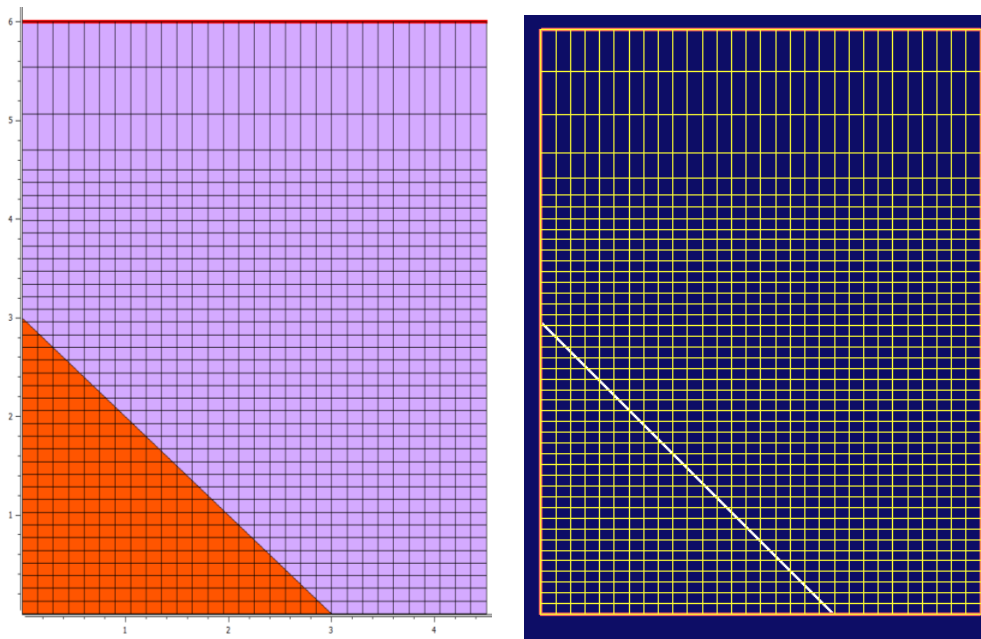


Figure 12. Computational domain, mesh and bed shape for the conical debris beds studied at KTH in the MEWA simulation (left) and in the study of Yakush & Kudinov (2014) (right).

4.2 MEWA results

The maximum particle temperature as a function of the simulation time in the MEWA simulations for the 1, 2, and 3 mm particle cases are plotted in Figure 13, Figure 14, and Figure 15, respectively. Contour plots for the void fraction and solid particle temperature are shown in Figure 16, Figure 17, and Figure 18.

Considering the cases with $D_p = 1$ mm (cf., Table 2, Figure 13, and Figure 16), dryout does not occur with the specific power of 50 W/kg. In case of the 100 W/kg specific power, a dryout zone develops slowly and stabilises to steady-state post-dryout conditions in about 20 000 s. For the specific powers of 150 and 200 W/kg, the MEWA results indicate that in both cases the corium melting temperature of 2700 K would certainly be achieved.

In the 2-mm cases (Table 2, Figure 14, and Figure 17) steady-state post-dryout conditions with dryout zones are obtained for the specific powers of 150, 200, and 250 W/kg. With larger heating power, the corium melting would eventually occur.

The coolability of the 3 mm particle bed is significantly better than in the cases for smaller particles (Table 2, Figure 15, and Figure 18). Steady-state post-dryout conditions with a dryout zones are obtained for the specific powers from 200 to 400 W/kg, although with the largest heating powers the maximum particle temperature is high enough for zirconium oxidation. In the simulations, the zirconium oxidation model was turned on.

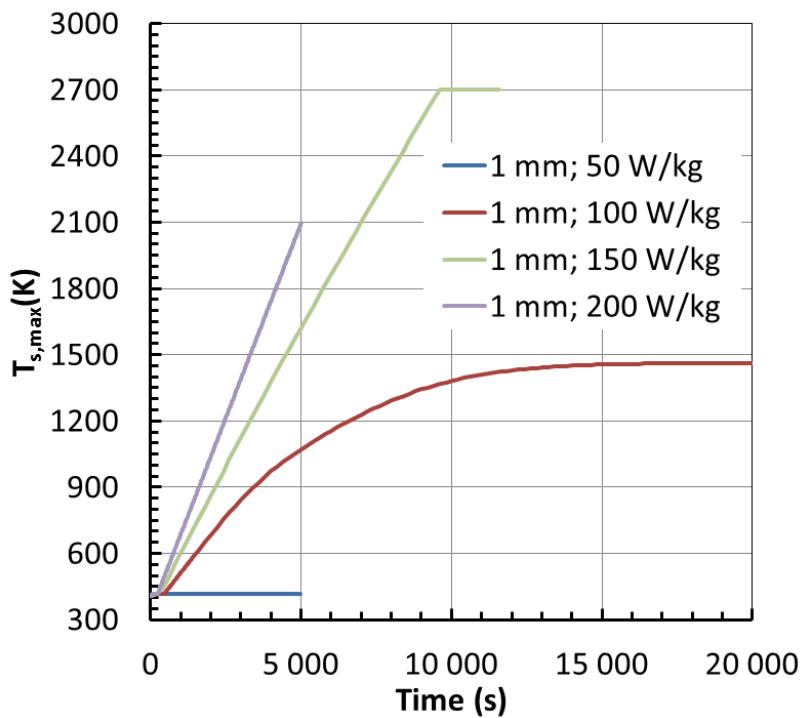


Figure 13. Influence of the specific power on the evolution of the maximum particle temperature in the MEWA simulations for 1 mm bed particles.

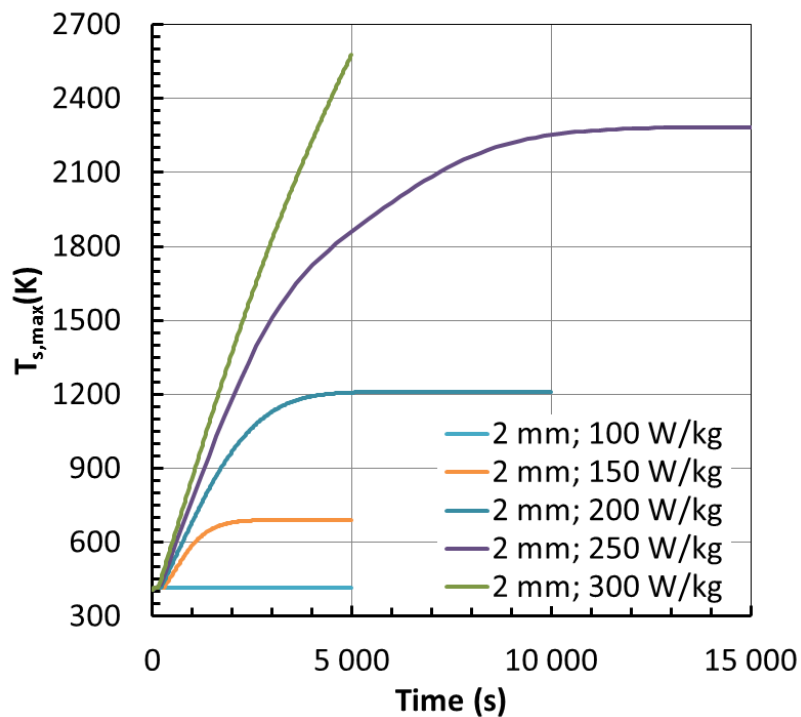


Figure 14. Influence of the specific power on the evolution of the maximum particle temperature in the MEWA simulations for 2 mm bed particles.

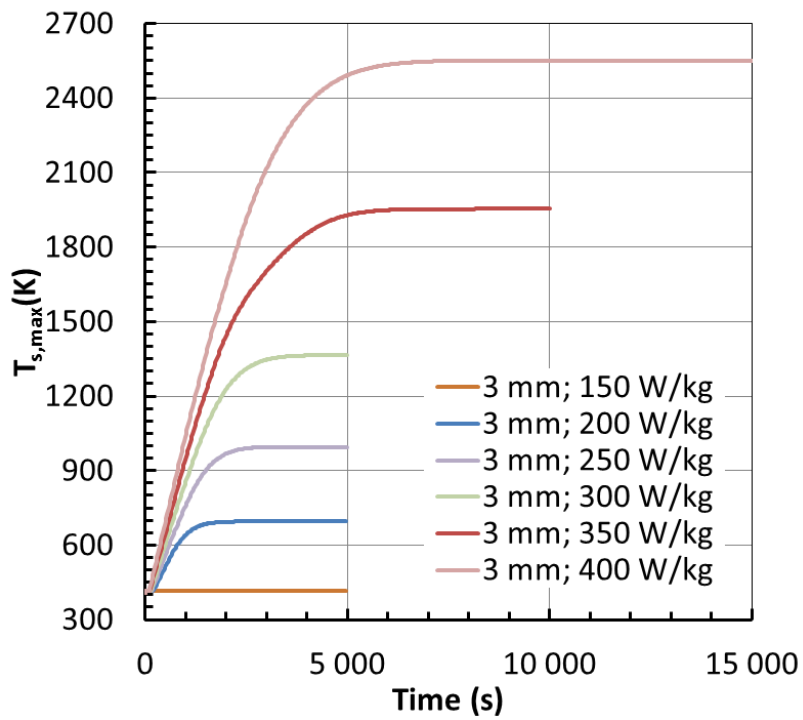


Figure 15. Influence of the specific power on the evolution of the maximum particle temperature in the MEWA simulations for 3 mm bed particles.

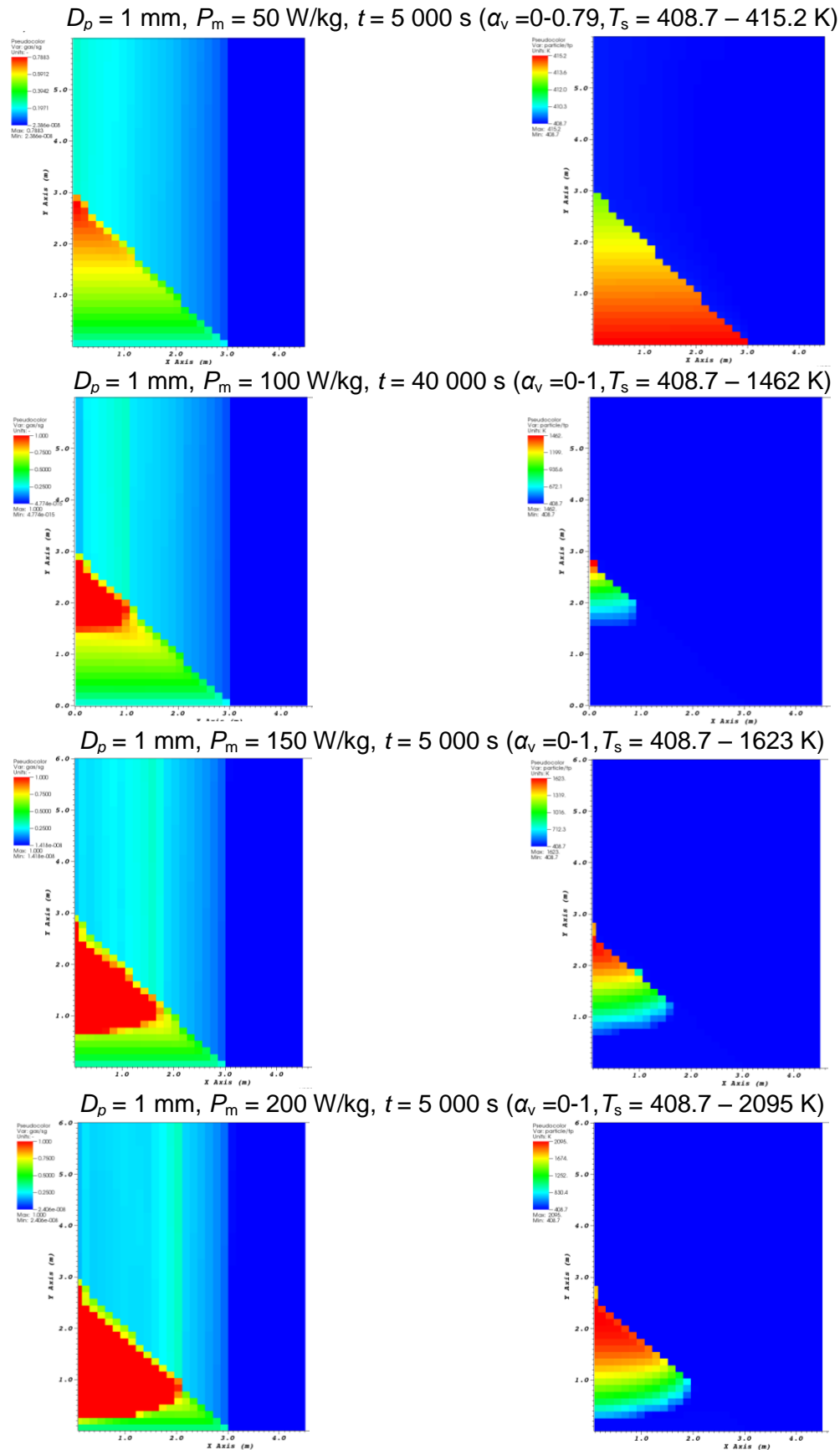


Figure 16. Void fraction (left) and solid particle temperature (right) in the MEWA simulations for 1 mm bed particles with different specific powers P_m . (Note: the contour range varies and is given in parentheses.)

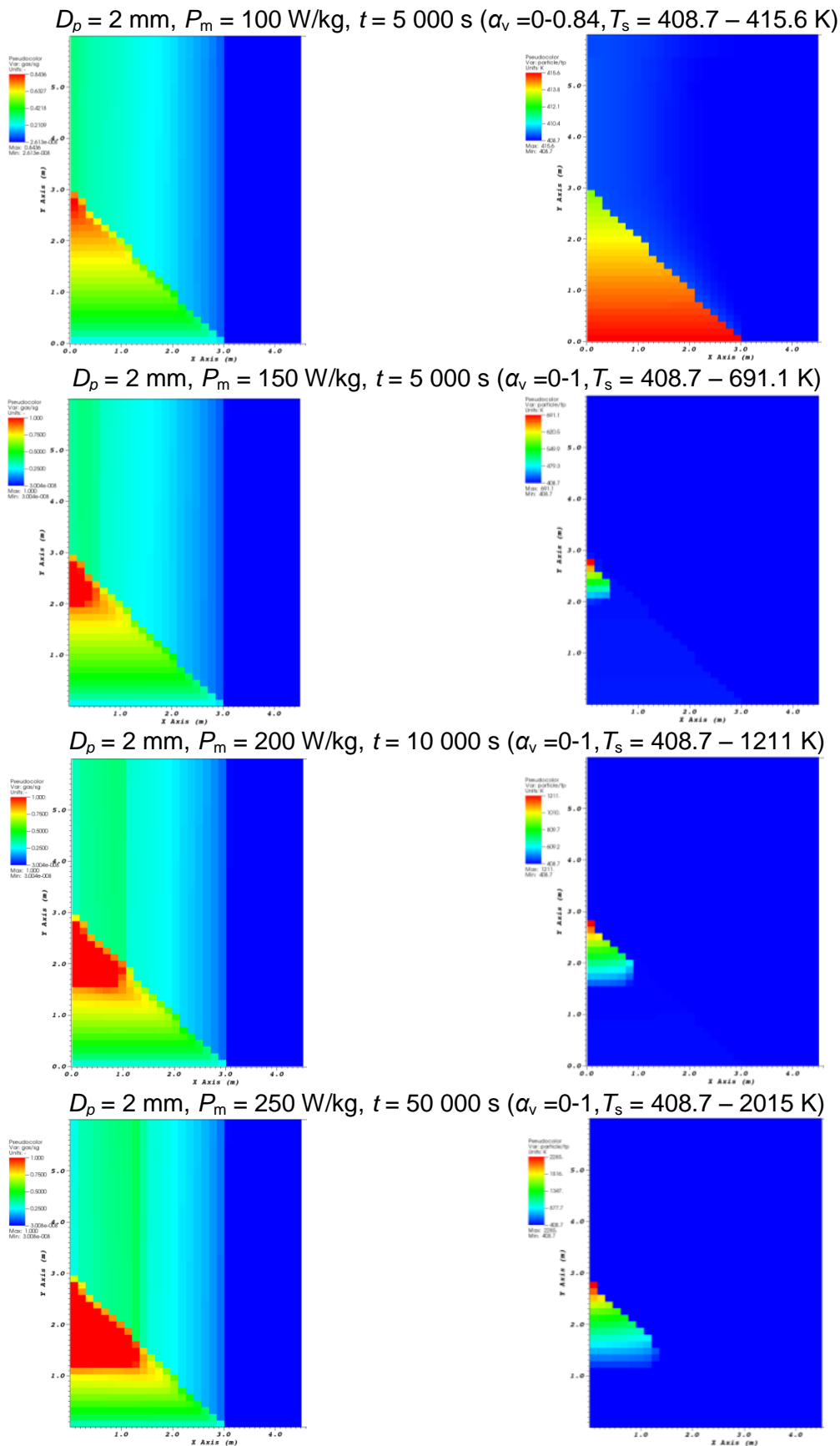


Figure 17. Void fraction (left) and solid particle temperature (right) in the MEWA simulations for 2 mm bed particles with different specific powers P_m . (Note: the contour range varies and is given in parentheses.)

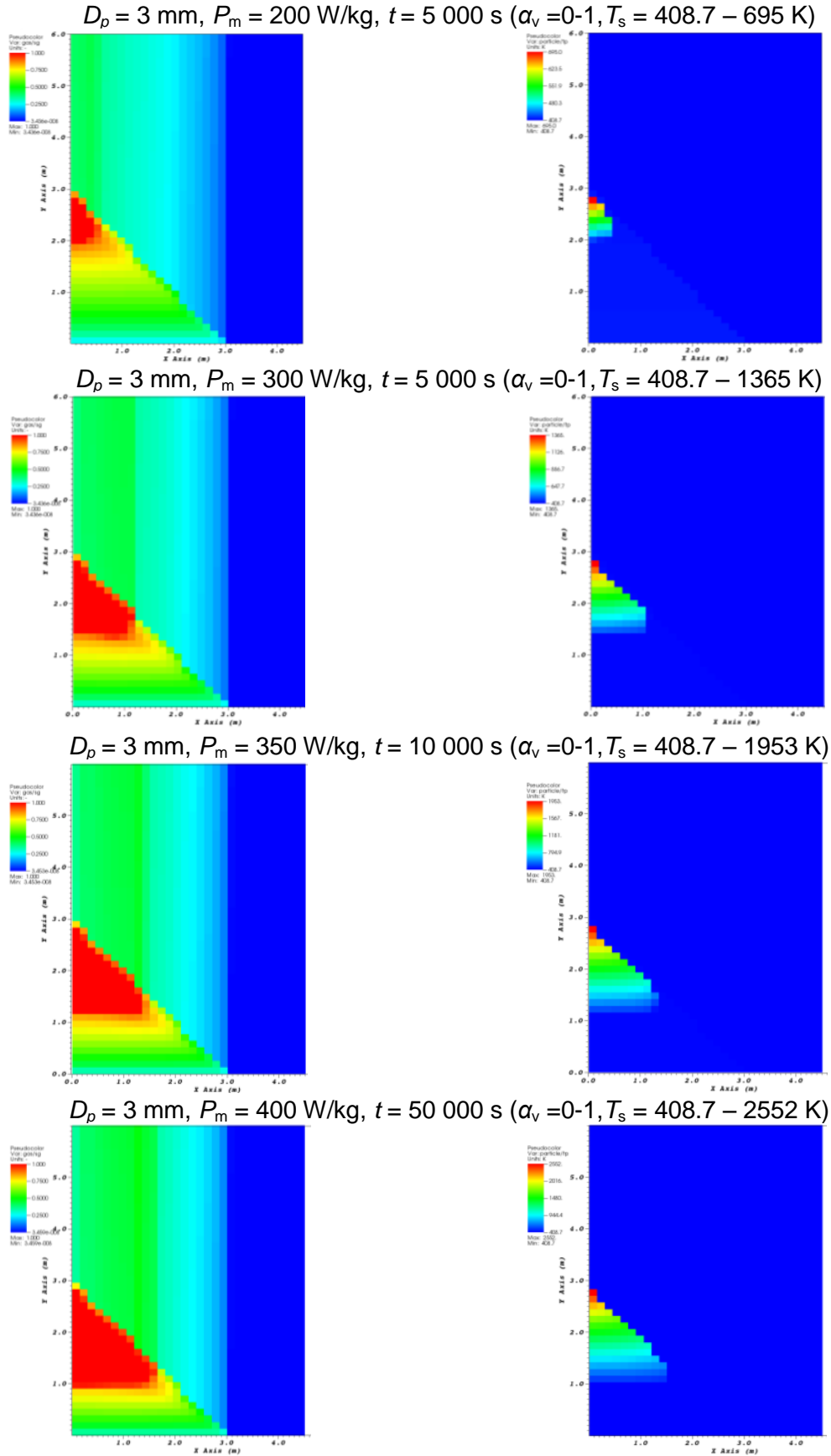


Figure 18. Void fraction (left) and solid particle temperature (right) in the MEWA simulations for 3 mm bed particles with different specific powers P_m . (Note: the contour range varies and is given in parentheses.)

4.3 Comparison of the MEWA and DECOSIM results

The MEWA and DECOSIM results for the void fraction and solid particle temperature at the time of 4000 s are compared in Figure 19 in those conical bed cases for which contour plots are given in Yakush & Kudinov (2014). The contour plots look reasonably similar. However, for the case of 2 mm particle, the maximum particle temperature in the MEWA simulation is 1192 K but DECOSIM gives 1485 K.

The maximum particle temperature predictions of both codes as a function of the simulation time are plotted in Figure 20 in the conical bed cases studied by Yakush & Kudinov (2014). The maximum particle temperatures at the time of 5000 s are compared in Table 3.

The agreement between the MEWA and DECOSIM results is satisfactory in the cases of the 1-mm particles. Simulation results agree reasonably well in the case with $D_p = 3$ mm and $P_m = 200$ W/kg. However, in the other cases, the differences are large. The evolutions of the maximum particle temperature are different. In the DECOSIM simulations, steady-state post-dryout conditions are not achieved and the maximum temperature would eventually likely stabilise to different values than in the MEWA simulations.

It was noticed, that the saturation temperature seems to be different in the MEWA and DECOSIM simulations. In the MEWA simulations, the saturation temperature is a function of the pressure and thus a function of the vertical position. For the bed area, MEWA calculates a saturation temperature of about 409 K. In the DECOSIM results, the saturation temperature is about 387 K (Yakush & Kudinov, 2014, Table 1) and thus close to a value which would be obtained, if the top boundary pressure were 1 bar. However, most likely this is not the reason for the large differences between the results of the simulations.

Table 3. Comparison of the maximum solid temperature computed with MEWA and DECOSIM at the time of 5000 s for the conical bed cases studied by Yakush & Kudinov (2014).

Particle diameter (mm)	Specific power (W/kg)	Maximum particle temperature (K)	
		MEWA	DECOSIM (Yakush & Kudinov,2014)
1	150	1622*	1587*
1	200	2095*	1699*,**
2	150	691	1008
2	200	1208*	1837*
3	200	695	729
3	250	996	1250

*No dryout. Values given for the time of 5000 s.

** Probably a typing error in the table. The correct number is about 2100 (cf., Figure 20).

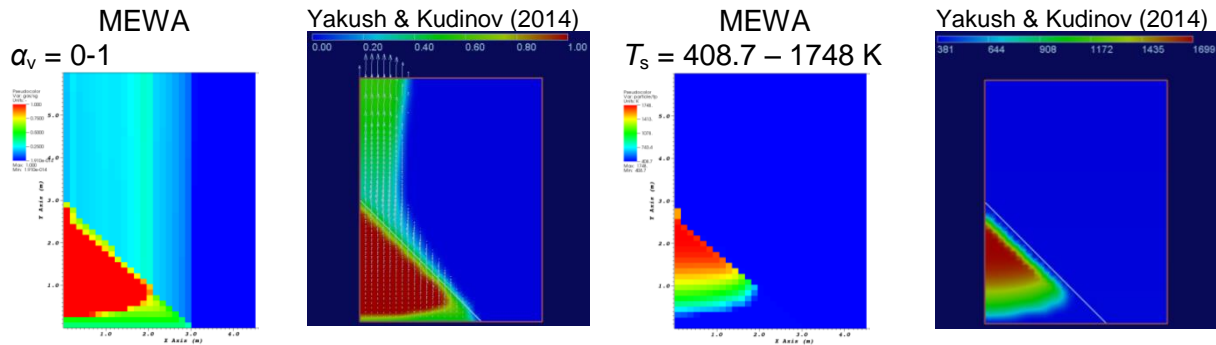
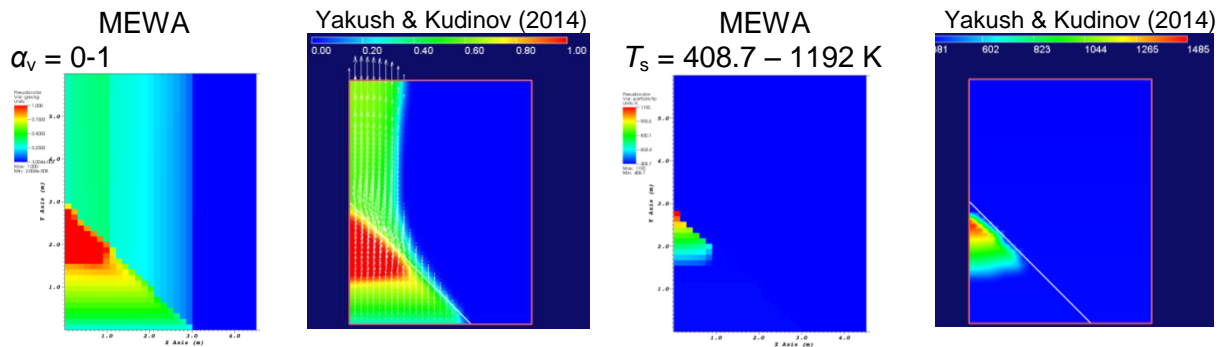
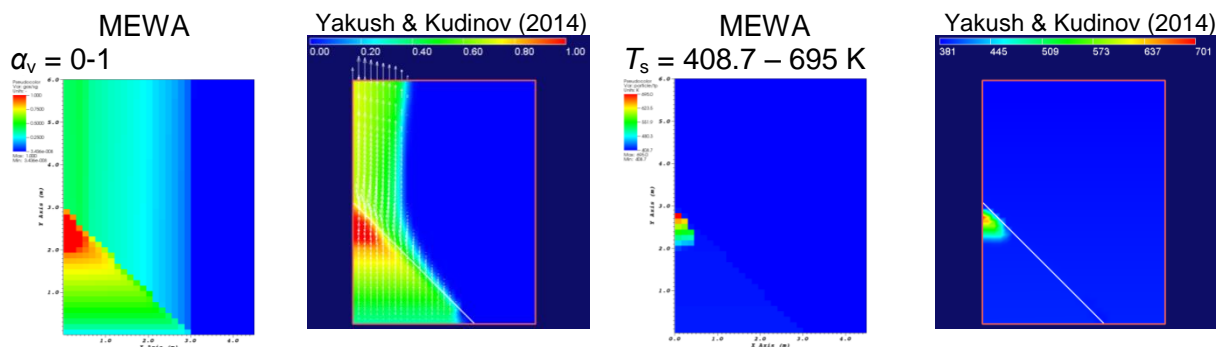
$D = 1 \text{ mm}, P_m = 200 \text{ W/kg}, t = 4000 \text{ s}$

 $D = 2 \text{ mm}, P_m = 200 \text{ W/kg}, t = 4000 \text{ s}$

 $D = 3 \text{ mm}, P_m = 200 \text{ W/kg}, t = 4000 \text{ s}$


Figure 19. Void fraction (two left columns) and solid particle temperature (two right columns) in the MEWA simulations and in the DECOSIM simulations according to Yakush & Kudinov (2014) at the time of 4000 s.

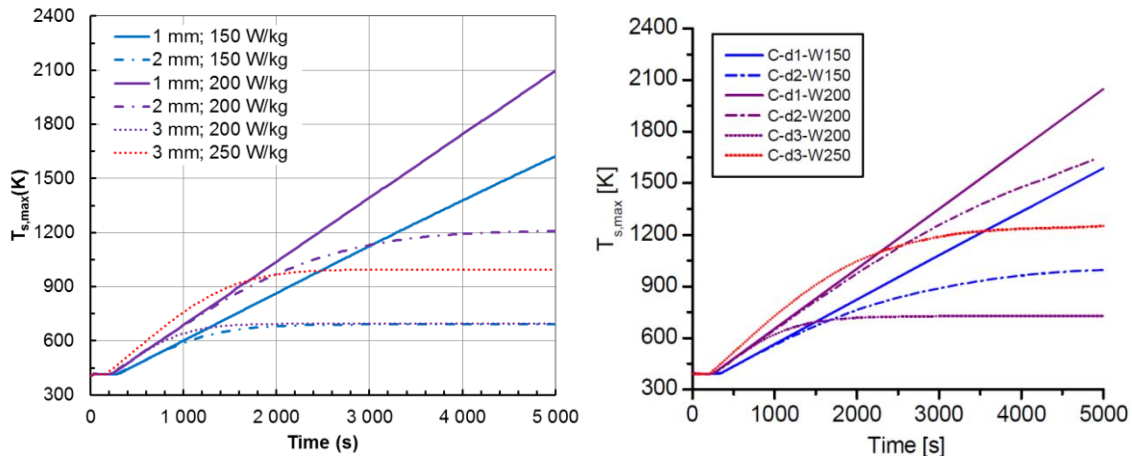


Figure 20. Maximum solid particle temperature as a function of time in the MEWA simulations (left) and in the DECOSIM simulations according to Yakush & Kudinov (2014) (right) for the same conical bed.

4.4 Effects of heat transfer models

Since the differences between the MEWA and DECOSIM results are so large in some case and DECOSIM uses different models, the influence of model selections in the MEWA simulations was studied. The case of the 2 mm particles and 150 W/kg specific power was computed by applying alternative models for the solid-to-gas heat transfer coefficient $\kappa_{s,g}$ and for the effective dry-bed thermal conductivity $\lambda_{s,eff}$. In this case, MEWA predicts a significantly lower maximum particle temperature than in the model selection study for the reference reactor debris bed in Section 3.3.3 so the results of this sensitivity study might be different.

The maximum particle temperature as a function of the simulation time is plotted in Figure 21 and Figure 22 for different model selections. The differences remained small also for the conical bed of Yakush & Kudinov (2014) with a lower maximum particle temperature and are always within 3 K.

4.5 Discussion

In the MEWA simulations for the conical debris bed studied at KTH (Yakush & Kudinov, 2014), for each particle size, 1, 2, and 3 mm, several specific heating powers were used to cover conditions from no-dryout to (or close to) the corium remelting temperature. The MEWA results behave logically and smoothly as a function of the particle size and heating power. Alternative models for solid-to-gas heat transfer coefficient $\kappa_{s,g}$ and for the effective dry-bed thermal conductivity do not change the results meaningfully.

According to the MEWA results the temperature-based dryout criterion increases the coolability limit compared to the void-based criterion (i.e., the dryout heat flux). MEWA predicts that for all studied particle sizes, coolable steady-state conditions are obtained with heat fluxes higher than the dryout heat flux. For 1 mm bed particles, the temperature-based dryout criterion would roughly double the coolability limit relative to the coolability limit determined by the dryout heat flux.

However, the comparison of the MEWA and DECOSIM results brought out significant differences in the predictions of the post-dryout conditions. The differences are even largest in those conditions which would be used to determine the temperature-based coolability limit. The origin of the differences is not known and further investigations are needed before trying to determine the temperature-based coolability limit.

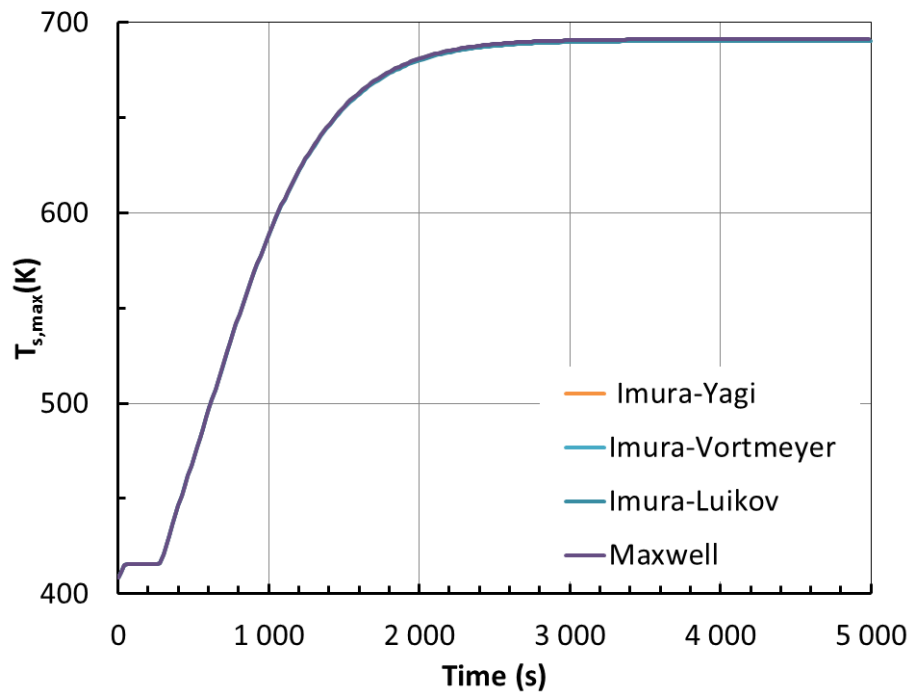


Figure 21. Influence of the model for the effective dry-bed thermal conductivity $\lambda_{s,eff}$ (Section 2.2) on the evolution of the maximum particle temperature in the MEWA simulations for the conical debris bed studied at KTH (Yakush & Kudinov, 2014) in the case of 2 mm particles and 150 W/kg specific power.

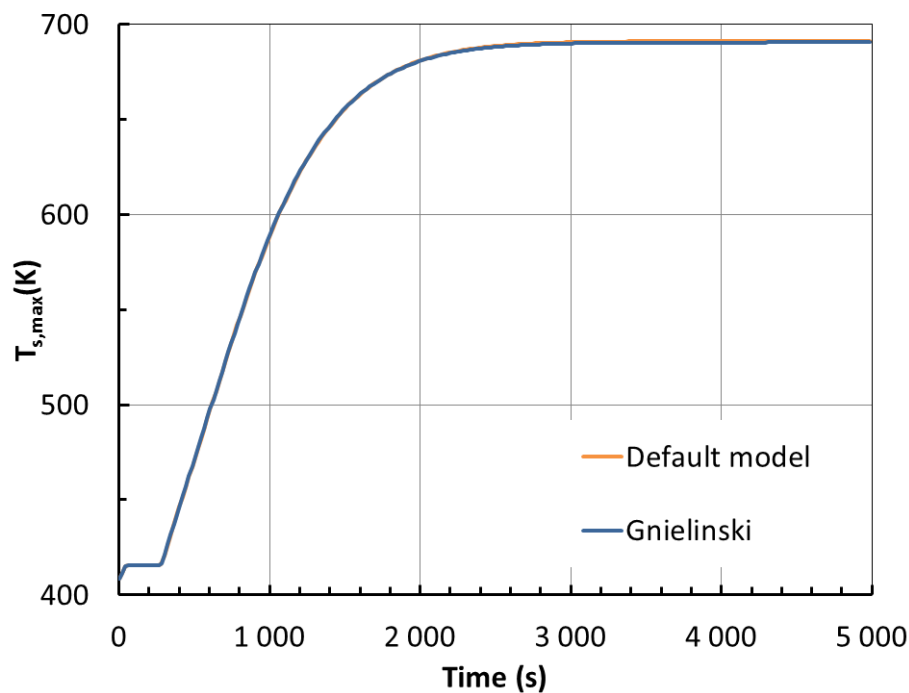


Figure 22. Influence of the model for the solid-to-gas heat transfer coefficient $\kappa_{s,g}$ (Section 2.3) on the evolution of the maximum particle temperature in the MEWA simulations for the conical debris bed studied at KTH (Yakush & Kudinov, 2014) in the case of 2 mm particles and 150 W/kg specific power.

5. Post-dryout steady-state conditions

By assuming vertical vapor flow and assuming that the vapor produced in a wet part flows to the dry part above at the saturation temperature as well as ignoring the heat transfer mechanisms between the particles, Yakush & Kudinov (2014) developed the following simple analytical correlation for the maximum bed particle temperature as a function of the height of the dry zone:

$$T_{s,max} = T_{sat} + \frac{h\xi}{c_{p,g}(1 - \xi)} \quad (11)$$

where h is the heat of evaporation (J/kg), $c_{p,g}$ the specific heat capacity of the vapor phase (J/kgK) and ξ the relative height of the dry zone

$$\xi = \frac{z_t - z_b}{z_t} \quad (12)$$

Here z_t and z_b are the top and bottom coordinates of the dry zone, respectively.

The MEWA results for the reference reactor debris bed as well as for the conical debris bed studied at KTH are plotted in Figure 23 with the analytical correlation of Yakush & Kudinov (2014). The agreement is satisfactory especially for the low heating powers (i.e., for low dry zones and thus for low maximum particle temperatures). The coarseness of the meshes results in uncertainties in the relative height of the dry zone. On the other hand, the zirconium oxidation model was turned on in the MEWA simulations and that might further increase high temperatures well above the analytical prediction. This is expectable as the analytical model ignores zirconium oxidation.

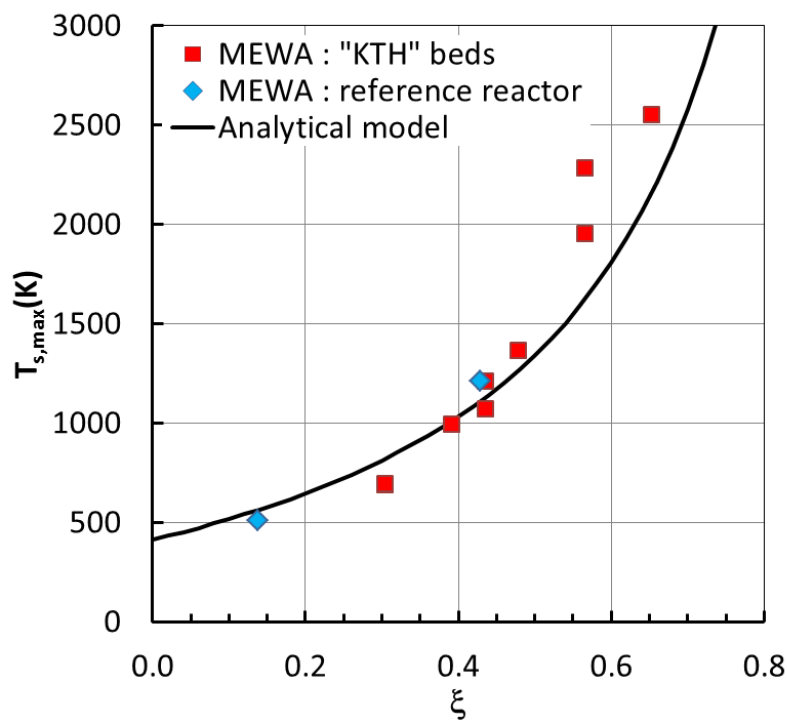


Figure 23. Maximum particle temperature as a function of the relative height of the dry zone (Eq., 12) for MEWA simulations and the analytical model of Yakush & Kudinov (2014) (Eq. 11).

6. Conclusions

Behaviour of two hypothetical conical debris beds was studied by performing MEWA (Bürger et al., 2006) simulations. Coolability and especially conditions after dryout were analysed for the reference reactor debris bed and for the conical debris bed studied at KTH by Yakush & Kudinov (2014).

The MEWA results show that the temperature-based dryout criterion increases the coolability limit compared to the void-based criterion (the dryout heat flux). In the dryout conditions, after the bed temperature stabilization, i.e., after achieving a steady-state, the bed temperature might locally be considerably higher than the saturation temperature. For 1 mm bed particles, the temperature-based dryout criterion would roughly double the coolability limit relative to the dryout-heat-flux-based limit. The increase in the coolability limit would be larger for larger particles, but a small particle bed is considered more representative for realistic beds of random irregular particles (Chikhi et al., 2014).

However, the simulation results of the MEWA code are not in fully agreement with the DECOSIM results reported by Yakush & Kudinov (2014). For small particle cases without temperature stabilization, the codes agree satisfactorily. On the other hand, these cases are not interesting because the maximum particle temperature eventually exceeds the temperatures where zirconium oxidation or even corium remelting begins. In the other conical bed cases studied by Yakush & Kudinov (2014), according to the both codes the beds are coolable but MEWA and DECOSIM predict different transient behaviours and final steady-state conditions. Therefore, before trying to quantify the temperature-based dryout criterion, the origin of the significant differences between the MEWA and DECOSIM results need to be identified. Some differences in the simulation setups and models are known or probable but most likely they do not cause those large differences in simulation results for post-dryout conditions.

References

- Atkhen, K. & Berthoud, G., 2006. SILFIDE experiment: Coolability in a volumetrically heated debris bed. *Nuclear Engineering and Design*, 236, pp.2126–2134.
- Bürger, M. et al., 2006. Validation and application of the WABE code: Investigations of constitutive laws and 2D effects on debris coolability. *Nuclear Engineering and Design*, 236, pp.2164–2188.
- Chikhi, N. et al., 2014. Evaluation of an effective diameter to study quenching and dry-out of complex debris bed. *Annals of Nuclear Energy*, 74, pp.24–41.
- Imura, S. & Takegoshi, E., 1974. Effect of Gas Pressure on the Effective Thermal Conductivity of Pack Beds. *Heat Transfer Japanese Research*, 3(4).
- Luikov, a. V. et al., 1968. Thermal conductivity of porous systems. *International Journal of Heat and Mass Transfer*, 11(2), pp.117–140.
- Maxwell, J.C., 1873. *A treatise on electricity and magnetism | Vol. 1*,
- Rahman, S., 2013. *Coolability of Corium Debris under Severe Accident Conditions in Light Water Reactors*. Insitut für Kernenergetik und Energiesysteme, University of Stuttgart.
- Song, J.H. et al., 2006. The effect of corium composition and interaction vessel geometry on the prototypic steam explosion. *Annals of Nuclear Energy*, 33(17-18), pp.1437–1451.
- Stephan, P., Martin, H., Kabelac, S., Mewes, D., Kind, M., & Schaber, K. ed., 2010. VDI Heat Atlas.
- Takasuo, E., 2016. An Experimental Study of the Coolability of Debris Beds with Geometry Variations. *Annals of Nuclear Energy*, 92, pp.251–261. Available at: <http://www.sciencedirect.com/science/article/pii/S0306454916300408>.
- Takasuo, E., 2015. *Coolability of porous core debris beds: Effects of bed geometry and multi-dimensional flooding*. VTT Technical Research Centre of Finland Ltd. D.Sc. thesis. <http://www.vtt.fi/inf/pdf/science/2015/S108.pdf>. Available at: <http://www.vtt.fi/inf/pdf/science/2015/S108.pdf>.
- Vortmeyer, D., 1978. Radiation in Packed Solids. In *6th International Heat Transfer Conference, Toronto, Canada*.
- Yagi, S. & Kunii, D., 1957. Studies on effective thermal conductivities in packed beds. *AIChE Journal*, 3(3), pp.373–381. Available at: <http://onlinelibrary.wiley.com/doi/10.1002/aic.690030317/full>.
- Yakush, S. & Kudinov, P., 2014. A model for prediction of maximum post-dryout temperature in decay-heated debris bed. In *22nd International Conference on Nuclear Engineering. July 7-11, 2014, Prague, Czech Republic*.

ANNEX 2
Hydrogen fire risk in BWR simulations with MELCOR



RESEARCH REPORT

VTT-R-00669-17

Hydrogen fire risk in BWR simulations with MELCOR

Authors: Magnus Strandberg

Confidentiality: Public

Report's title Hydrogen fire risk in BWR simulations with MELCOR	
Customer, contact person, address SAFIR2018 Research Program	Order reference SAFIR 6/2016
Project name Comprehensive Analysis of Severe Accidents	Project number/Short name 108735/CASA
Author(s) Magnus Strandberg	Pages 21
Keywords Hydrogen, MELCOR, Severe accidents	Report identification code VTT-R-00669-17
<p>Summary</p> <p>In order to better study the hydrogen fire effects and risk the Olkiluoto MELCOR model needed to be updated to run on the new 2.1 MELCOR version. This new version of MELCOR included among other things, significant changes to the input model syntax. For this reason the specialised tool, SNAP, was used to convert the old model to the new version.</p> <p>This report includes a brief comparison of the old and new model simulated as a station blackout scenario. The largest differences seem to be from changes in the COR-package which is visible in for example differences in time of RPV breach.</p> <p>The later parts of the report focuses on hydrogen fire scenarios. Both analysing the risk of hydrogen burns in the reactor building volumes of the model, and then with a modified model studies the effect of a non-inerted containment.</p> <p>Results show that there are very small amounts of hydrogen that leak into the reactor building, average volume concentrations stay well below the theoretical limit for hydrogen gas combustion.</p> <p>The results from the modified model with non-inerted containment show higher temperatures in containment atmosphere but the lower pressure, compared to the unmodified model. Also, the time of RPV failure is very similar in both cases.</p>	
Confidentiality	Public
Espoo, 06.02.2017	
Written by  Magnus Strandberg, Research Scientist	Reviewed by  Tuomo Sevon, Senior Scientist
Accepted by  Anitta Hämäläinen, Research Team Leader	
VTT's contact address P.O. Box 1000, FI-02044 VTT, Finland	
Distribution (customer and VTT) SAFIR2018 Reference Group 2 VTT	
<i>The use of the name of VTT Technical Research Centre of Finland Ltd in advertising or publishing of a part of this report is only permissible with written authorisation from VTT Technical Research Centre of Finland Ltd.</i>	

Contents

1. Introduction	3
2. Changes in MELCOR Version 2.1	3
3. Update process	3
4. Comparison of the results between the different versions	4
5. Analysis of the effects and risks of hydrogen burns	15
5.1 Hydrogen concentrations in the reactor building	15
5.2 Non-inerted containment analysis	16
6. User experience with MELCOR 2.1	19
7. Conclusions	19
References	21

1. Introduction

The main focus of this task was to study the risk and effects of hydrogen burns in the containment and reactor building. To accomplish this the MELCOR [1] model of the Olkiluoto 1&2 BWR plant needed to be updated from the old version 1.8.6 to new version 2.1. The updated model would also be able to take advantage of the new features available and updates introduced to the new version of MELCOR.

MELCOR is a computer code used in analysis of severe accidents in nuclear power plants. It is developed by Sandia National Laboratories in Albuquerque, New Mexico. MELCOR handles a wide variety of phenomena related to severe accidents, it is modularly built with different packages that handle the different phenomena.

In the following chapter (2) of the report the changes incorporated into MELCOR version 2.1 are described, followed in chapter 3 with a description of the update process. In chapter 4 is presented a comparison of the results from the 2.1 version of the model with the results from the old 1.8.6 model. The hydrogen fire scenarios are presented in chapter 5. Chapter 6 describes the user experiences of using the new model.

2. Changes in MELCOR Version 2.1

Version 2.1.6840 of MELCOR was released in August 2015. The largest change is in the input model syntax, which in principle does not add any major changes to the way the calculations are performed but requires a major restructure of the input model.

There are however some smaller updates done to the different packages of MELCOR, and some changes to how some default parameters are defined. There is no complete list of changes between the version, but the manual provides insight into the different changes. The reader is referred to the MELCOR manuals [1] for details, but it is clear that at least the updates to the COR-package¹ affect the simulation results.

3. Update process

The original input model for Olkiluoto 1 and 2 was written by Ilona Lindholm at VTT for MELCOR 1.8.2 in 1994. In 1997 it was updated to to MELCOR 1.8.3 by Heikki Sjövall from TVO. It was later updated to version 1.8.5 by Ilona Lindholm in 2002. In 2006 Tuomo Sevón updated the model to version 1.8.6 which is the model that was used as in this update process[2]. During the update process the parameter values used were only taken from the previous models. That is there were no systematic check of the new input model or comparison to plant data made. If the model is to be used in licensing work, a comparison to plant data would be required and modifications done accordingly.

The updating process was simplified with the SNAP tool [3], as this enabled automatic conversion of the bulk of the input from the old version to the new. However, some manual post-processing was required to check some parameters that were flagged with warnings.

The changes in how some of the default values have been defined did not cause any extra problems for the conversion program, and the values were the same in both the 1.8.6 and 2.1 version of the code.

¹The COR-package of MELCOR handles the core degradation calculations.

Time (h:mm:ss)	Time (s)	Event
00:00	0	Reactor scram
23:30	1410	Core water level below top of active fuel
30:00	1800	Pedestal flooding from wetwell
30:30	1830	Reactor depressurization
42:10	2530	Core water level below bottom of active fuel
46:50	2810	Zr oxidation begins (1100 K)
48:20	2900	Gap release in rod group 1
48:21	2901	Gap release in rod group 2 and 3
48:26	2906	Gap release in rod group 4
50:02	3002	Gap release in rod group 5
1:05:10	3910	Control rod melting starts
1:18:29	4709	Core support plate yields in ring 2
1:23:30	5010	Collapse of fuel rods begins
1:32:37	5557	Core support plate yields in ring 1
4:41:40	16900	All water in the RPV has boiled away
4:55:37	17737	Core support plate yields in ring 3
5:03:50	18230	Core support plate yields in ring 4
5:07:40	18460	Core support plate yields in ring 5
5:20:37	19237	Core support structure fails in ring 3, fuel rods collapse
5:22:16	19336	Core support structure fails in ring 4, fuel rods collapse
5:22:51	19371	Core support structure fails in ring 5, fuel rods collapse
5:23:22	19403	Core support structure fails in ring 2, fuel rods collapse
5:33:45	20025	Core support structure fails in ring 1, fuel rods collapse
6:18:46	22726	RPV lower head fails in ring 6, Thru-wall yielding
7:32:40	27160	RPV lower head fails in ring 3, Thru-wall yielding
10:00:00	36000	Simulation stops

Table 1. Progression of the 2.1 version model calculations.

An unfortunate side effect of using the SNAP tool is that the exported model is not as readable as in the the previous version. So future updates might be best handled inside the SNAP model editor.

4. Comparison of the results between the different versions

The newer version was compared to the older simulations to make sure that the conversion was successful. From the results presented in this chapter it is clear that the changes to the MELCOR code have some impact on the calculated results, where the biggest differences seem to originate from the COR package. The calculated scenario was a station blackout, with reactor scram at 0 s.

Table 1 contains the major events as they occur in the simulations with 2.1 model, and table 2 the events in version 1.8.6. From here some differences are already noticeable such as the core degradation and Reactor Pressure Vessel (RPV) failure. The core degradation from the 2.1 simulations are visualized in Fig. 1, for four different times.

In Fig. 2 the pressure in the RPV is shown up until the moment of depressurization. From the figure it is clear that both versions of the code produce very similar results. In Fig. 3 the pressure

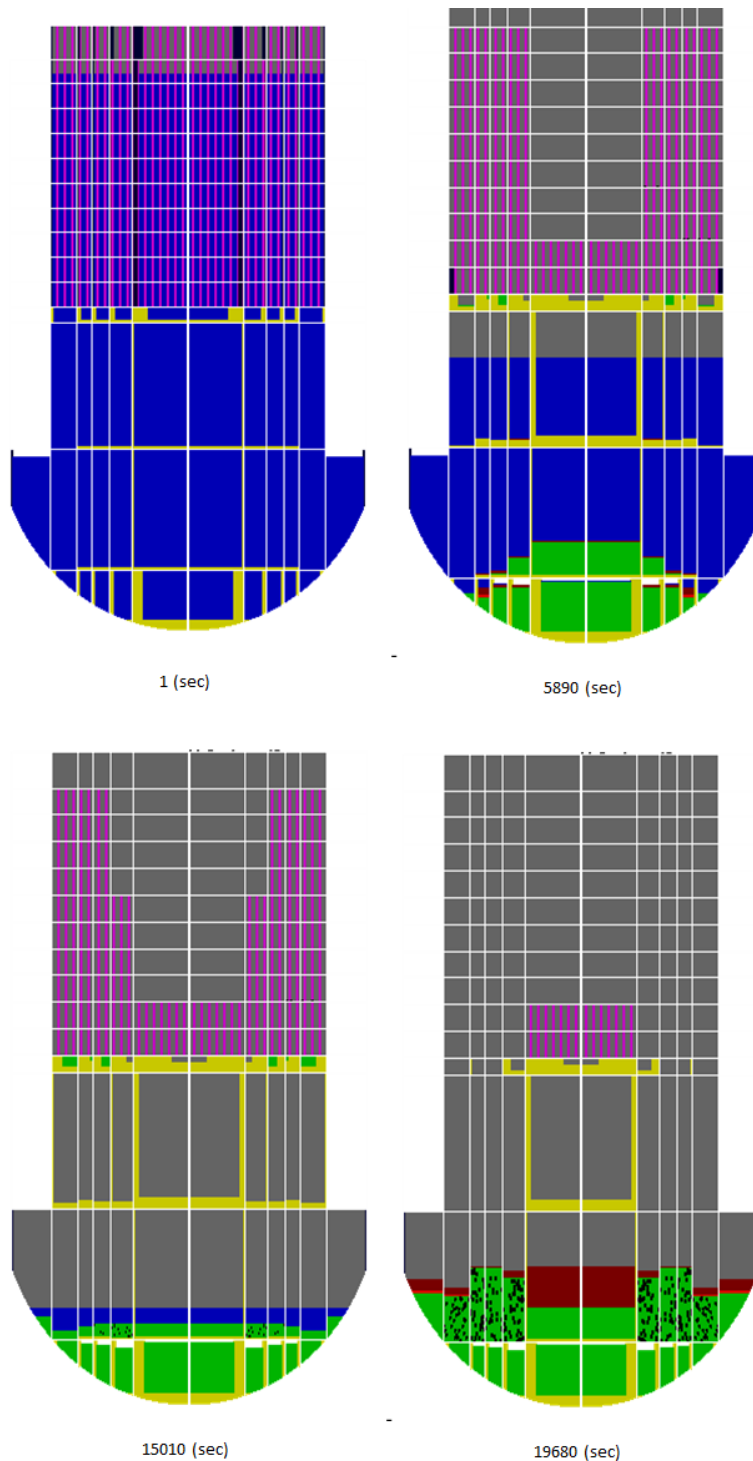


Figure 1. Four snapshots of the core degradation at different times. Pink represents the fuel rods, black the control rods, yellow core support plates and control rods guide tubes. Grey represents void and blue is liquid water. Green color represents particle debris. Red and brown represents molten oxides and metal, respectively. The placement of the yellow color is not correctly rendered in the mesh, and the small green spots suspended in mid air are small amounts due to rounding errors.

Time (h:mm:ss)	Time (s)	Event
00:00	0	Reactor scram
23:30	1410	Core water level below top of active fuel
30:00	1800	Pedestal flooding from wetwell
30:30	1830	Reactor depressurization
41:50	2510	Core water level below bottom of active fuel
46:50	2810	Zr oxidation begins (1100 K)
48:29	2909	Gap release in rod group 1 and 2
48:30	2910	Gap release in rod group 3 and 4
50:10	3010	Gap release in rod group 5
1:04:10	3850	Control rod melting starts
1:23:30	5010	Collapse of fuel rods begins
1:25:49	5149	Core support plate yields in ring 2
1:29:43	5383	Core support plate yields in ring 3
3:31:30	12690	All water in the RPV has boiled away
3:53:32	14012	Core support plate yields in ring 5
4:11:49	15109	Core support structure fails in ring 5, fuel rods collapse
4:12:57	15177	Core support structure fails in ring 2, fuel rods collapse
4:14:58	15298	Core support structure fails in ring 4, fuel rods collapse
4:17:41	15461	Core support structure fails in ring 3, fuel rods collapse
4:34:00	16440	Core support structure fails in ring 1, fuel rods collapse
5:28:56	19736	RPV lower head fails in ring 1, Thru-wall yielding
10:00:00	36000	Simulation stops

Table 2. Progression of the 1.8.6 version model calculations.

for the RPV is shown for the period after the depressurization, here the differences between the versions are noticeable. The peaks at around 5000 seconds are larger in 1.8.6 than in 2.1, whereas in 2.1 there are spikes at approximately 9500 seconds that are not present in old version. Also noticeable is the time difference between the RPV breaks, visible in the figure as instantaneous drops of pressure at around 19700 s (1.8.6) and 22800 s (2.1).

Figure 4 shows the maximum fuel cladding temperature for the first 5000 s of the simulation. Both versions show very similar results up until cladding temperatures of 1800K.

The average corium temperature in the cavity after RPV breach is shown in Fig. 5, here is again quite different results between the versions, but this was indicated already earlier as the RPV in v2.1 took 50 more minutes to break, which would be an indication of lower corium temperature. The extra rise in corium temperature in version 2.1 at 4500 s is due to a second release of corium into the cavity at that time as shown in Fig. 6.

The lower corium temperature leads to a significantly lesser amount of concrete ablation in the newer model, illustrated in figure Fig. 7. This also leads to a lower hydrogen production in the later stage of the simulation as the concrete ablation is a source of hydrogen. As seen from Fig. 8 the hydrogen production in the core is also lower in the new model.

Figure 9 shows the pressure increase in the drywell during the simulation. The pressurization starts of very similar but as it starts to rise the older version consistently holds a higher pressure than the new model. Also the effect of the RPV vessel breach is much larger in the old version than in the new. Which is to be expected due to the lower average temperature of the corium in the cavity. The larger amount of hydrogen in the older version is also a probable reason for this.

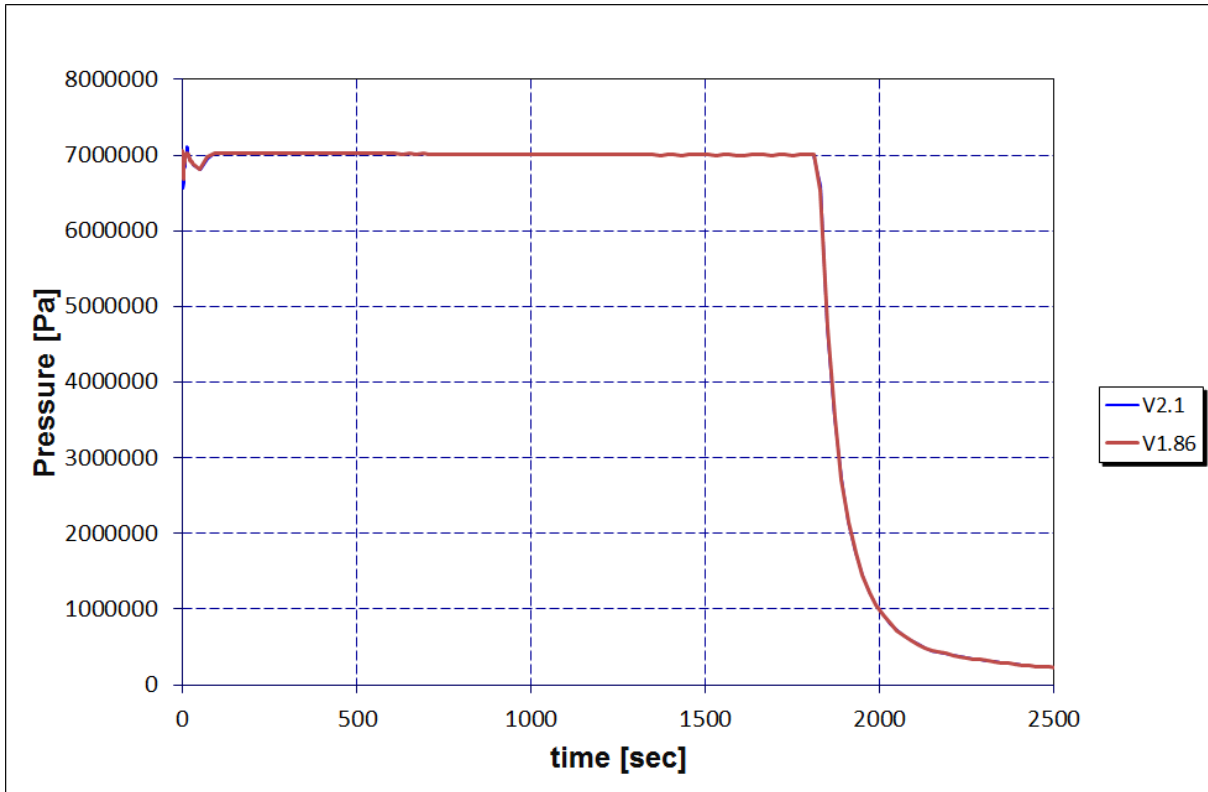


Figure 2. RPV pressure up until the depressurization. Calculated with MELCOR 1.8.6 and 2.1.

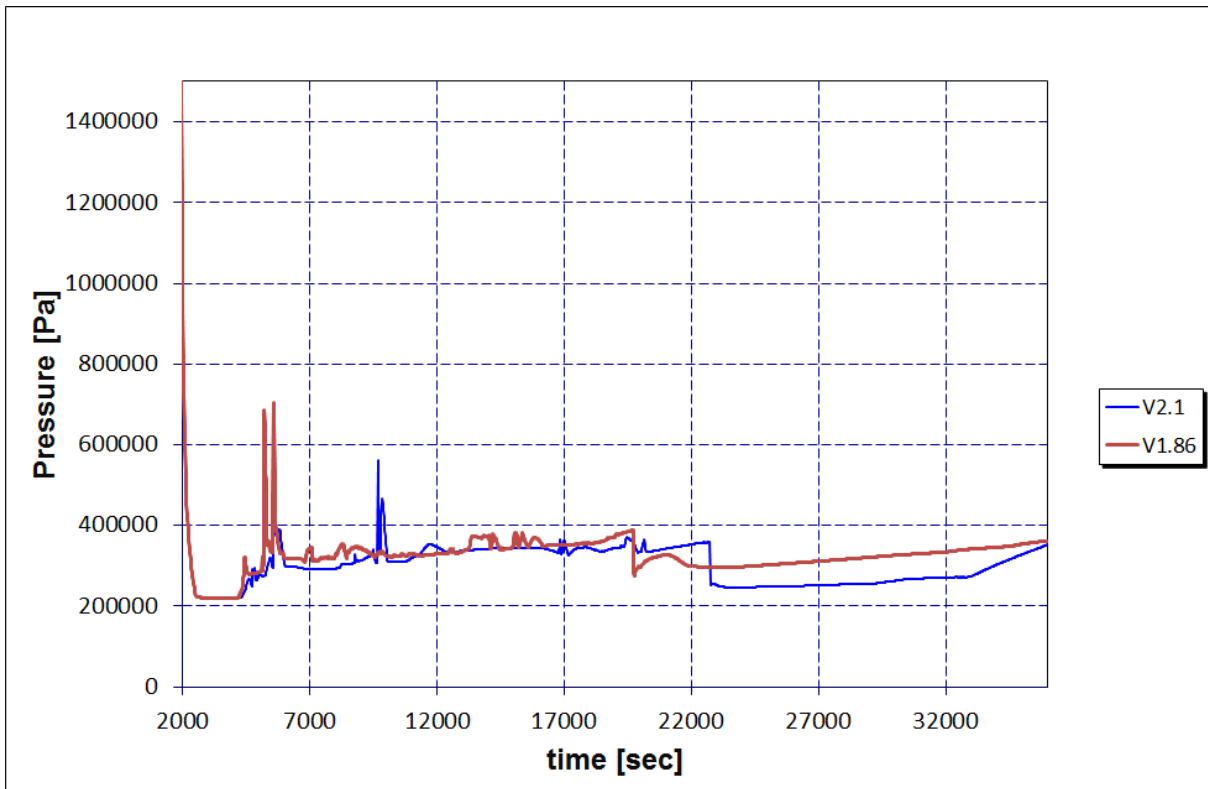


Figure 3. RPV pressure after depressurization. Calculated with MELCOR 1.8.6 and 2.1.

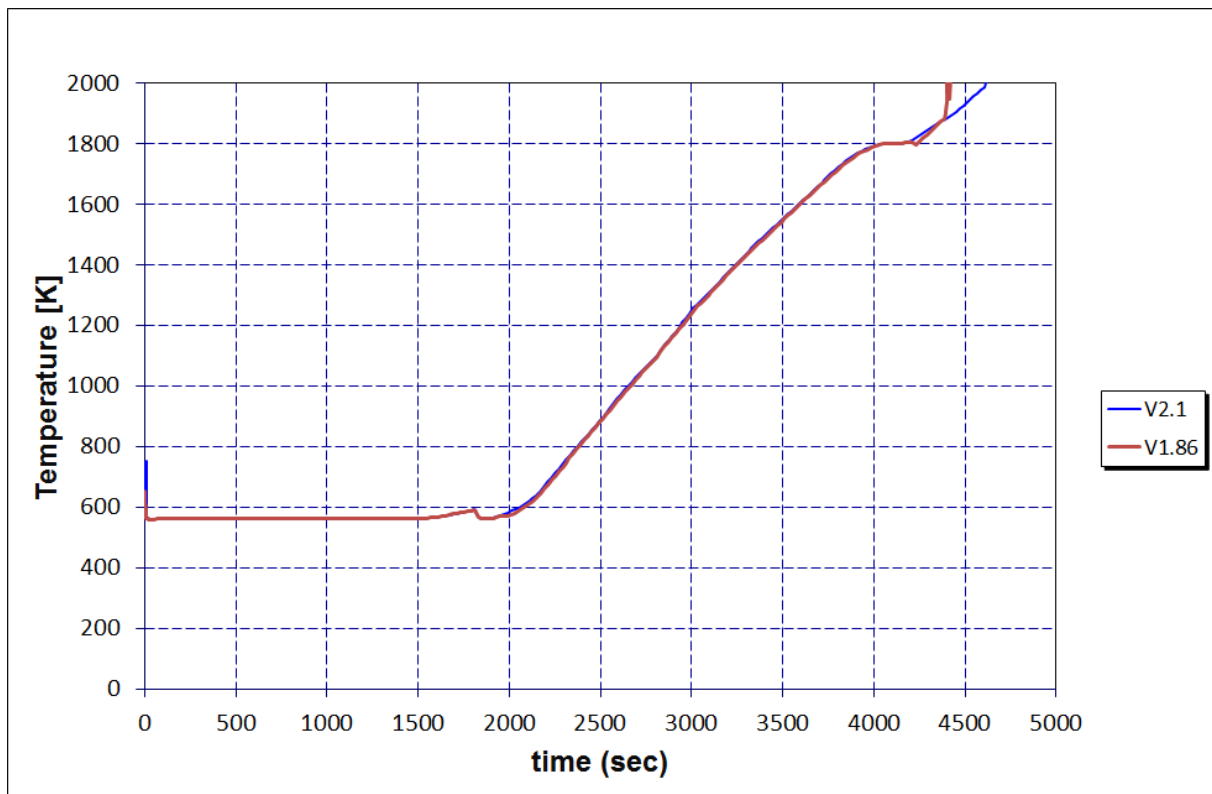


Figure 4. Maximum cladding temperature. Calculated with MELCOR 1.8.6 and 2.1.

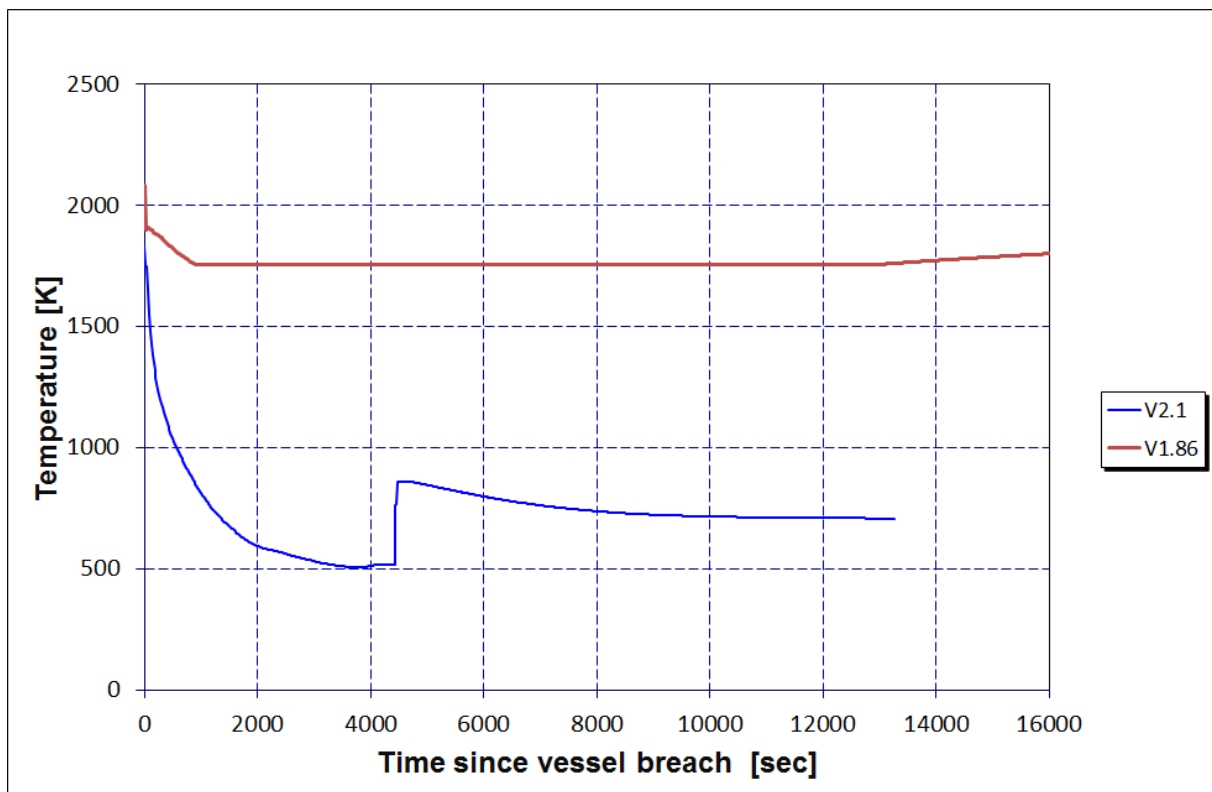


Figure 5. Average corium temperature in cavity, after PRV rupture. Calculated with MELCOR 1.8.6 and 2.1.

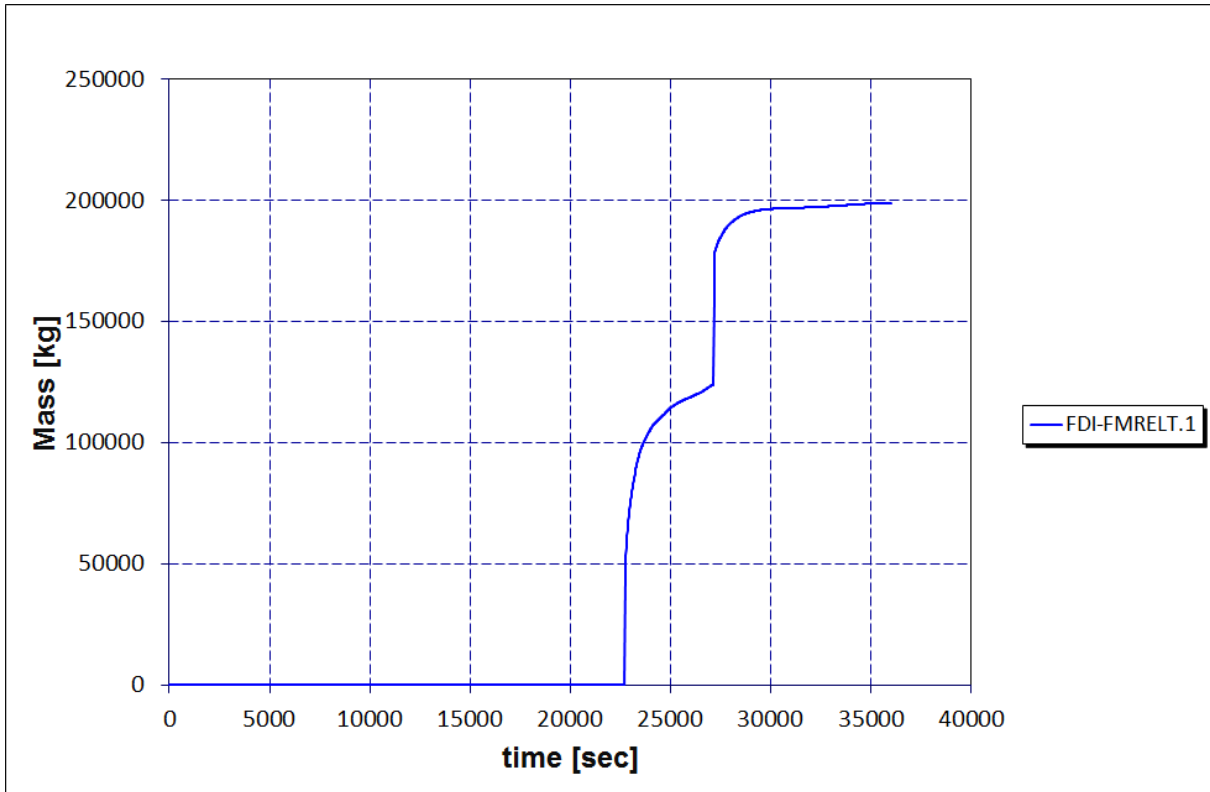


Figure 6. Corium release into cavity for the 2.1 MELCOR model.

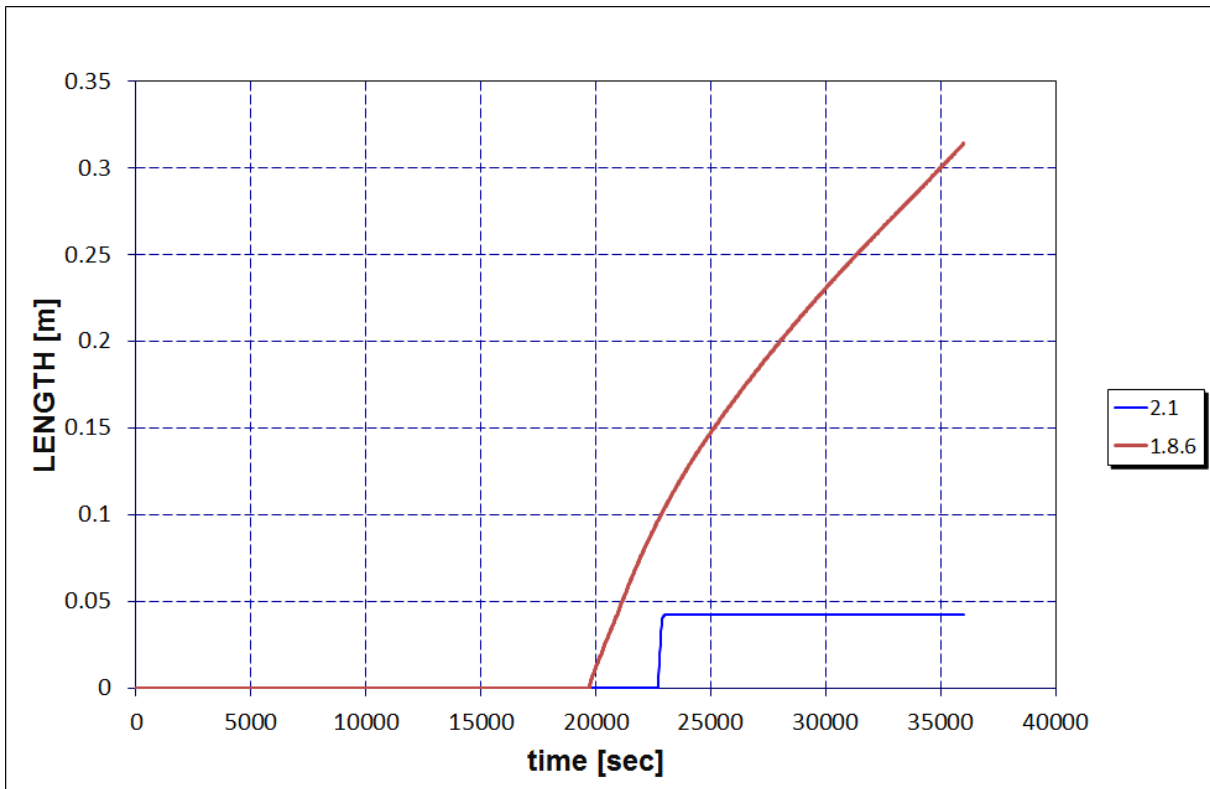


Figure 7. Concrete ablation depth. Calculated with MELCOR 1.8.6 and 2.1.

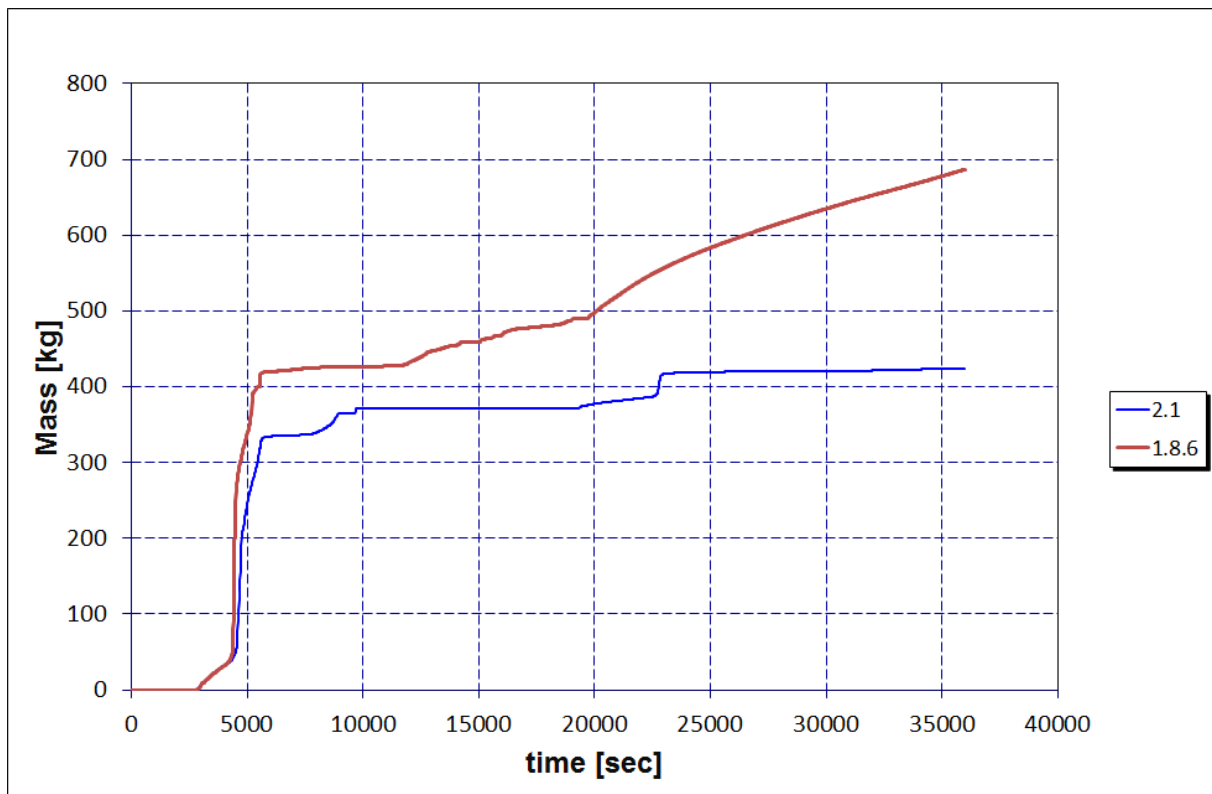


Figure 8. Comparison of the total hydrogen production in the two MELCOR models.

In Fig. 10 and 11 the temperature of the water pool in the wetwell and the pedestal is shown. For the wetwell the temperatures match quite well, but in the pedestal case the temperature starts rising at the time of RPV break which causes a delay in the temperature rise in the newer version.

The temperature of the atmosphere of the wet well and the dry well are presented in Fig. 12 and 13. In the wet well the temperatures match very well but the newer version produces much smoother results. In the dry well however, the temperature differences at the later stage of the simulations are large. The sharp increase in temperature in both versions occurs at the time of the RPV rupture but in the older version the drop off in temperature is much smaller than in the new one.

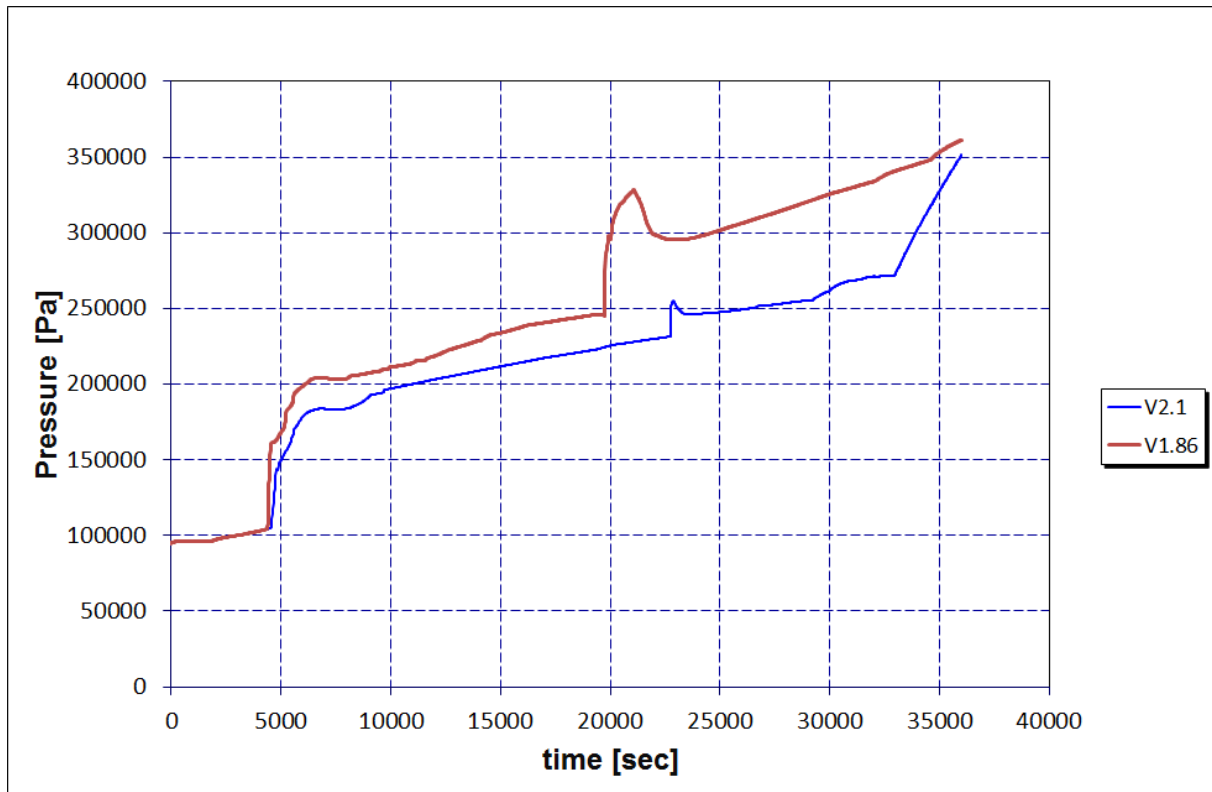


Figure 9. Drywell pressure calculated with MELCOR 1.8.6 and 2.1.

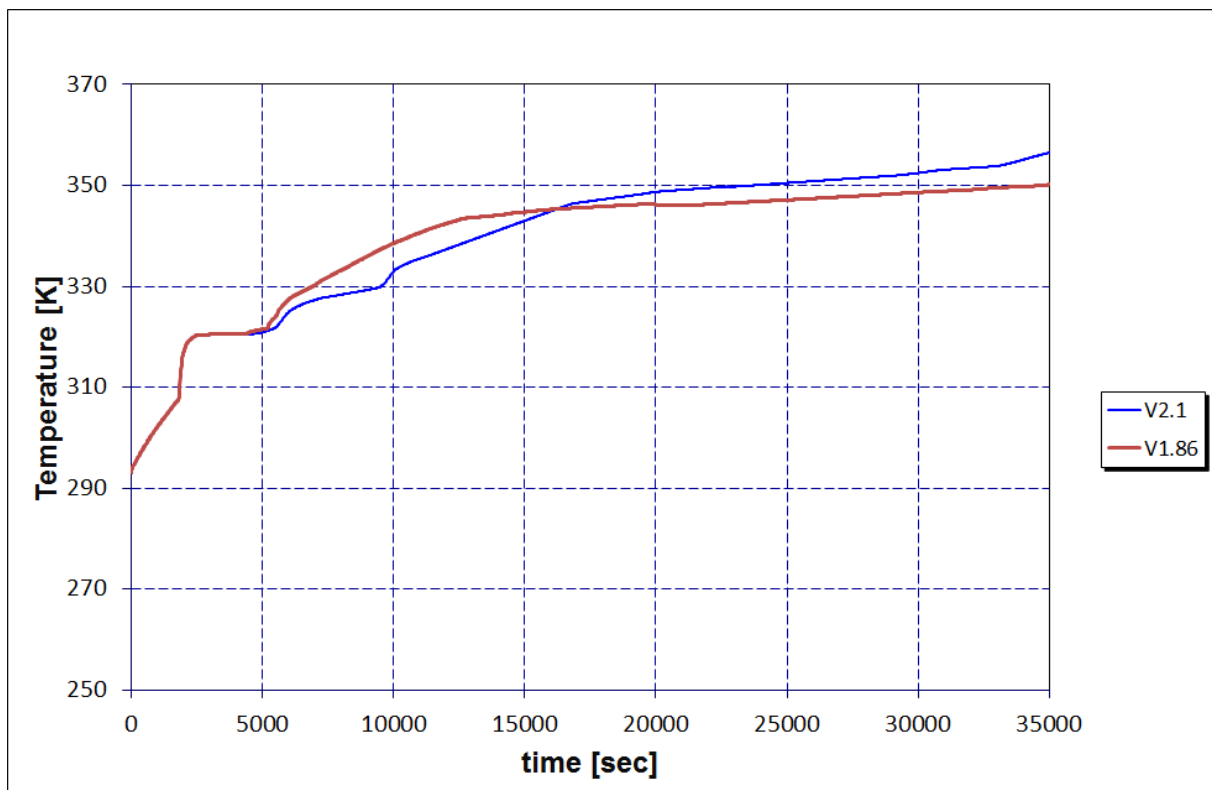


Figure 10. Wet well water pool temperature. Calculated with MELCOR 1.8.6 and 2.1.

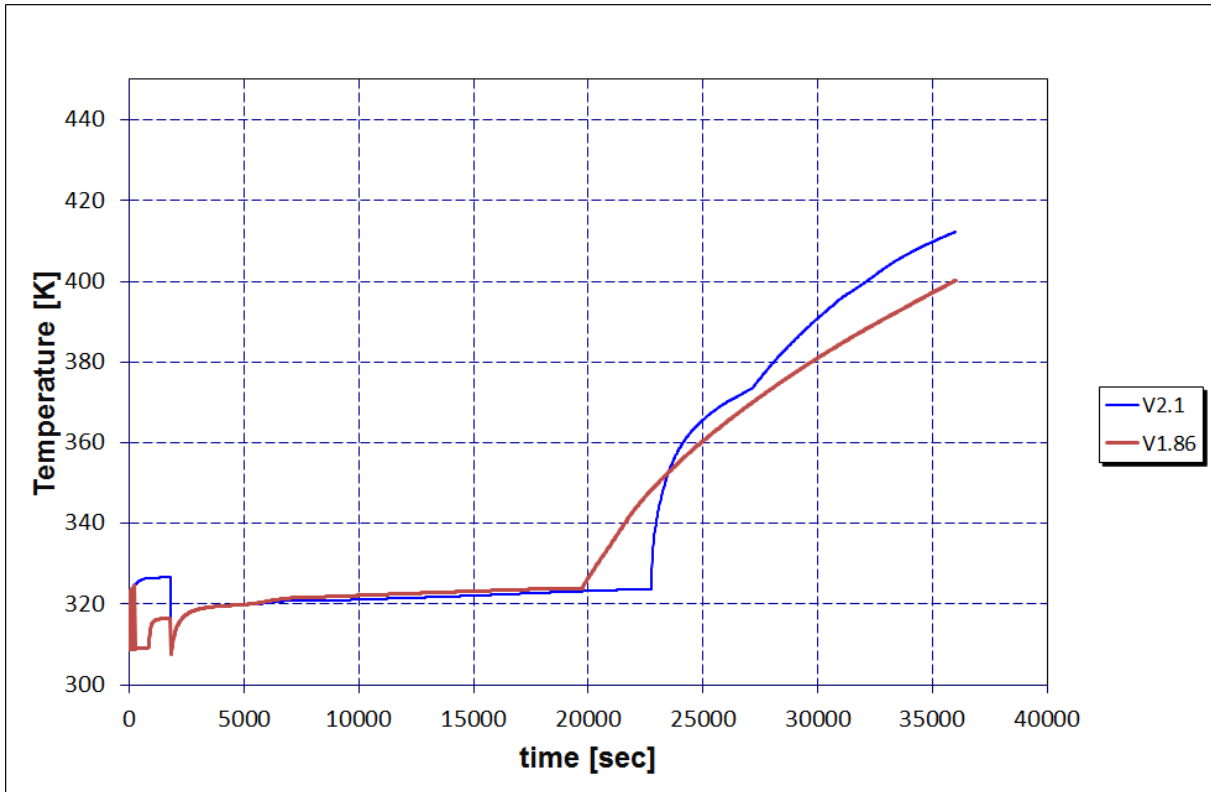


Figure 11. Pedestal water pool temperature. Calculated with MELCOR 1.8.6 and 2.1.

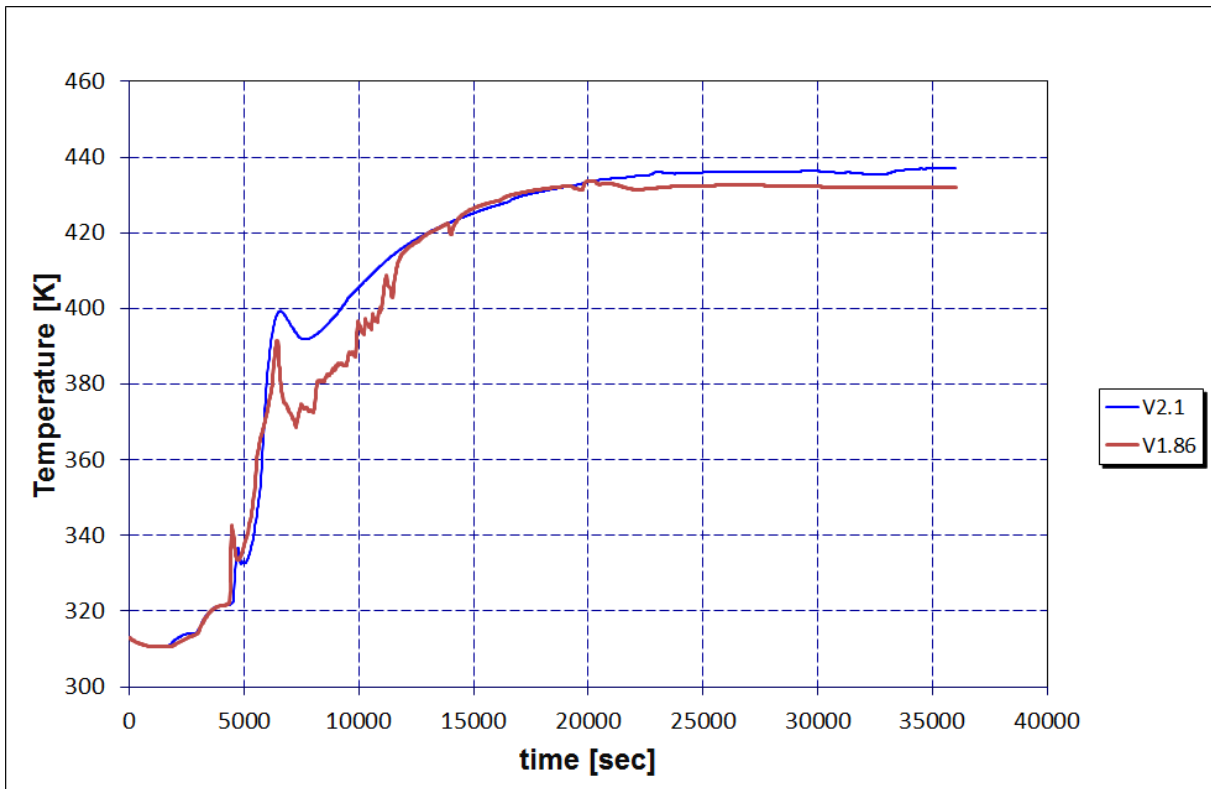


Figure 12. Wet well atmosphere temperature. Calculated with MELCOR 1.8.6 and 2.1.

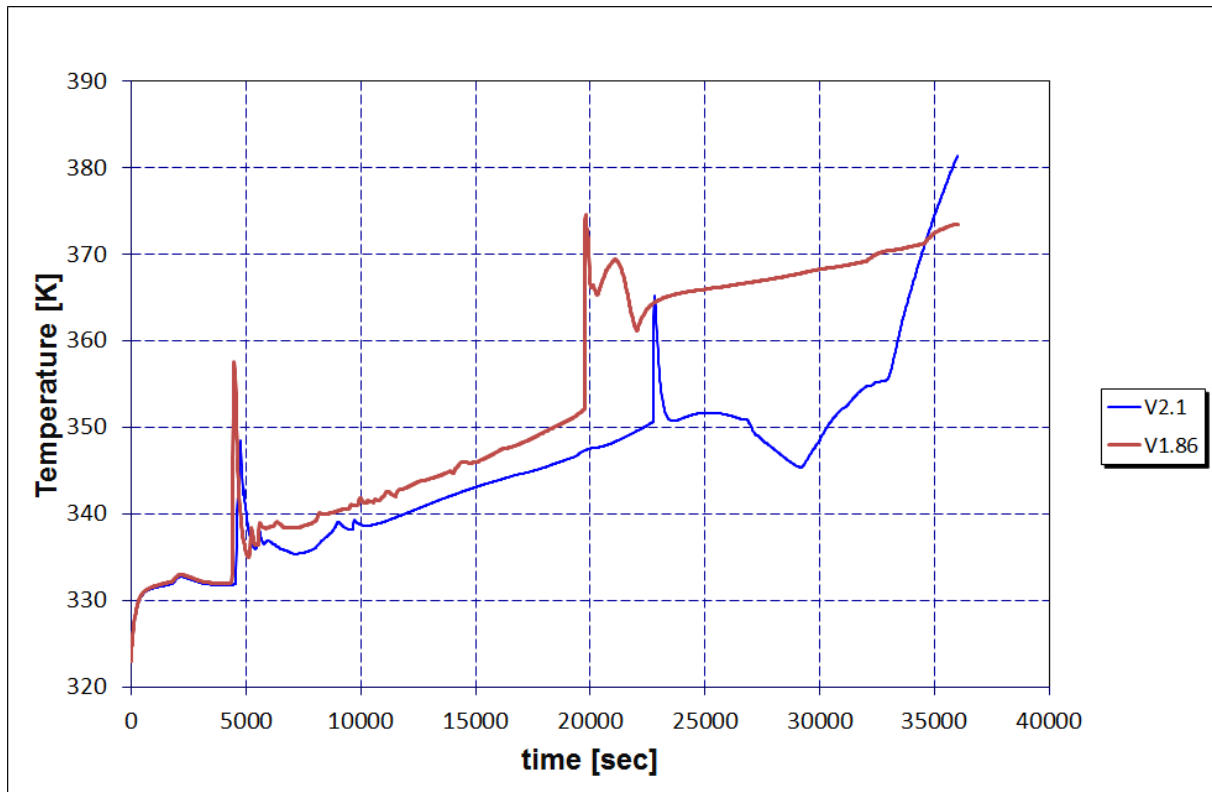


Figure 13. Dry well atmosphere temperature. Calculated with MELCOR 1.8.6 and 2.1.

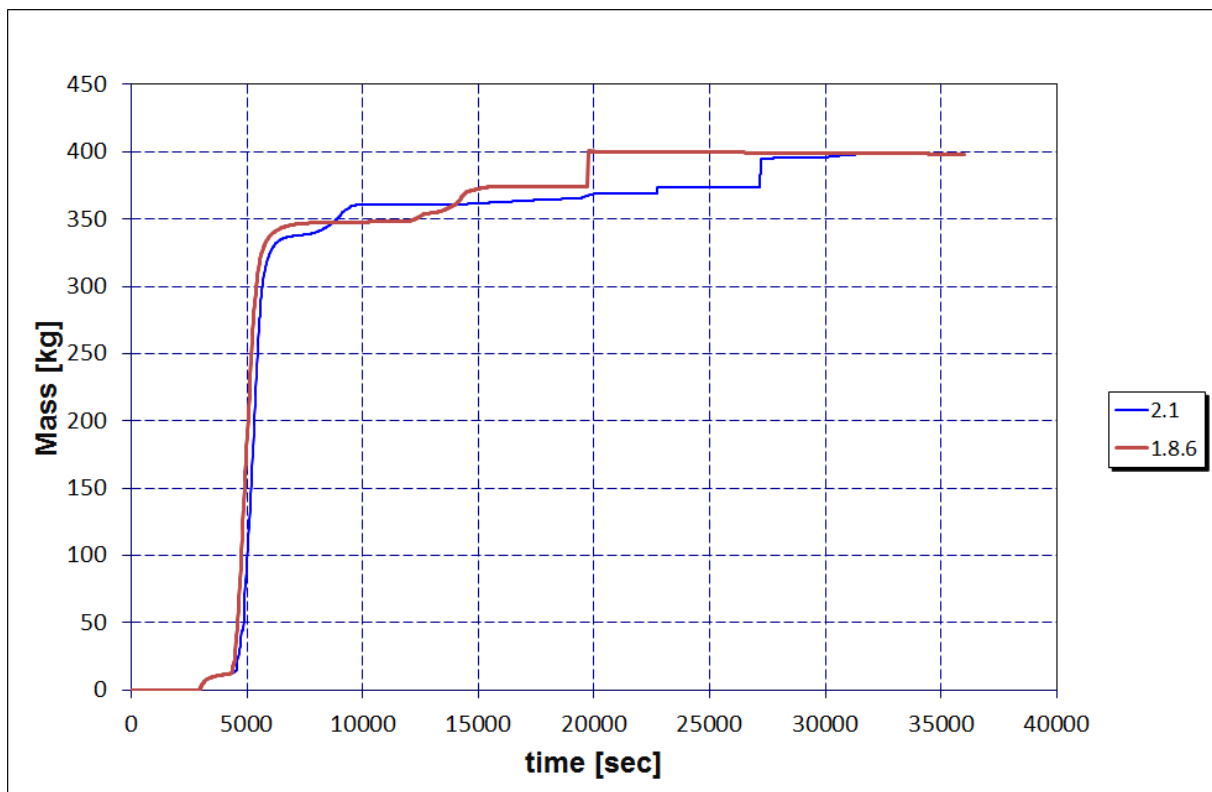


Figure 14. Radioactive noble gas in the containment volumes. Calculated with MELCOR 1.8.6 and 2.1.

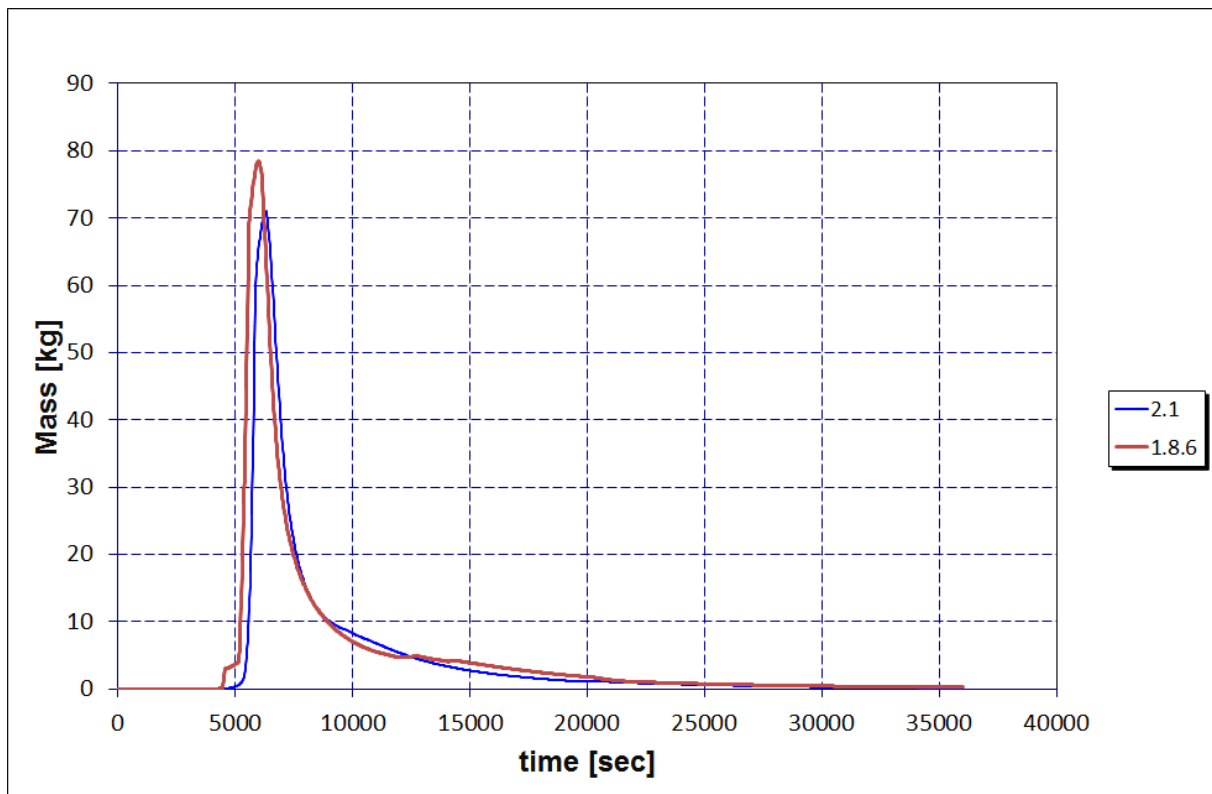


Figure 15. Radioactive cesium aerosol in the containment volumes. Calculated with MELCOR 1.8.6 and 2.1.

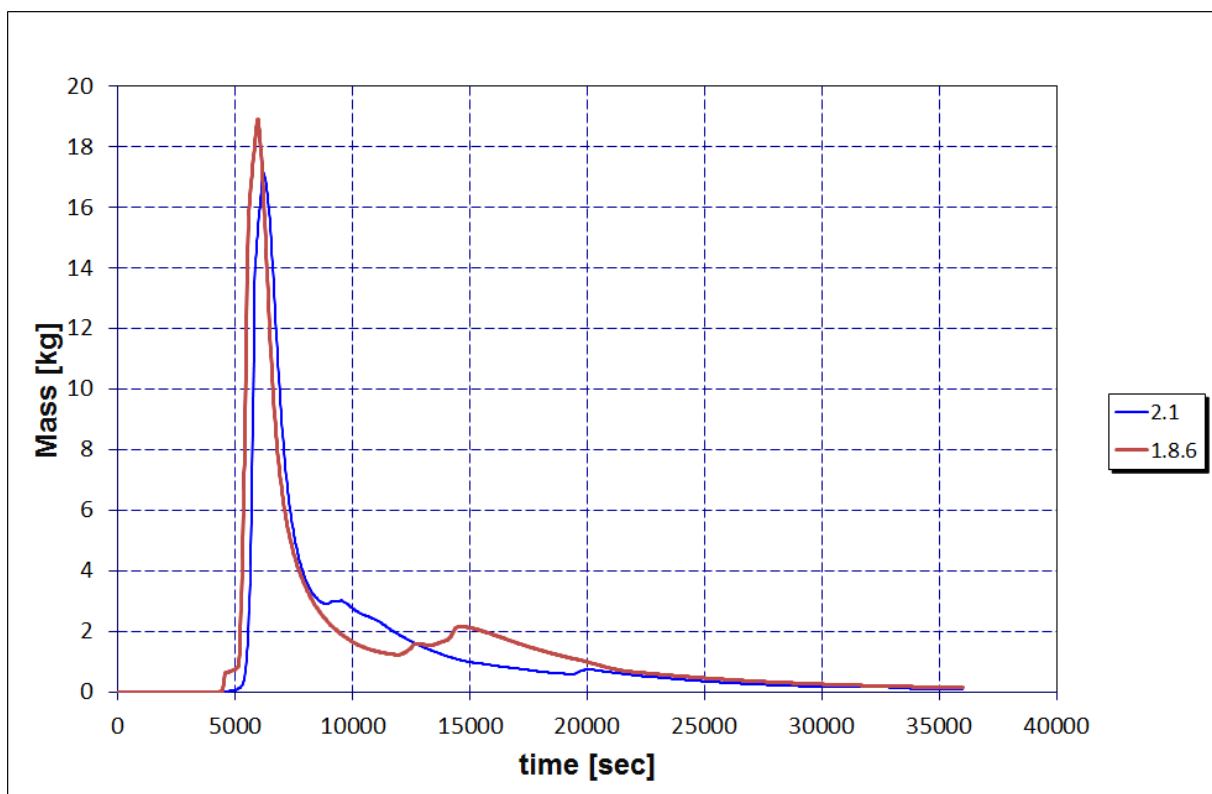


Figure 16. Radioactive cesium iodide aerosol in the containment volumes. Calculated with MELCOR 1.8.6 and 2.1.

5. Analysis of the effects and risks of hydrogen burns

5.1 Hydrogen concentrations in the reactor building

To assess the risks of hydrogen fire inside the reactor building the first step is to determine the amount of hydrogen that leaks into these areas from the containment. Figure 17 illustrates the hydrogen concentration in the volumes representing the reactor building that are present in the model.

The concentration is the overall average, and local concentration could be higher in some cases. However the amounts calculated in the simulations are very small for all volumes except number 500 (B1171) and 550(B564RRB) the calculated H₂ concentration were zero. The exceptions did also have a very low concentration, where the 500 volume had a concentration of about 0.05 per cent.

The 550 volume has an average concentration of maximum 3 per cent. According to [4] the lower theoretical limit for hydrogen combustion is 4 per cent, so taking higher local concentrations into account there seem to be a small theoretical risk for hydrogen fire in that volume. However, in case of a hydrogen fire in this volume the mass of available hydrogen is also of concern and in this case it is only about 0.58 kg.

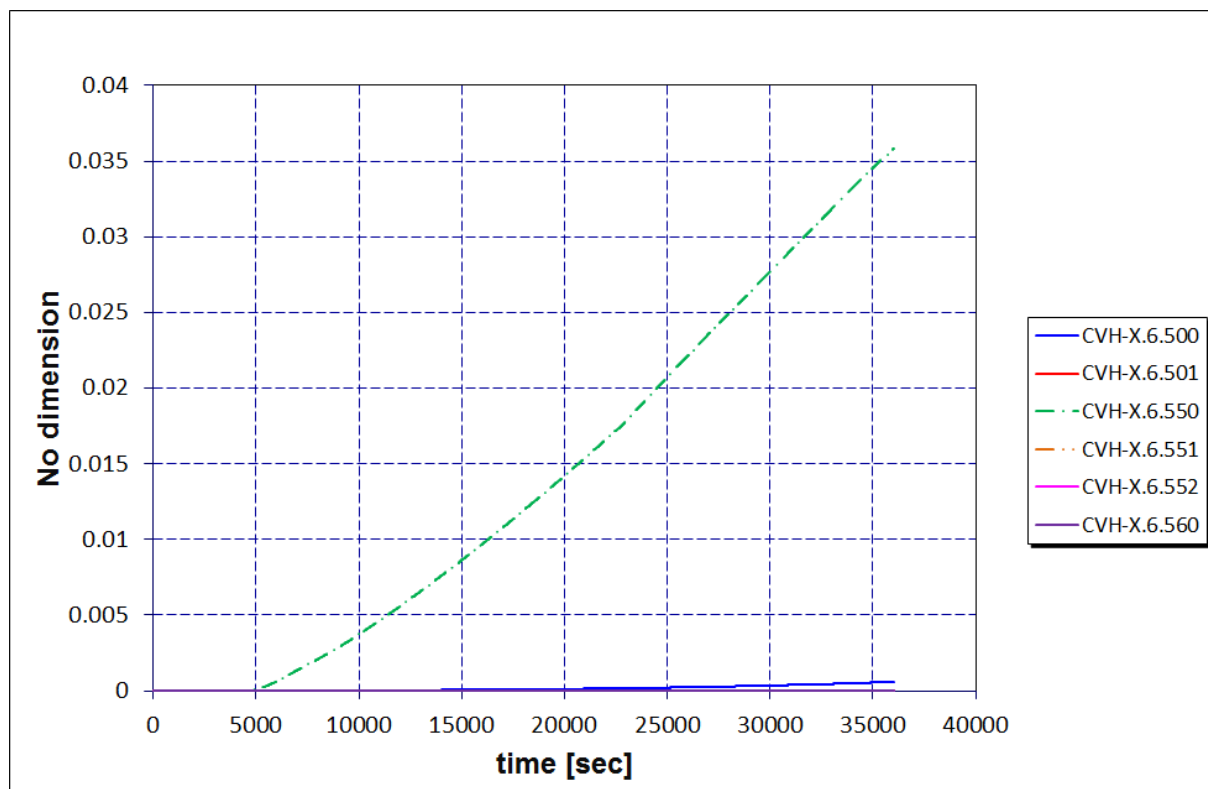


Figure 17. Concentration of hydrogen in different control volumes that make up the reactor building. Only volume 550 shows an noticeable increase of hydrogen concentration.

5.2 Non-inerted containment analysis

To be able to analyse the effects of an uninerted containment the 2.1 model was modified so that the containment volumes contained normal atmospheric mixture of gas (78% nitrogen, 21% oxygen and 1% argon) instead of the original inerted state (99% nitrogen and 1% oxygen).

This resulted in a large amount of hydrogen burns in the containment volumes, with MELCOR showing upwards to 19 000 deflagration burns ignited during the simulation. Most of these burns are very small and last only moments, the total amount of hydrogen burned in the different parts of the containment is illustrated in Fig. 18, and the average hydrogen concentration in the atmosphere can be seen in Fig. 19. The temperature increase caused by the fires is illustrated in Fig. 20, 21 and 22. However the pressure is noticeably lower in this scenario, Fig. 23. This could be because the burning of hydrogen consumes gas which lowers the overall pressure.

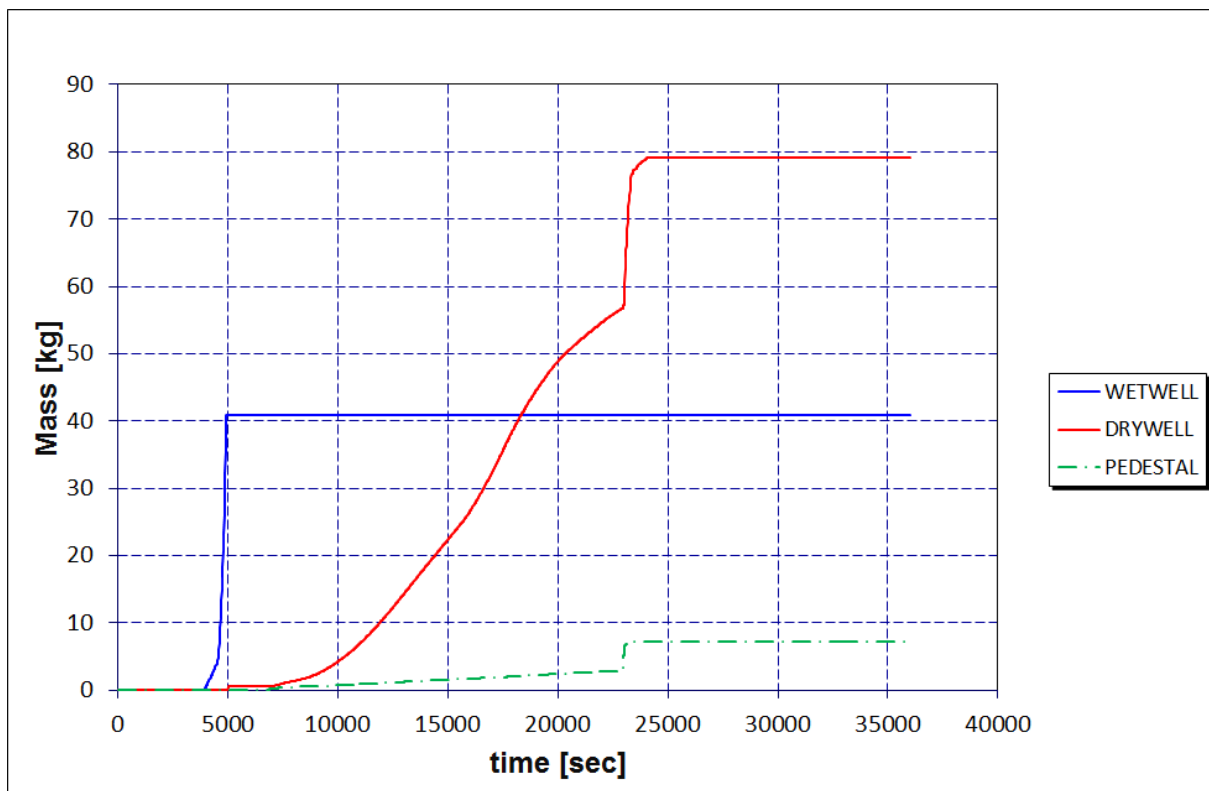


Figure 18. Total amount of hydrogen burned in the different containment volumes in the uninerted simulations with MELCOR 2.1

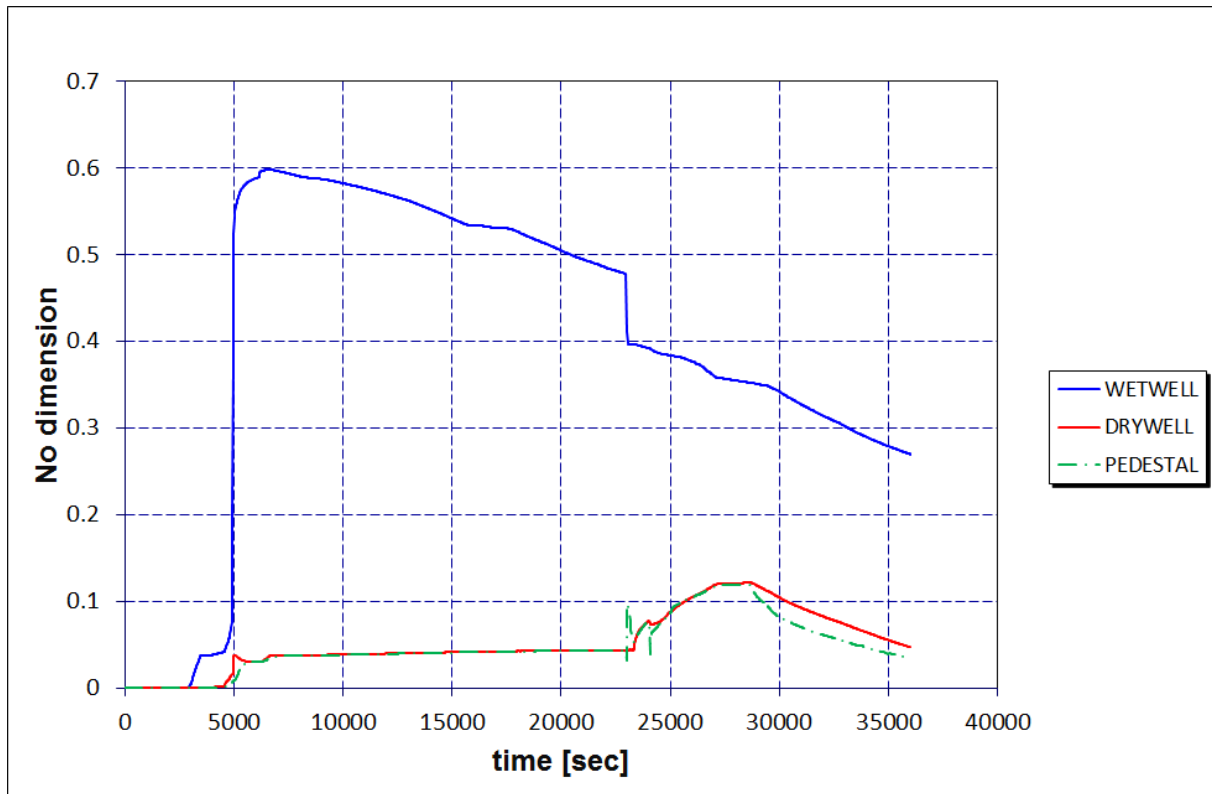


Figure 19. Hydrogen concentration in the different containment volumes in the uninerted simulations with MELCOR 2.1

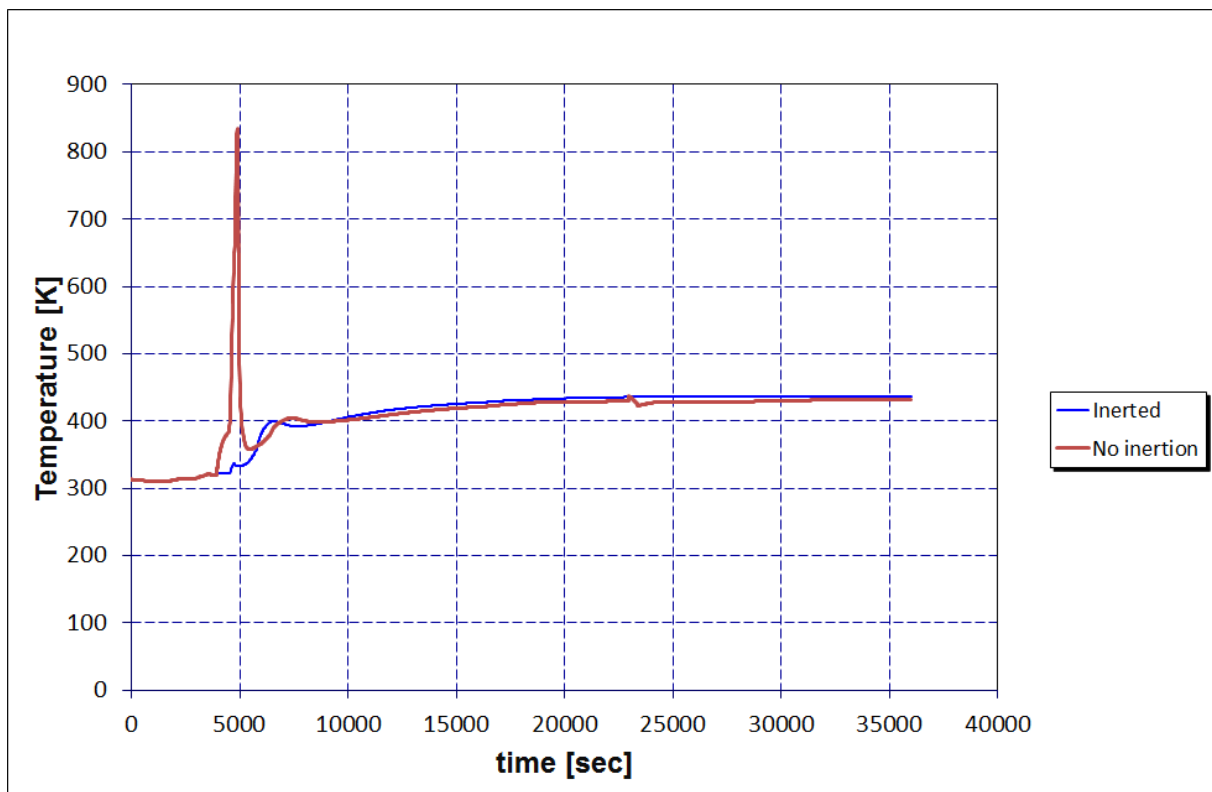


Figure 20. Comparison of atmosphere temperature in the wet well between the inerted and original MELCOR 2.1 models.

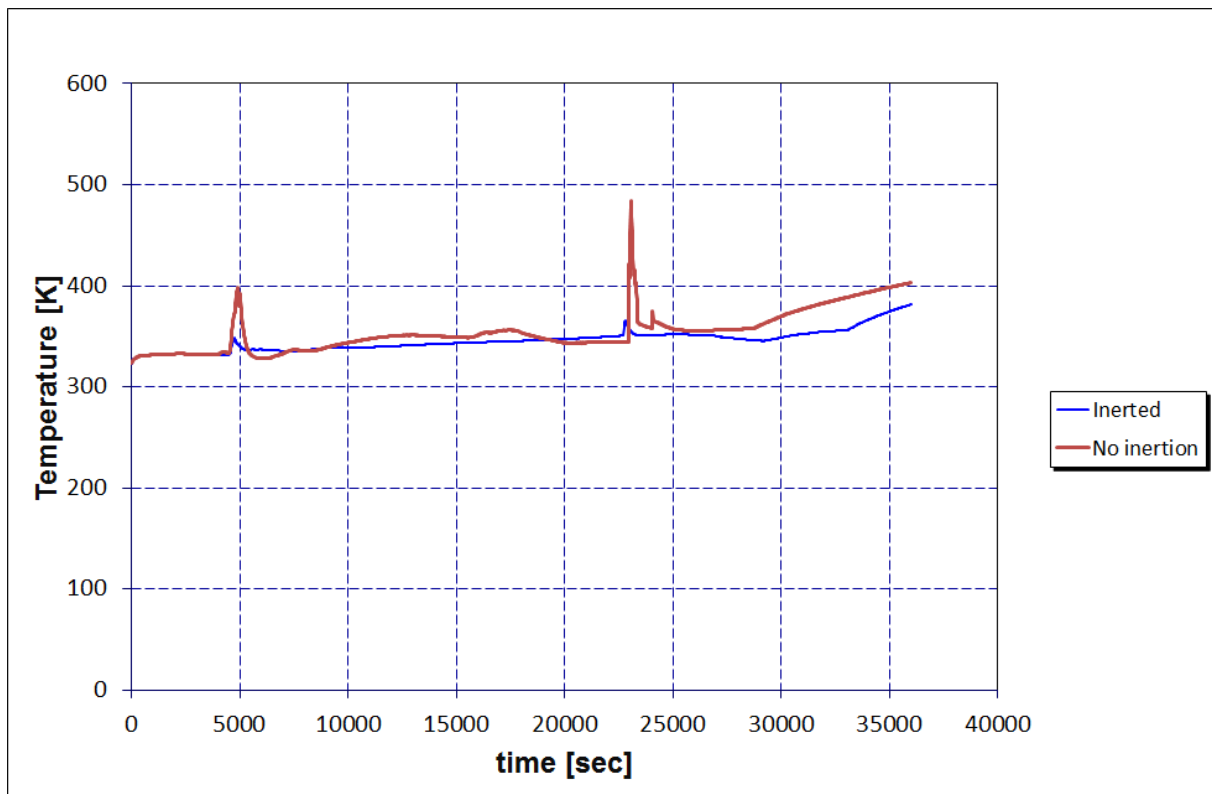


Figure 21. Comparison of atmosphere temperature in the dry well between the inerted and original MELCOR 2.1 models.

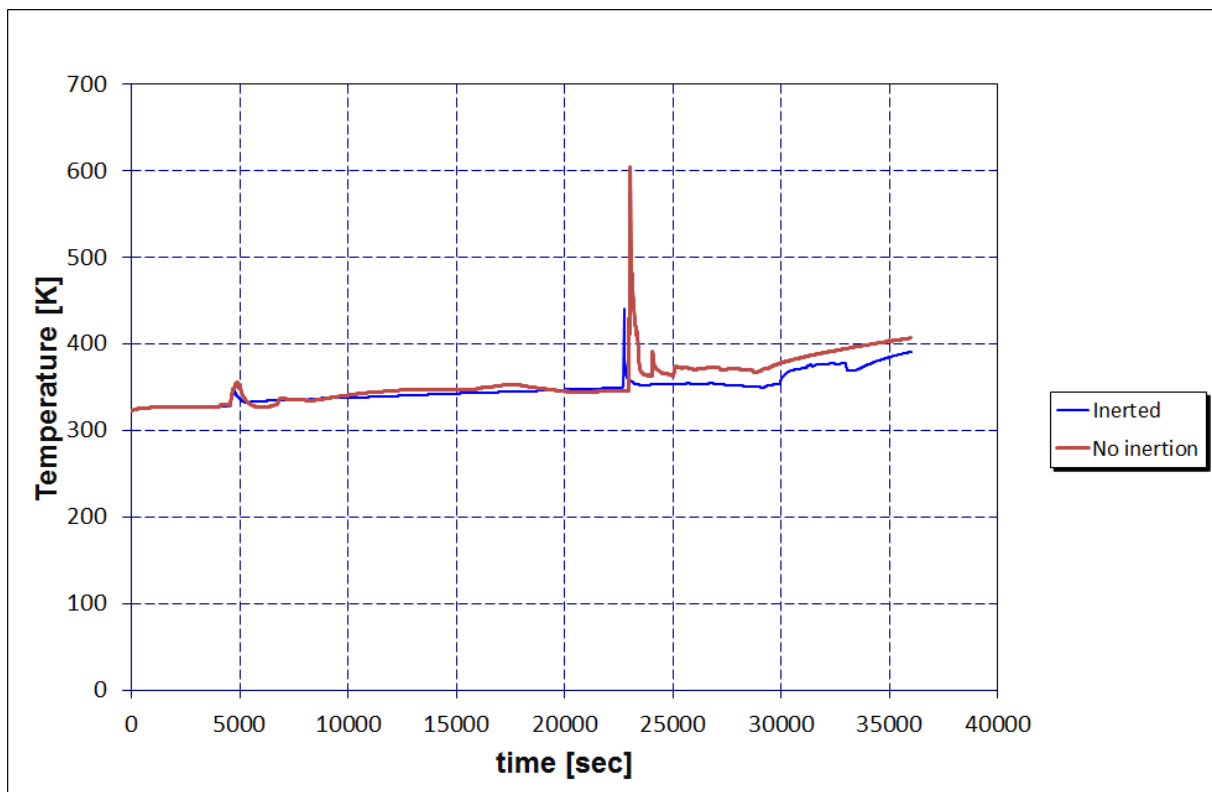


Figure 22. Comparison of atmosphere temperature in the pedestal between the inerted and original MELCOR 2.1 models.

6. User experience with MELCOR 2.1

The new model runs quite smoothly. However, there seem to be some stability issues, for example the code crashes early on in the calculations with the BUR package turned off. The crash was due to rounding errors from the COR-package, with the BUR-package switched back on every thing run smoothly though.

As mentioned already in chapter 3 the new versions of the model was created with SNAP. It now exists as a SNAP model and as a exported "text-file". The SNAP model is easily navigated and modifiable and the SNAP program is easy to start working with so an experienced MELCOR user should not have any problems adapting to using the SNAP model compared to the older text based version.

Editing the model via the exported files is not recommended, as the files lacks comments and does not have a layout that is easy to navigate and read without very good knowledge of both MELCOR and the structure model.

7. Conclusions

The SNAP tools offers a fast solution to updating MELCOR models to run on the new version of the code. And offers an easy editing environment with the drawback of making the "text" versions of the model less user friendly to work with directly.

The updated MELCOR model of the Olkiluoto 1 & 2 plant runs smoothly and produces results similar to the older model. There are differences, mostly due to differences in the COR-package

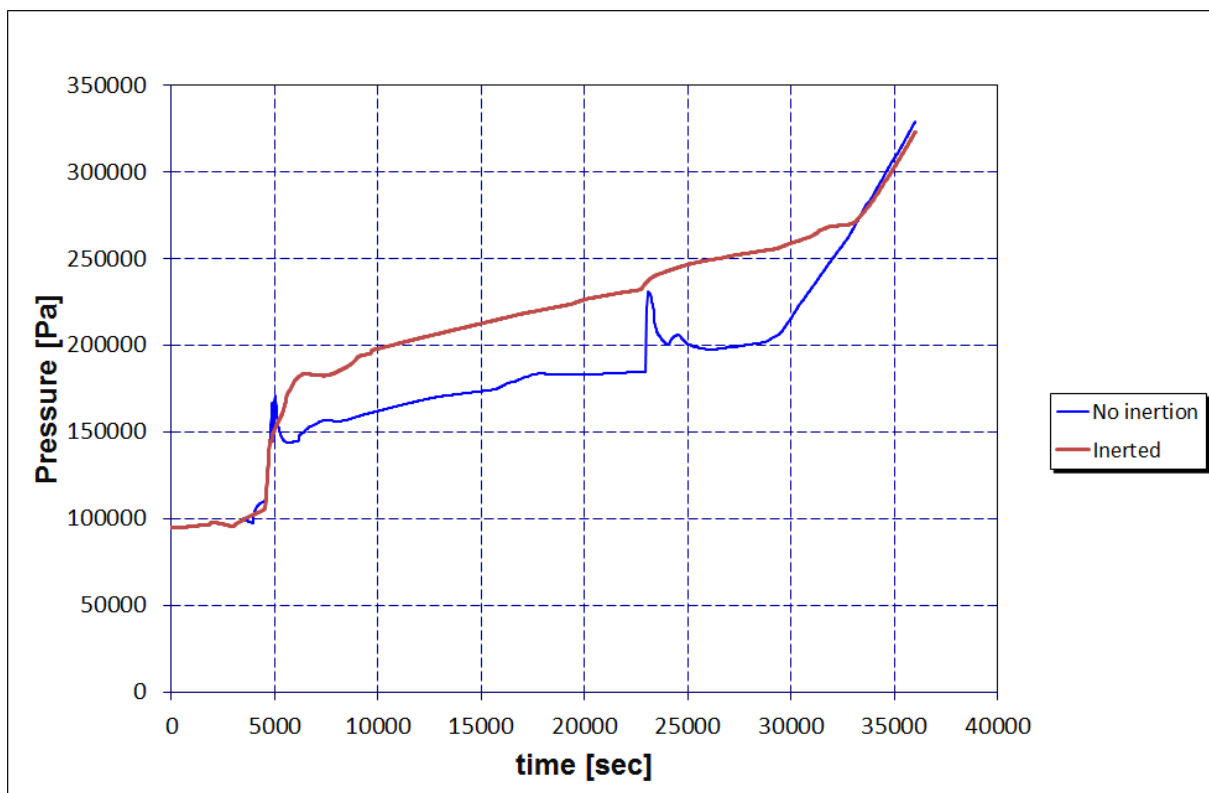


Figure 23. The calculated pressure in the dry well for the inerted and original MELCOR 2.1 models.

calculations. Most significantly later RPV breach and lower corium temperature in the cavity. The later causing secondary differences such as less concrete ablation in the cavity and less hydrogen production, compared to the older version.

The simulation calculations done with the new model shows that the hydrogen concentration in the reactor building volumes are very low, and also that the total mass of hydrogen in these volumes are very small. So even if the local concentrations could be high enough to be theoretically able to cause an ignitable mixture the assorted energy release is not very high.

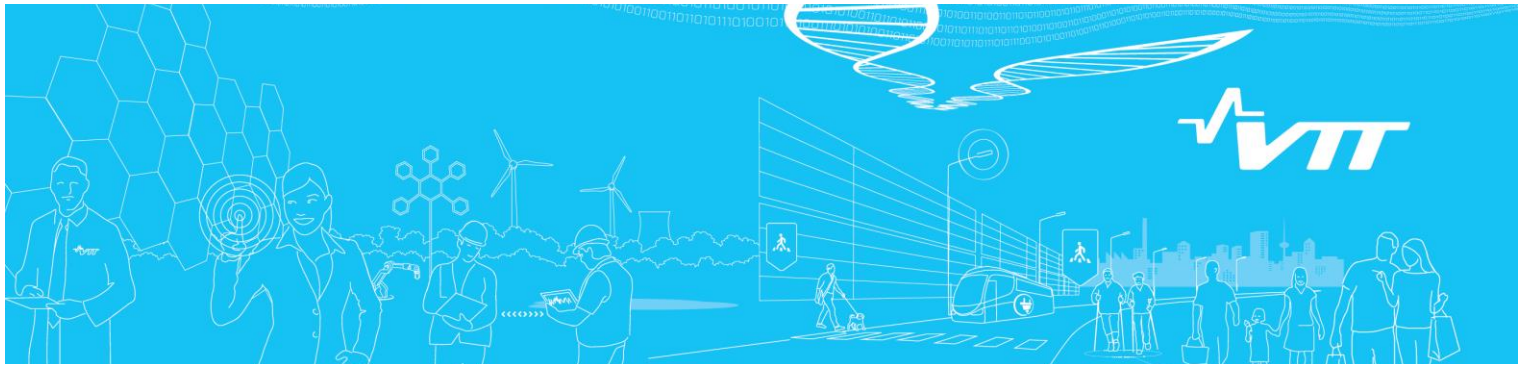
The modified model without containment inertion shows large amounts of hydrogen burns and also some temperature spikes in the containments atmosphere. However, these temperature spikes did not cause an overall increase in pressure, this was probably due to the flames consuming gas. Also the hydrogen fires did not cause the RPV to fail earlier than in the original model.

All in all the results seem reasonable, but the differences in simulation results between the old and the new version are for some properties quite large and could be investigated further.

References

- [1] D.L. Louie V.G. Figueroa M. F. Young L.L. Humphries, R.K. Cole. *MELCOR Computer Code Manuals Version 2.1.6840*. Sandia National Laboratories, Albuquerque, NM 87185-0748, 2015. SAND2015-6691 R, Vol 1 &2.
- [2] Tuomo Sevón. Updating of olkiluoto 1&2 bwr model to melcor version 1.8.6. Technical report, VTT Technical Research Centre of Finland Ltd, 2006. VTT-R-08033-06.
- [3] *Symbolic Nuclear Analysis Package, Version 2.4.5*, 2016.
- [4] Nilesh Agrawal, K. Velusamy, and Sarit K. Das. A method to characterize mixing and flammability of hydrogen–air mixtures in enclosures. *International Journal of Hydrogen Energy*, 36(19):12607 – 12617, 2011.

ANNEX 3
**Level 2 PRA studies – Source term characteristics and
hydrogen explosions**



RESEARCH REPORT

VTT-R-00354-17

Level 2 PRA studies – Source term characteristics and hydrogen explosions

Authors: Tero Tyrväinen, Ilkka Karanta

Confidentiality: Public

Report's title	
Level 2 PRA studies – Source term characteristics and hydrogen explosions	
Customer, contact person, address	Order reference
VYR	SAFIR 4/2016
Project name	Project number/Short name
Probabilistic risk assessment method development and applications	102420/PRAMEA
Author(s)	Pages
Tero Tyrväinen, Ilkka Karanta	19/2
Keywords	Report identification code
Probabilistic risk analysis, severe accident, source term, hydrogen explosion, uncertainty analysis	VTT-R-00354-17
Summary	
<p>This document studies probabilistic modelling of severe nuclear power plant accidents. Factors that affect the height and temperature of radioactive releases are identified, and hydrogen explosions in boiling water reactor (BWR) nuclear power plant are studied. A containment event tree model is developed for a BWR plant based on a model developed in a previous study. Uncertainty analysis is implemented for release probabilities, and release heights and temperatures are included in the model.</p> <p>The height and temperature of radioactive releases have typically not been included in level 2 probabilistic risk analyses (PRA), even though they are needed as inputs for level 3 PRA. Release height is usually the height of the location where the reactor building leaks (which depends on the containment failure mode), or the height of the chimney if the release is controlled. In an uncontrolled accident case, both the containment failure location and the flow path of radionuclides in the reactor building need to be analysed to determine the release height. The temperature of release from containment is in most cases close to 100°C, but the temperature of radionuclides can potentially change during their migration in the reactor building. Higher temperatures can be caused by fires and explosions. There are computer codes that can be used to analyse radionuclide flows in reactor building and determine the release heights and temperatures.</p> <p>Hydrogen explosions can occur inside BWR containment if the containment is not inert. Therefore, the risk of hydrogen explosions comes mainly from reactor start-up, shut-down and refuelling. Hydrogen explosions outside containment have usually not been modelled in PRA, even though they can affect the releases significantly.</p>	
Confidentiality	Public
Espoo 14.2.2017	
Written by	Reviewed by
	
Tero Tyrväinen Research Scientist	Kim Björkman Research Scientist
Accepted by	
	Eila Lehmus Research Team Leader
VTT's contact address	
VTT, PL 1000, 02044 VTT	
Distribution (customer and VTT)	
SAFIR reference group 2	
<p><i>The use of the name of VTT Technical Research Centre of Finland Ltd in advertising or publishing of a part of this report is only permissible with written authorisation from VTT Technical Research Centre of Finland Ltd.</i></p>	

Contents

1. Introduction.....	3
2. Containment performance and failure modes.....	3
3. Release height.....	5
4. Release temperature	7
5. Hydrogen explosions	7
5.1 Containment inerting.....	8
5.2 Analysis of explosions	9
5.3 Hydrogen explosions outside containment.....	9
6. Containment event tree model	10
6.1 Dynamic containment event tree analysis	10
6.2 Overview of the model	10
6.3 Release heights and temperatures	12
6.4 Uncertainty analysis.....	13
6.5 Results	15
7. Conclusions	18
References.....	18
Appendix A: Uncertainty distributions of parameters	20

1. Introduction

Level 2 probabilistic risk analysis (PRA) studies how a nuclear power plant accident progresses after core damage and how frequent and large radioactive releases are [1]. Severe accident phenomena, e.g. hydrogen explosions, and timings of events, such as cooling system recovery, play an important role in such analyses. Information on severe accident progression provided by deterministic analyses is crucial to the construction of proper level 2 PRA. Integrated deterministic and probabilistic safety analysis (IDPSA) aims to bring the two types of analysis closer and improve their co-operation.

The height and temperature of radioactive releases have typically not been included in level 2 probabilistic risk analyses (PRA), even though they are needed as inputs for level 3 PRA [2]. This report identifies which factors affect the height and the temperature.

Hydrogen explosions can occur in nuclear power plant containment if heated zirconium reacts with steam producing significant amount of hydrogen during severe accidents. These explosions have the potential to be powerful enough to break the containment and cause a large early release. Hydrogen explosions in a pressurized water reactor plant were studied in [3]. Hydrogen explosions in boiling water reactor (BWR) plants have been studied less because inerting of containment - filling the containment with a non-flammable gas (usually nitrogen) - prevents explosions with certainty. Inerting of containment is often used in BWR's, for example in the Olkiluoto 1 and 2 reactors for which the model presented in this report was built. However, an accident can also occur when the containment is not inert, e.g. during start-up or shut-down. Therefore, it is relevant to consider hydrogen explosions in BWR plants too.

This report continues the development of a level 2 containment event tree model for a BWR plant started in [4]. In [4], the focus of the research was on steam explosion modelling, and other phenomena were modelled in a very simple manner. In this report, uncertainty analysis is implemented for release probabilities. In addition, release heights and temperatures are included in the model.

2. Containment performance and failure modes

The purpose of a containment in a nuclear power plant is to isolate radioisotopes from the public (and also plant personnel and rescue workers) in case of a severe accident. Containment failure is necessary for an uncontrolled release. In PRA, it is also assumed that containment failure is sufficient for a release, although there are usually other structures (such as the outer walls) in a typical nuclear power plant unit that act as partial release barriers and may to a great extent affect the timing, radionuclide content and energy of the release to the atmosphere.

Uncertainty and variability are associated with many variables describing a structure's performance; this can be accounted for by the use of probability theory and structural reliability theory. As PRA is explicitly concerned with uncertainty and variability, containment performance is best analysed in its context using the methods of structural reliability analysis [5].

A containment may fail in different ways, called containment failure modes. The failure mode greatly influences release height and energy. Some general factors that affect what failure modes a containment might have and how vulnerable the containment is to that failure mode are [6]:

- General configuration

- Construction materials. For concrete, information on rebar, stiffeners, aggregate. For steel, type(s) and tension.
- The location and size of penetrations, including electrical penetrations and major openings
- Major discontinuities, such as the transition from the spherical top head to the cylindrical shell in many PWR's, and from the cylindrical cell to the basemat.
- Weld locations
- Layout and anchorage of the reinforcement
- Liner walls and anchoring
- Interactions with surrounding structures at large deformations

Failure modes - or the vulnerabilities of individual containment - and their significance vary widely due to different designs. However, some generic containment failure modes can be identified that apply to a large variety of designs. Some of those are listed in Table 1.

Table 1. Some generic containment failure modes for BWRs and PWRs.

Failure mode	Description	Location	Causes and influencing factors	Consequences	Notes
Isolation failure or bypass	Containment leaks through a penetration, door, manhole or such	Depends on the geometry of the containment. Usually close to the bottom.	Explosions, static overpressure, hot temperature	Radionuclides enter the reactor building	The height of the release depends on which penetration is lost. Usually the penetrations are close to the bottom of the containment.
Over-pressure	Over-pressure develops slowly in the containment, until a part of the containment yields	Most probably a penetration, door, manhole or such.	Boiling of coolant water	Radionuclides enter the reactor building	
Corium-concrete interaction	Hot corium melts its way through the bottom of the	Basemat	Insufficient cooling of corium	Radionuclides, mixed with water, enter the ground below	Occurs at late phase of accident

	containment			the plant.	
Containment rupture	Containment fails due to a pressure impulse from an explosion or rapid fire	Anywhere except the basemat, most probably through a door or such	Steam explosions, hydrogen explosions	Radionuclides enter the reactor building	Failure of containment structure is unlikely; it is more likely that a penetration, door or such fails
Steam generator tube rupture	The tube from the containment to the steam generator is broken, volatile radionuclides may enter the tube (PWR)	Steam generator tube, usually close to the top of the containment.	Heat, pressure	Radionuclides may enter the turbine hall if the pipeline is not closed.	

3. Release height

The height of a radioactive release affects the spreading of the radioactive substances in the atmosphere which in turn affects the consequences of a nuclear power plant accident. Therefore, the height of the release is important information for atmospheric dispersion analyses and level 3 PRA [2]. Release height can be defined either based on the release from containment or release from reactor building. Before entering open environment, radionuclides are released from the containment to the reactor building. Even though PRA and safety analyses focus mostly on the events occurring inside the containment, the reactor building can affect significantly to the migration path of the radionuclides. This is a challenge for the determination of the release height.

To estimate release height accurately, some fluid dynamics analyses would be needed for radionuclides considering the architecture and conditions of the reactor building. Radionuclide flows in reactor building can be modelled using some deterministic computer code, such as OpenFOAM [7], FDS [8], MELCOR [9] or RADTRAD-NAI [10]. The fluid dynamics model could likely be quite simple because only rough estimates for the height are needed and no complex fluid phenomena are relevant for this problem. It also needs to be noticed that radionuclides can escape only from known holes in the reactor building or holes that are created by severe accident phenomena, such as hydrogen explosions. Possibly, in some cases, the correct hole can be identified based on reactor building architecture without any calculations.

Roughly speaking, there are three different types of release cases with regard to the release height:

- The release height is the height of the location where the reactor building leaks after containment failure.

- The release height is the height of the chimney if filtered venting is performed.
- An explosion throws the releases in the air above/surrounding the containment and reactor building.

Literature search gives very little about the release heights directly. There are some estimates for the heights of the releases of Fukushima Daiichi accident [11]. In containment leakage cases, the height was 20 meters. In the case of filtered venting, the height was 120 meters. In the two hydrogen explosion cases that occurred outside the containment, the maximum heights were 100 and 300 meters, and the centre heights were 50 and 150 meters. It is also given that the releases spread up to 100 meters away from the plant in different horizontal directions due to explosions. Reference [12] gives some slightly different numbers.

In most cases, the location of the containment failure is the basis for the analysis of the release height even though the reactor building has to also be taken into account. Structural reliability analysis [5] can be used to determine the location where the containment fails. Usually, penetrations and doors fail more likely than the concrete wall. PRA containment failure modes for which some structural analysis could be performed include

- Isolation failure, containment not leak-tight
- Containment over-pressurisation
- Containment rupture (e.g. due to hydrogen explosion or steam explosion)

The location of an explosion affects the location of the containment failure. Hydrogen explosions occur most likely in the upper part of the containment, and therefore, some weak point in the upper part of the containment would most likely be broken. Ex-vessel steam explosions occur in the lower part of the containment, whereas in-vessel steam explosions occur in the lower part of the pressure vessel, which is typically somewhere in the middle part of the containment. These locations, of course, depend on the reactor type and plant design. Previous statements are not necessarily applicable to all the nuclear power plants in the world. BWR plant of Olkiluoto is used as the main reference in this report.

For explosions, the determination of the release height is not straightforward. The release height can depend on the volume of the explosion. Explosion cases may require their own release height analyses using some proper deterministic explosion model. It is also noteworthy that an explosion can spread the release to a wider area in both horizontal and vertical directions, which could require special handling in atmospheric dispersion and level 3 PRA analyses, as well as in level 2 PRA model. However, explosions that occur inside the containment would likely not throw the radionuclides as far as hydrogen explosions outside the containment did at Fukushima.

For some containment failure modes, such as failure of containment penetration or basemat melt-through, the location of the containment failure is clear. If there are penetrations at different heights, a probability distribution covering different penetrations can be used in PRA. In these cases, the final height of the release from the reactor building may however be different than the height of the release from the containment.

It is difficult to determine accurate release heights for all accidents, because there are different release paths, and instead of single height, the release can be distributed at different heights in continuous or discontinuous manner. But for PRA, simplifications are justified because the release height has small importance with regard to level 3 results compared to the amounts of radionuclides. Mainly the magnitude of the release height is important.

4. Release temperature

Temperatures of releases from containment are in most cases close to 100°C because radioactive substances are usually released among steam. It is possible to calculate accurate temperatures using deterministic severe accident analysis software such as MELCOR [9].

The temperature of radionuclides can change during their migration through reactor building to environment. Reactor building structures can cool down radionuclides if they are in contact for a sufficient time. If radionuclides leak from a small crack, the temperature of the radionuclides will be the same as the temperature of the wall because the flow rate is so slow that the radionuclides have enough time to cool down. On the other hand, if there is a fire in the reactor building, e.g. due to hydrogen explosion, the temperature of the radionuclides can rise. The release temperature could be calculated, taking fire into account, using some deterministic fluid dynamics software, such as OpenFOAM [7] or FDS [8]. It would be possible to determine both the release height and temperature in the same analysis.

An explosion can be a special case with regard to release temperature too. During an explosion, the temperature is very high, but the release cools down fast. Some special explosion analysis would be required to determine the temperature of a radioactive release after an explosion.

5. Hydrogen explosions

Hydrogen produced inside the containment during severe accident can lead to an explosion that jeopardizes the integrity of the containment. Potential hydrogen sources are metallic materials inside and outside the vessel. Significant amount of hydrogen can be produced when hot zirconium reacts with steam. In addition to the hydrogen concentration, hydrogen combustions can occur only with particular steam and air concentrations. Hydrogen combustion can be mild deflagration, detonation or something in between. Explosions can be prevented using pre-inertization, igniter or passive autocatalytic recombiners. Igniter can burn off hydrogen before an explosive concentration is reached. Passive autocatalytic recombiners reduce hydrogen concentration in the atmosphere by spontaneous reactions.

Hydrogen explosions in pressurized water reactor plant were studied in [3]. Deterministic MELCOR [9] analyses were performed to find out if atmospheric conditions of hydrogen explosion are met in different scenarios. Particularly, the capability of passive autocatalytic recombiners to prevent explosions was studied. Probability of containment failure due to hydrogen explosion was calculated based on deterministic analyses and reliability analysis of passive autocatalytic recombiners. The probability was highly dependent on whether the containment was reflooded in critical time window.

Hydrogen management in BWR plants is significantly different from pressurized water reactor plants. Typically in BWR plants, the containment is inert during operation which prevents the hydrogen explosions with certainty. However, the containment is not inert during start-up and shut-down, and accidents occurring at those times can lead to hydrogen explosions. Also, it is possible that the inerting system fails.

Hydrogen explosions are typically modelled in level 2 PRAs of BWRs in very simple ways. For example, in the model presented in the next section, probability 0.3 is given for containment not being inert, and if the containment is inert, hydrogen explosion breaks the containment with probability 0.5. These probabilities have been assumed to be conservative. The model could be made more accurate by modelling the dependence of the hydrogen explosion probability on different events, such as cooling system recovery and depressurisation. In addition, it is possible to include physical variables, such as hydrogen

concentration, in the model, and that way model physical dependencies explicitly. On the other hand, it is good practise to avoid unnecessary complexity in PRA models, and therefore, complex modelling should be well justified.

In practice, there are three probabilities that need to be determined for a given accident scenario:

1. the probability that the containment is not inert
2. the probability that an explosion occurs if the containment is not inert
3. the probability that the containment is broken if an explosion occurs.

Often, two latter probabilities are merged into one, like in the example model of this report. PRA model could be improved by determining these probabilities more accurately because the current probability estimates are very rough.

5.1 Containment inerting

The probability that the containment is not inert during an accident is the sum of the following probabilities of mutually exclusive events:

- the probability that reactor start-up is going on
- the probability that reactor shut-down is going on
- the probability that the containment is not inert due to the failure of the inerting system during operation
- the probability that the reactor is being refuelled.

The probabilities of start-up, shut-down and refuelling can be taken from level 1 results. Significant portion of transient and reactor over-pressurisation accidents occur during these phases. The probabilities must be calculated separately for each plant damage state.

The probability that the inerting system is failed during accident is likely small compared to start-up and shut-down accident probabilities. However, to assess the significance of inerting system failure, reliability analysis should be performed for the system. It is also important to determine how long the containment is non-inert if the system fails.

It seems that inerting system failure and its consequences have not received much attention in research literature, and there are some potentially important research questions to which more detailed studies could shed light on, such as:

- If the inerting is incomplete during accident, what is the sufficient level of inerting to prevent an accident?
- How does the probability of hydrogen explosion behave as the function of the level of inerting? It seems that hydrogen flammability has been studied mainly as a function of oxygen and steam content of the containment atmosphere, and the proportion of inerting gas(es) have not been taken into account.
- How long does the inerting take? This information is obviously available to NPP operators. A useful piece of information would be the proportion of oxygen (or more generally, non-inert gases) in the containment atmosphere, tabulated as a function of time from the start of inerting.

- How long does the deinerting take? A reasonable guess is that it takes significantly shorter time than inerting, but again the proportion of oxygen tabulated as a function of time would be useful.

A report from 1980 [13] states that the containment is inerted in 24 hours after start-up and deinerted 24 hours before shutdown for the reference plant, but today's plants might have different time frames.

Inerting could possibly be analysed using MELCOR [9] or based on measurement data of a BWR plant.

It is also worth considering whether the probability that the reactor start-up or shut-down is on is exactly the probability from level 1 PRA. It is possible that a small portion of accidents counted as normal operation accidents occur before inerting is completed after start-up or after the inerting has been removed before shut-down.

5.2 Analysis of explosions

The probability that an explosion occurs if the containment is not inert, can be analysed based on deterministic analyses in the same way as in [3], i.e. determining hydrogen and steam volumes in different accident scenarios. Deterministic analyses could be performed using MELCOR. However, different models are needed for start-up, shut-down and refuelling than for normal operation. VTT does not have such models at the moment, so they should be developed first.

The conditional probability that the containment is broken given that an explosion occurs can be analysed based on pressure impulses and the strength of the containment. Deterministic computer codes exist for the computation of pressure impulses. For example, in [14], pressure impulses were calculated using DETO software for hydrogen explosions in reactor building. The containment failure probabilities could be calculated using load vs. strength approach in the same way as for steam explosions in [4]. Also some literature in the response of structures to impulse loads exists (e.g. [15]).

5.3 Hydrogen explosions outside containment

Hydrogen explosion can also occur outside the containment if hydrogen leaks from the containment to the reactor building. This kind of hydrogen explosions occurred at Fukushima causing significantly larger releases than what had occurred before that [11] because the roofs were destroyed. Such explosions have not usually been modelled in PRA. It is theoretically possible that a hydrogen explosion could break the containment from the outside (causing larger containment leak than from which the hydrogen entered to the reactor building), but it has not been considered likely.

Hydrogen explosion outside containment has to be related to some containment failure mode, e.g. failure of containment penetrations, because otherwise hydrogen could not leak to the reactor building. If it is assumed in PRA that such explosion can possibly break the containment, a new containment failure mode needs to be introduced, e.g. "failure of penetrations with ex-containment hydrogen explosion." The probability that the leak leads to an explosion and the containment failure probability need to be estimated. Load vs. strength approach could be applied to the latter. Hydrogen and steam volumes outside the containment and pressure impulses can be calculated using deterministic software. The distribution of the time of the explosion should also be estimated, and the effects of the explosion on the releases should be included in the source term model.

A more realistic scenario is that an ex-containment hydrogen explosion does not break the containment but breaks the reactor building. In that case, the containment failure mode is the

cause of the leak. The difference to the previous case is that the reactor building failure probability needs to be estimated, and source term modelling is slightly different.

Source term modelling could be performed so that the amount of radionuclides accumulated in the reactor building would be calculated, like in [3], and when an explosion occurs, all those radionuclides could be assumed to be released. Furthermore, after the explosion, all releases from the containment can be assumed to be released to environment. More detailed modelling of the reactor building could possibly be performed too. If the explosion breaks the containment, the releases from the containment are larger (than with the leak that led to the hydrogen explosion).

6. Containment event tree model

A containment event tree (CET) model for a boiling water reactor plant was developed in [4]. This CET represented a station blackout scenario, and the plant damage state covered both low and high pressure transients. The CET was built originally using SPSA software [16] and later using FinPSA software [17]. In this study, FinPSA is used.

6.1 Dynamic containment event tree analysis

Software tools FinPSA [17] and SPSA [16] offer dynamic containment event tree approach that supports IDPSA. FinPSA is an updated version of SPSA (currently developed and maintained by VTT).

The level 2 modelling in FinPSA and SPSA is based on dynamic containment event trees and containment event tree programming language (CETL). The CETL language is used to define functions to calculate conditional probabilities of event tree branches, timings of the accident progression and amounts of releases. A CETL function is defined for each branch of a dynamic containment event tree, and a CET also contains an initial conditions section, where some probability and process variable values are defined. In addition, the model contains a global “common section”, where some global variables and functions can be defined. CETL programming is very flexible. At any branch, new value can be set or calculated for any global variable, and that way accident progression can be modelled dynamically. Binning rules can also be defined to divide the end points of the CET into release categories.

To account for uncertainties related to variable values, it is possible to define value distributions and perform Monte Carlo simulations. At each simulation run, a value is sampled from each defined distribution, and based on that, conditional probabilities are calculated for all the branches, and values are calculated for all variables at each end point of the CET. After the simulations, statistical analyses are performed to calculate frequency and variable value distributions for each end point and release category among other statistical results and correlation analyses. It is also possible to just calculate point values of the CET based on the mean values of distributions.

6.2 Overview of the model

The CET model is presented in two parts in Figures 1 and 2. The CET structure is otherwise similar to the CET presented in [4] except that sections have been added for lower drywell (LDW) flooding and filtered venting. In the model, core cooling systems are assumed unavailable until the possible AC power recovery. The sections of the CET, except LDW flooding and filtered venting, as well as source term computation are gone through in detail in [4]. Containment failure modes are presented in Table 2.

Transient	ISOL Containment leak-tightness	DEPR RCS depressurization	ECCS ECCS recovery	Flood LDW flooding	VEF Very early containment failure	VF Vessel failure	EF Early containment failure	LF Late containment failure	FV Filtered venting	
	ISOL_OK	DEPR_OK	REC	FL	NO_VEF	NO_VF	NO_EF	NO_LF	NO_FV	#1
									FV	#2
						VF	NO_EF	NO_LF	NO_FV	#3
									FV	#4
								LF		#5
							EF	NO_LF		#6
					VEF	NO_VF	NO_EF	NO_LF		#7
						VF	NO_EF	NO_LF		#8
			NO_REC	NO_FL	NO_VEF	VF	NO_EF	NO_LF	NO_FV	#9
									FV	#10
								LF		#11
							EF	NO_LF		#12
					VEF	VF	NO_EF	NO_LF		#13
				FL	NO_VEF	VF	NO_EF	NO_LF	NO_FV	#14
									FV	#15
								LF		#16
							EF	NO_LF		#17
					VEF	VF	NO_EF	NO_LF		#18

Figure 1: The CET model (part 1).

Transient	ISOL Containment leak-tightness	DEPR RCS depressurization	ECCS ECCS recovery	Flood LDW flooding	VEF Very early containment failure	VF Vessel failure	EF Early containment failure	LF Late containment failure	FV Filtered venting	
		NO_DEPR	REC	FL	NO_VEF	NO_VF	NO_EF	NO_LF	NO_FV	#19
									FV	#20
						VF	NO_EF	NO_LF	NO_FV	#21
									FV	#22
								LF		#23
							EF	NO_LF		#24
					VEF	NO_VF	NO_EF	NO_LF		#25
						VF	NO_EF	NO_LF		#26
			NO_REC	NO_FL	NO_VEF	VF	NO_EF	NO_LF	NO_FV	#27
									FV	#28
								LF		#29
							EF	NO_LF		#30
					VEF	VF	NO_EF	NO_LF		#31
				FL	NO_VEF	VF	NO_EF	NO_LF	NO_FV	#32
									FV	#33
								LF		#34
							EF	NO_LF		#35
					VEF	VF	NO_EF	NO_LF		#36
	NO_ISOL	DEPR_OK	NO_REC	NO_FL	NO_VEF	VF				#37

Figure 2: The CET model (part 2).

Table 2: Containment failure categories and the corresponding failure modes used in the CET model.

Release category	Containment failure/vent mode
No containment failure of filtered venting (OK)	-
Isolation failure (ISOL)	1. Containment not leak-tight (ISOL)
Very early containment failure (VEF)	1. Containment over-pressurization (COP) 2. Hydrogen deflagration/detonation (H2) 3. Alpha-mode failure (ALPHA)
Early containment failure (EF)	1. Ex-vessel steam explosion (STEAM) 2. Failure of containment penetrations (PENE)
Late containment failure (LF)	1. Non-coolable ex-vessel debris causes basemat melt-through (BASE)
Filtered venting (FV)	1. Very early venting (VEFV) 2. Early venting (EFV) 3. Late venting (LFV)

6.3 Release heights and temperatures

A release height variable and temperature variable were added to the model. Their values are set always after the containment failure mode is defined. Table 3 presents the values that are used in the model. The values are however not based on any real data because the authors had no possibility to perform any deterministic calculations and had no access to any reactor building architecture document from which potential release heights could have been identified. It was assumed that hydrogen explosions and alpha mode steam explosions lead to higher release heights than the other failure modes because they occur high in the containment. Basemat release was assumed to occur at ground level, and the height of the stack was assumed to be 110 meters. It was assumed that release temperatures are higher than 100 °C if explosions occur. Without explosions the temperatures were assumed to be 100 °C with exception of basemat melt-through. In that case, it was assumed that the radionuclides are cooled down to a lower temperature by building structures. These values were chosen just for the sake of having an example and they should not be adapted to any real PRA.

Table 3: Release heights and temperatures for different containment failure modes.

Containment failure mode	Release height	Release temperature (°C)
Containment not leak-tight	5 m with prob. 0.5, 20 m with prob. 0.5	100
Containment over-pressurization	5 m with prob. 0.5, 20 m with prob. 0.5	100
Hydrogen deflagration/detonation	30 m with prob. 0.5, 50 m with prob. 0.5	Lognormal distribution with mean 500 and error factor 1.5
Alpha-mode failure	20 m with prob. 0.5, 30 m with prob. 0.5	Lognormal distribution with mean 200 and error factor 1.5
Ex-vessel steam explosion	5 m with prob. 0.5, 20 m with prob. 0.5	Lognormal distribution with mean 500 and error factor 1.5
Failure of containment penetrations	5 m with prob. 0.5, 20 m with prob. 0.5	100
Non-coolable ex-vessel debris causes basemat melt-through	0 m	Lognormal distribution with mean 50 and error factor 1.5
Filtered venting	110 m	100

6.4 Uncertainty analysis

In the original model [4], uncertainty analysis was not performed for release probabilities. Instead, only one sequence (or in some cases two sequences) was realised in a single simulation cycle. For this study, the model was changed so that results were calculated for all sequences in all simulation cycles, and uncertainty distributions were assigned to probability parameters. The parameters are presented in Table A-1 in Appendix A. The distributions were chosen so that the mean values remained same as in the original model, and the model was kept as close to the original as possible, though many parts required significant modifications.

A significant change is that previously some physical parameters, e.g. ECCS recovery time and core release fraction, determined which sequence is realised, but in the new model, the values of those parameters depend on the accident sequence. Hence, the logic is kind of reversed and emphasises probabilistic analysis, while the physical modelling is more on background. But still the source term results remain approximately the same.

A good and simple example of modifications that were made is the emergency core system recovery. The failure probability of recovery is now drawn from a lognormal distribution, which differs depending on whether the depressurisation is successful. Previously, the recovery time was drawn from a distribution and compared to time available which was also drawn from a distribution. On each simulation cycle, either the recovery occurred in time or not, but the updated version of the model covers both scenarios at the same time. The mean values of failure probability distributions (of high and low pressure cases) were taken from the results of the previous model. Also, in the updated model, for relevant accident sequences, the recovery time is drawn from the distribution as many times as it takes for the recovery time to be smaller than the time available for the recovery.

A new section was added for the LDW flooding so that both flooded and unflooded scenarios can be calculated in same simulation cycle. Previously, flooding was handled in ECCS recovery section.

In the old model, very early containment failure either occurred or not in a simulation cycle, but the new model calculates a probability for it as a sum of the probabilities of different failure modes. Still, only one failure mode is realised in one simulation cycle. The failure mode is drawn based on the fractions of the failure mode probabilities.

In the old model, the vessel failed if the core release fraction was larger than a given limit value. Both the core release fraction and the limit value were drawn from a distribution. In the new model, a probability is drawn for the vessel failure instead. In addition, a large value is given for the core release fraction if the vessel fails, and a small value is given if the vessel does not fail so that the source term calculation will work in the same way as in the old model.

Again, in the old model, early containment failure either occurred or not in a simulation cycle, but the new model calculates a probability for it as a sum of the probabilities of different failure modes. Only one failure mode is realised in one simulation cycle. The failure mode is drawn based on the fractions of the failure mode probabilities. In the old model, ex-vessel steam explosion induced containment failure was evaluated by drawing LDW strength and pressure impulses from distributions, but in the new model, failure probabilities taken from [4] are used directly as the mean values of the probability distributions.

The new model also includes a probability parameter for high amount of melt being ejected to the LDW. The mean probability was calculated from the results of the old model. Also, in the case of ex-vessel steam explosion and ECCS working, the core release fraction and debris fraction are updated because high amounts of melt are more likely. The distribution for these fractions was estimated from the results of the old model, but it is quite rough.

In the old model, late containment failure either occurred or not, but the new model calculates a probability for it. The probability is the product of the probability that debris exists, the probability that the debris is not coolable and the probability that the basemat melt-through occurs if the debris is not coolable. In the old model, debris coolability fraction needed to be small enough, and the debris needed to exist so that the basemat melt-through could occur. Probabilities for these conditions were estimated from the results and are used in the new model. A small value is also given for debris coolability fraction if basemat melt-through occurs, and it is ensured that the core release fraction and debris fraction are larger than 0.

A new section was also added for filtered venting. In the old model, the possibility of filtered venting was considered in NO_VEF, NO_EF and NO_LF functions of VEF, EF and LF sections. Because of this, there were sequences that could lead either to release category OK or FV depending on the drawn input parameters. The new filtered venting section was added so that these release categories can be analysed in different sequences in the same simulation cycle. This way the uncertainty distributions are calculated correctly. Very early, early and late filtered venting are all considered in this same section. The venting probability is calculated based on the probabilities of these venting modes as

$$p_{VEFV} + (1 - p_{VEFV})(p_{EFV} + (1 - p_{EFV})p_{LFV}).$$

One of these venting modes is realised in a simulation cycle. The venting mode is drawn based on the fractions of the probabilities.

6.5 Results

Table 4 presents the results including the conditional probabilities and release fractions for all release categories. The four values in the cells of the table are mean, 5th percentile, median and 95th percentile. The Prob. column shows the percentile values of the new uncertainty distributions. When uncertainty analysis is correct, FinPSA also produces a set of proper graphs presenting the uncertainty distributions, e.g. those in Figures 3-6.

Table 4: The summary of results.

Bin	Prob.	S_Xe	S_Cs	S_Ru
OK	2.24E-01	7.58E-11	0.00E+00	0.00E+00
	1.09E-01	1.76E-11	0.00E+00	0.00E+00
	2.25E-01	9.97E-11	0.00E+00	0.00E+00
	3.39E-01	1.00E-10	0.00E+00	0.00E+00
ISOL	9.98E-03	8.41E-01	2.55E-01	8.90E-03
	4.54E-03	4.50E-01	6.46E-02	0.00E+00
	9.19E-03	9.98E-01	2.41E-01	3.50E-03
	1.82E-02	1.00E+00	4.75E-01	3.40E-02
VEF	1.86E-01	7.58E-01	1.13E-01	3.77E-03
	9.34E-02	1.76E-01	9.01E-03	2.10E-06
	1.71E-01	9.97E-01	8.52E-02	7.51E-04
	3.27E-01	1.00E+00	3.15E-01	1.75E-02
EF	3.09E-02	7.80E-01	1.57E-01	5.49E-03
	8.49E-03	2.28E-01	2.16E-02	2.00E-06
	2.43E-02	9.97E-01	1.39E-01	1.71E-03
	7.58E-02	1.00E+00	3.71E-01	2.31E-02
LF	1.99E-02	7.90E-01	1.54E-01	4.49E-03
	6.66E-03	2.76E-01	2.36E-02	0.00E+00
	1.74E-02	9.97E-01	1.36E-01	1.01E-03
	4.11E-02	1.00E+00	3.54E-01	1.99E-02
FV	5.29E-01	7.57E-01	9.82E-04	2.90E-05
	3.97E-01	1.74E-01	2.62E-06	0.00E+00
	5.28E-01	9.97E-01	6.57E-05	3.19E-07
	6.67E-01	1.00E+00	3.58E-03	6.25E-05
Weighted Total	1.00E+00	5.90E-01	3.18E-02	1.06E-03
	1.00E+00	1.41E-01	4.69E-03	5.01E-07
	1.00E+00	6.90E-01	2.40E-02	3.03E-04
	1.00E+00	8.67E-01	8.58E-02	4.46E-03

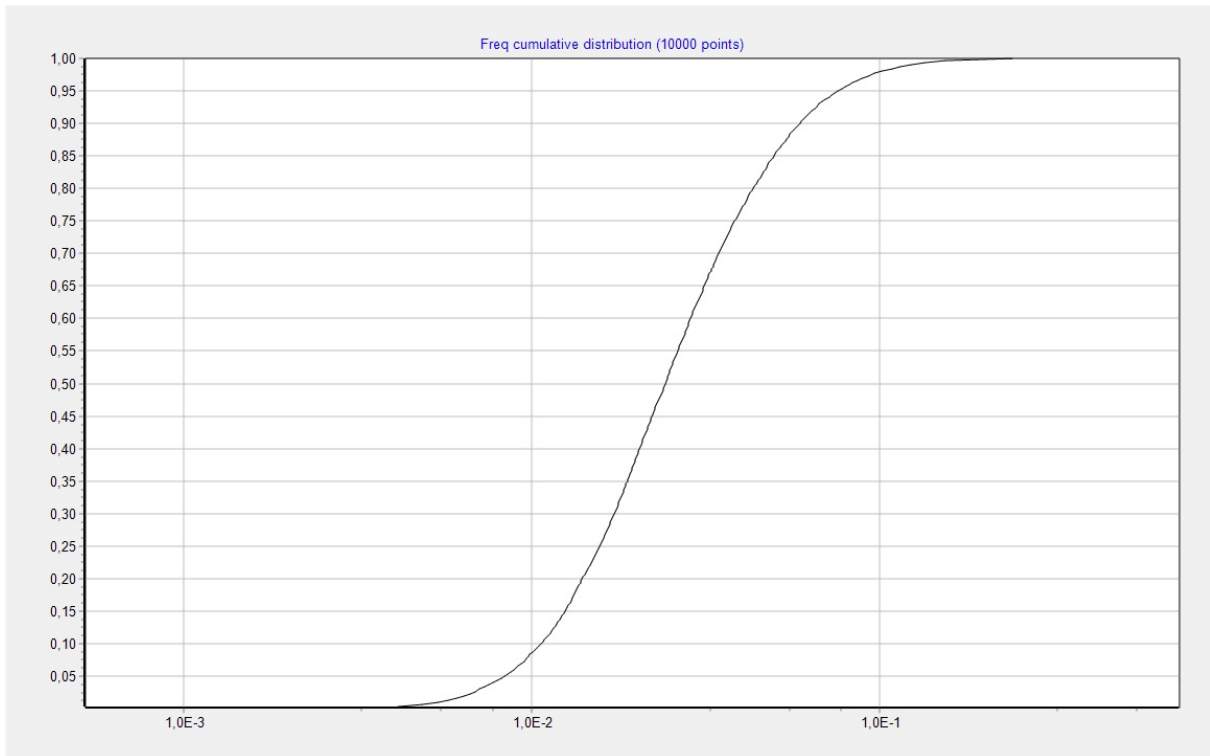


Figure 3: Cumulative distribution of the conditional probability of early containment failure.

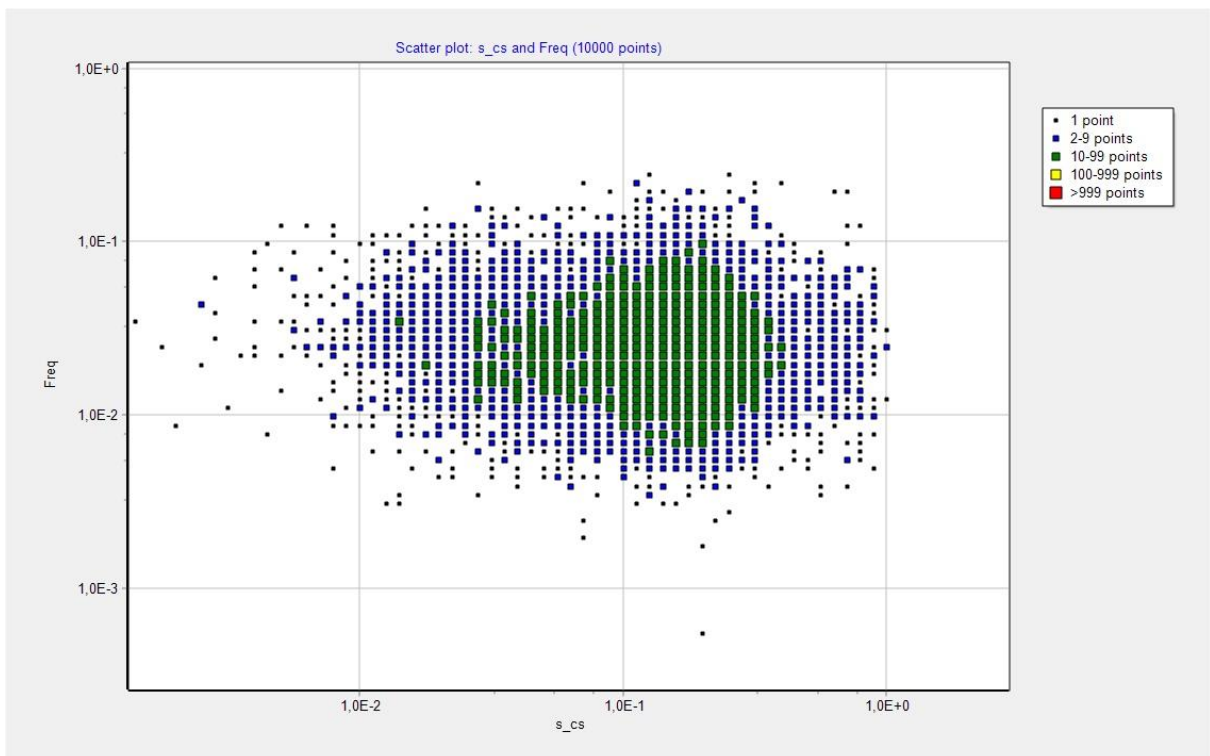


Figure 4: Scatter plot between conditional probability and cesium release fraction in early containment failure based on weighted point values.

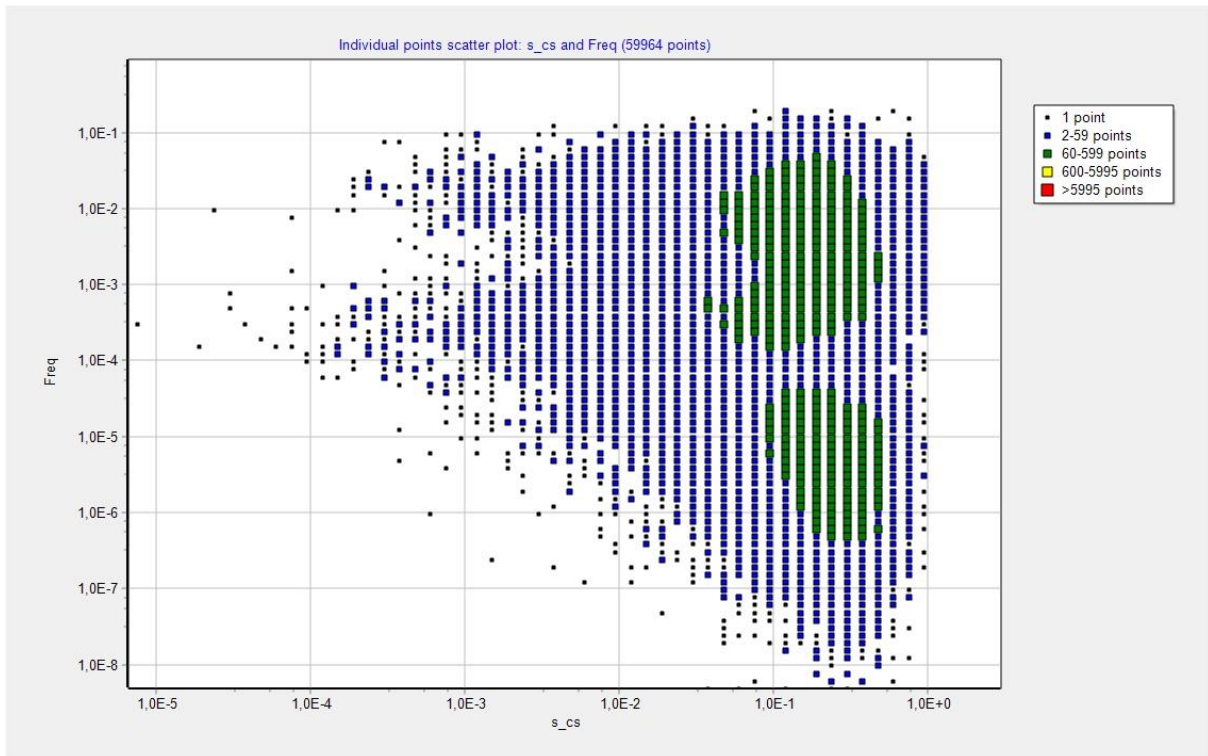


Figure 5: Scatter plot between conditional probability and cesium release fraction in early containment failure based on individual simulation points.

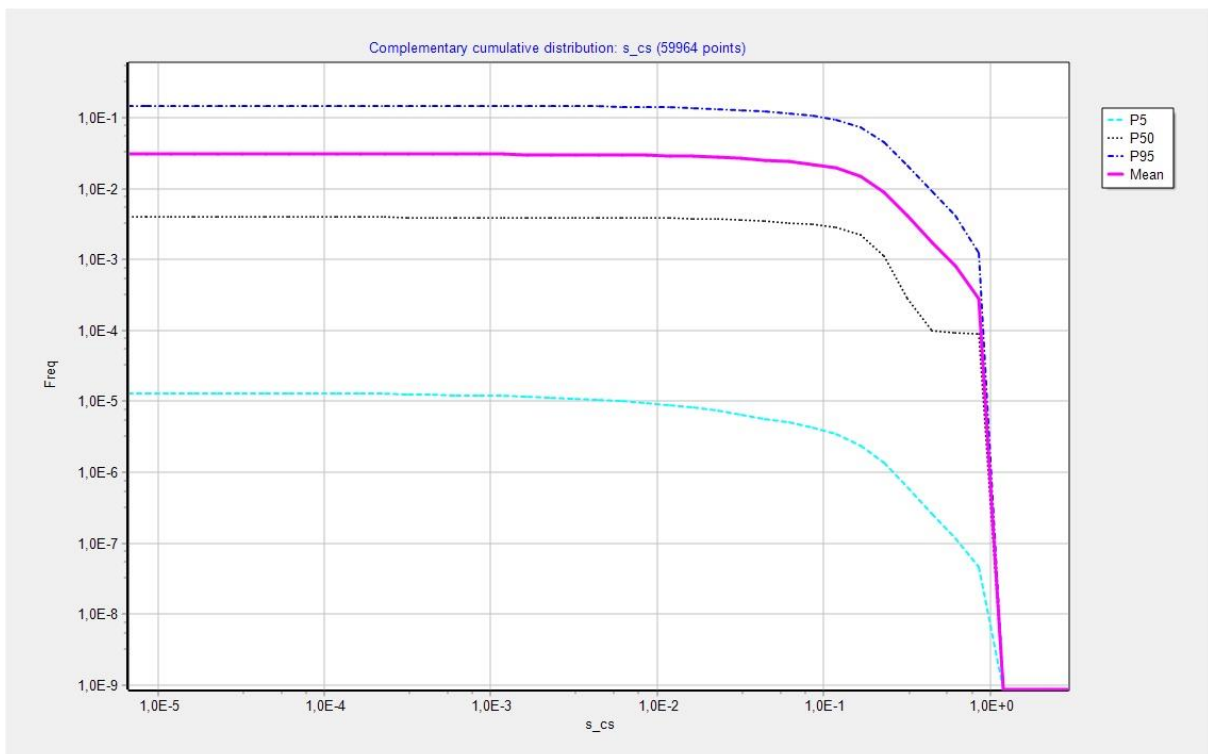


Figure 6: Complementary cumulative distribution of cesium release fraction in early containment failure.

7. Conclusions

This report studied nuclear power plant accident source term characteristics and hydrogen explosions from the PRA point of view. Release height and temperature were considered for different accident scenarios based on general knowledge, literature and discussions with deterministic safety analysis experts. Release height is usually the height of the location where the reactor building leaks (which depends on the containment failure mode), or the height of the chimney if the release is controlled. In an uncontrolled accident case, both the containment failure location and the flow path of radionuclides in the reactor building need to be analysed to determine the release height. The determination of the accurate release height distribution is very difficult in some cases, especially when an explosion occurs. The temperature of release from containment is in most cases close to 100°C, but the temperature of radionuclides can potentially change during their migration in reactor building. Higher temperatures can be caused by fires and explosions. There are computer codes that can be used to analyse radionuclide flows in reactor building and determine the release heights and temperatures. Both release heights and temperatures can be included in PRA models easily if their probability distributions are known.

Hydrogen explosions in BWR were considered. Different areas of the analysis concerning both explosions inside and outside containment were discussed. Hydrogen explosions can occur in BWR containment even if it is normally inerted, if accident occurs during start-up, maintenance or shut-down, or if the inerting system fails. Hydrogen explosions outside containment have not usually been modelled in PRA, even though they can affect the releases significantly.

Complete uncertainty analysis was developed for an existing simplified BWR containment event tree model. This required significant changes in the model. The original model was heavily based on computation with physical parameters, whereas in the new version, the focus is on probabilistic modelling. The mean values of the probability distributions used in the new model were derived from the original model and its results. If there had not been the original model, other supporting analyses to estimate those mean probabilities would have been needed instead. It can actually be a good idea to perform the modelling in two phases like this: first focusing on physical modelling to obtain preliminary results and implementing the uncertainty analysis later.

References

- [1] International Atomic Energy Agency, IAEA. Development and application of level 2 probabilistic safety assessment for nuclear power plants: Specific safety guide No: SSG-4. Vienna, 2010.
- [2] Lee JC and McCormick NJ. Risk and safety analysis of nuclear systems. Wiley, Hoboken NJ, USA, 2011.
- [3] Silvonen T. Reliability analysis for passive autocatalytic hydrogen recombiners of a nuclear power plant. VTT Technical Research Centre of Finland, Espoo. 2013. VTT-R-08535-12.
- [4] Silvonen T. Steam explosion case study using IDPSA methodology. VTT Technical Research Centre of Finland, Espoo. 2013. VTT-R-05974-13.
- [5] Ditlevsen O and Madsen HO. Structural reliability methods. Wiley, New York NY, USA, 1996.

- [6] Fullwood R. Probabilistic safety assessment in the chemical and nuclear industries. Butterworth-Heinemann, Boston MA, USA, 2000.
- [7] OpenCFD Ltd (ESI Group). OpenFOAM. <http://www.openfoam.com/>
- [8] McGrattan K, Hostikka S, McDermott R, Floyd J, Weinschenk C, Overholt K. Fire dynamics simulator – User’s guide, NIST special publication 1019, Sixth edition. National Institute of Standards and Technology, 2013.
- [9] Sandia National Laboratories. MELCOR computer code manuals, Vol 2: Reference manuals, Version 1.8.6. Albuquerque, 2005.
- [10] Harrell J. RADTRAD-NAI, Numerical applications, A division of Zachry nuclear engineering, inc. http://www.numerical.com/radtrad_details.php.
- [11] Katata G, Chino M, Kobayashi T, Terada H, Ota M, Nagai H, Kajino M, Draxler R, Hort MC, Malo A, Torii T and Sanada Y. Detailed source term estimation of the atmospheric release for the Fukushima Daiichi nuclear power station accident by coupling simulations of the atmospheric dispersion model with an improved deposition scheme and oceanic dispersion model. Atmospheric chemistry and physics, 15, 1029-1070, 2015.
- [12] Korsakissok I, Mathieu A and Didier D. Atmospheric dispersion and ground deposition induced by the Fukushima nuclear power plant accident: a local-scale simulation and sensitivity study. Atmospheric environment, 70, 267-279, 2013.
- [13] Heising CD. Analyzing the safety impact of containment inerting at Vermont Yankee. Massachusetts Institute of Technology, Cambridge, Massachusetts, USA, 1980. MIT-NE-240.
- [14] Silde A and Lindholm I. On detonation dynamics in hydrogen-air-steam mixtures: theory and application to Olkiluoto reactor building. Nordic nuclear safety research, Roskilde, Denmark, 2000. NKS-9.
- [15] Jones, N. Structural impact, 2nd edition. Cambridge University Press, New York NY, USA, 2012.
- [16] Sandberg J and Virolainen R. Comparison of the core damage probability by the SPSA computer program and by analytical methods - a simplified loss of off-site power, Validation of the SPSA program, STUK-YTO-TR 62. Department of Nuclear Safety, Finnish Centre for Radiation and Nuclear Safety, STUK, Helsinki, 1993.
- [17] VTT Technical Research Centre of Finland Ltd. FinPSA – Tool for promoting safety and reliability. 2016. <https://www.simulationstore.com/finpsa>.

Appendix A: Uncertainty distributions of parameters

Table A-1: Uncertainty distributions of probability parameters.

Parameter	Distribution	Mean	Error factor (P95/P50)
Failure probability of ECCS recovery in pressurised case	Lognormal	0.024	2.0
Failure probability of ECCS recovery in depressurised case	Lognormal	0.078	2.0
Recriticality probability	Lognormal	0.5	1.5
Failure probability of LDW flooding if ECCS does not work	Lognormal	0.05	3.0
Probability that containment is not inert	Lognormal	0.3	2.0
Probability that over-pressurisation breaks the containment if the core is recritical	Lognormal	0.1	2.0
Probability that hydrogen explosion breaks the containment if it is not inert	Lognormal	0.5	1.5
Probability that an alpha mode steam explosion breaks the containment	Lognormal	0.0001	10
Probability of very early filtered venting in depressurised case if the core is recritical	Lognormal	0.25	2.0
Probability of very early filtered venting in pressurised case if the core is recritical	Lognormal	0.5	1.5
Probability of no vessel failure	Lognormal	0.5	1.5
Failure probability of containment penetrations in pressurised case if LDW has been flooded and vessel has failed	Lognormal (multiplied by 2)	0.05	3.0
Probability that only little melt is ejected to the containment if ECCS works and vessel has failed	Lognormal	0.45	1.5
Failure probability of containment penetrations if LDW has not been flooded and vessel has failed	Lognormal	0.5	1.5
Probability of no early filtered venting in pressurised case if ECCS works and the core is recritical	Lognormal	0.01	5.0
Probability of early filtered venting in pressurised case if ECCS works and the core is not recritical	Lognormal	0.5	1.5

Probability of early filtered venting in depressurised case if ECCS works and the core is recritical	Lognormal	0.5	1.5
Probability of early filtered venting in pressurised case if ECCS recovery has failed and the core is recritical	Lognormal	0.5	1.5
Probability of early filtered venting in depressurised case if ECCS works and the core is not recritical	Lognormal	0.25	2.0
Probability of early filtered venting in depressurised case if ECCS recovery has failed and the core is recritical	Lognormal	0.25	2.0
Containment failure probability due to ex-vessel steam explosion in pressurised case if much melt is ejected	Lognormal	0.091	3.0
Containment failure probability due to ex-vessel steam explosion in pressurised case if little melt is ejected	Lognormal	0.003	3.0
Containment failure probability due to ex-vessel steam explosion in depressurised case if much melt is ejected	Lognormal	0.207	3.0
Containment failure probability due to ex-vessel steam explosion in depressurised case if little melt is ejected	Lognormal	0.021	3.0
Probability of no ex-vessel steam explosion triggered if melt is ejected in high pressure	Lognormal	0.01	10
Probability of ex-vessel steam explosion triggered if melt is ejected in low pressure	Lognormal	0.5	1.5
Probability of basemat melt-through if the debris is not coolable	Lognormal	0.1	2.0
Probability of no late filtered venting in pressurised case	Lognormal	0.1	2.0
Probability of late filtered venting in depressurised case	Lognormal	0.5	1.5
Probability of no debris if ECCS recovery failed and vessel has failed	Lognormal	0.006	5.0
Probability that the debris is not coolable if LDW is flooded and the debris exists	Lognormal	0.5	1.5

Title	Phenomena Threatening Containment Integrity and Evaluating Source Term Characteristics
Author(s)	Veikko Taivassalo ¹ , Eveliina Takasuo ¹ , Magnus Strandberg ¹ , Tero Tyrväinen ¹ , Ilkka Karanta ¹ , Anna Nieminen ¹
Affiliation(s)	¹ VTT Technical Research Centre of Finland Ltd
ISBN	978-87-7893-497-0
Date	June 2018
Project	NKS-R / SPARC
No. of pages	7 + 76
No. of tables	0
No. of illustrations	3
No. of references	3
Abstract max. 2000 characters	<p>To assess phenomena threatening the BWR containment integrity more reliably, long-term debris bed coolability and possibility of hydrogen explosions to occur were analysed deterministically. When comparing VTT's MEWA results on the debris bed post-dryout temperature to KTH's DECOSIM results, a good agreement was achieved while the temperatures continued to increase, but the stabilized temperatures differed notably. Hydrogen explosions are possible in the containment only if the inertion is lost. This is most probable during the shutdown or start-up.</p> <p>In addition, factors affecting source term characteristics, i.e. release temperature, altitude and probability were considered for different accident scenarios to further develop the methods and tools for PRA. Source term release height is usually the height of the location where the reactor building leaks or the height of the chimney if release is controlled. The temperature of release from containment is in most cases close to 100 °C but the temperature of radionuclides can potentially change during their migration in the reactor building.</p>
Key words	Debris bed coolability, MEWA, hydrogen explosions, MELCOR, source term, PRA, FinPSA